

9

PLUMES DURING DREDGING

LYTTELTON HARBOUR/WHAKARAUPŌ CHANNEL PROJECT

Simulations of Dredge Plumes from Dredging Activities in the Channel

Prepared for Lyttelton Port Company Limited



*PO Box 441, New Plymouth, New Zealand
T: 64-6-7585035 E: enquiries@metocean.co.nz*

MetOcean Solutions Ltd: P0201-03

May 2016

Report status

Version	Date	Status	Approved by
RevA	22/12/2015	Initial draft for internal review	Weppe
RevB	18/05/2016	Updated draft for internal review	Weppe
RevC	01/06/2016	Draught for internal review	Beamsley
RevD	07/06/2016	Draught for internal review	Thiebaut
RevE	07/06/2016	Draught for Client review	Beamsley
RevF	04/08/2016	Updated draft for Client review	Beamsley
Rev0	21/09/2016	Approved for release	Beamsley

It is the responsibility of the reader to verify the currency of the version number of this report.

The information, including the intellectual property, contained in this report is confidential and proprietary to MetOcean Solutions Ltd. It may be used by the persons to whom it is provided for the stated purpose for which it is provided, and must not be imparted to any third person without the prior written approval of MetOcean Solutions Ltd. MetOcean Solutions Ltd reserves all legal rights and remedies in relation to any infringement of its rights in respect of its confidential information.

TABLE OF CONTENTS

1.	Introduction	9
2.	Methods	11
2.1.	Approach	11
2.2.	Hydrodynamics	11
2.3.	Trajectory Modelling	13
2.4.	Particle Size Distribution and Settling Velocity	15
2.5.	Disposal scenarios	17
2.6.	Post-Processing	21
2.6.1.	Concentration and depositional thickness computation	21
2.6.2.	Application to the present study	22
3.	Results	24
3.1.	Existing and post-dredging hydrodynamics	24
3.2.	Dredging plumes during peak tidal flows	33
3.2.1.	Dredging and overflow modes	33
3.2.1.	Existing, Scenario 2 and seiching hydrodynamics	33
3.3.	Probabilistic dredging plumes	41
3.4.	Dredging plume concentration exceedence maps	50
4.	Summary	54
5.	References	55
	Appendix – Supplementary Figures	56
A1.	Dredging plumes during peak tidal flows	57
A1.1	Dredging Mode	57
A1.1.1	Existing bathymetry	57
A1.1.2	Stage3 bathymetry	60
A1.1.3	Existing bathymetry with surge signal	63
A1.1.4	Scenario 2 bathymetry with surge signal	66
A1.2	Overflow Mode	69
A1.2.1	Existing bathymetry	69
A1.2.2	Stage3 bathymetry	72
A1.2.3	Existing bathymetry with surge signal	75
A1.2.4	Scenario 2 bathymetry with surge signal	78
A2.	Probabilistic dredging plumes	81
A2.1	Dredging Mode	81
A2.1.1	Existing bathymetry	81
A2.1.2	Scenario 2 bathymetry	84
A2.1.3	Existing bathymetry with surge signal	85
A2.2	Overflow Mode	88
A2.2.1	Existing bathymetry	88
A2.2.2	Scenario 2	92
A2.2.3	Existing with surge signal	93
A2.2.4	Stage3 with surge signal	94
A2.3	Comparison of 10, 20, 30 min overflow scenario	95
A2.3.1	Existing bathymetry	95
A3.	Concentration exceedence	98

A3.1 Existing bathymetry.....	98
-------------------------------	----

LIST OF FIGURES

Figure 1.1	Footprints of the new proposed shipping channel and offshore disposal ground.	10
Figure 2.1	SELFE model mesh and bathymetry.	12
Figure 2.2	Particle size distribution of sediment to be dredged in the Lyttelton Harbour/Whakaraupō. The vertical dashed lines indicate the clay, silt, and sand size ranges.	15
Figure 2.3	Simulated release sites along the proposed channel (see Table 2.2 for actual positions).	17
Figure 2.4	Sources of a dredge plume for a Trailing Suction Hopper Dredger: 1-Drag Head, 2-Overflow, 3-Propeller wash (after Becker J. et al., 2015).	18
Figure 2.5	Three main phases occurring during the disposal of dredged material: 1) Convective descent, 2) Dynamic Collapse, and 3) Passive plume dispersion.	19
Figure 2.6	Percentages of sediment transferred from the near-field density driven plume to the far-field plume during overflowing	21
Figure 2.7	Receptor grid for the SSC plumes. The resolution ranges from 30 m in the channel to ~500 m offshore.	23
Figure 3.1	Bathymetric changes associated with the Scenario 2 scenario including an extended and deeper channel and reclaimed land east of Gollans Bay. Negative depth changes indicate a deepening relative to the existing bathymetry.	25
Figure 3.2	Snapshots of peak ebb flows during spring tides over the existing and Scenario 2 bathymetries, representative of the bathymetry expected at the completion of the dredging program. The proposed channel polygon is show in black.	26
Figure 3.3	Snapshots of peak flood flows during spring tides over the existing and Scenario 2 bathymetries, representative of the bathymetry expected at the completion of the dredging program. The proposed channel polygon is show in black.	27
Figure 3.4	Snapshots of peak ebb flows during neap tides over the existing and Scenario 2 bathymetries, representative of the bathymetry expected at the completion of the dredging program. The proposed channel polygon is show in black.	28
Figure 3.5	Snapshots of peak flood flows during neap tides over the existing and Scenario 2 bathymetries, representative of the bathymetry expected at the completion of the dredging program. The proposed channel polygon is show in black.	29
Figure 3.6	Rose of existing tidal currents at study sites C1 to C11 (see Figure 2.3 for site position).	30
Figure 3.7	Rose of tidal currents for the Scenario 2 bathymetry at study sites C1 to C11 (see Figure 2.3 for site position).	31
Figure 3.8	Seiche signal super-imposed over tidal signal. The blue line represents the combined tidal and seiche signal, while the red line represents the seiche component only.	32
Figure 3.9	SSC plumes during dredging (left) and overflow (right) phases at site C1, C5 and C11 at peak ebb flow during spring tides, at three levels in the water column. These results are obtained using the existing hydrodynamics. ...	34
Figure 3.10	SSC plumes during dredging (left) and overflow (right) phases at site C1, C5 and C11 at peak flood flow during spring tides, at three levels in the water column. These results are obtained using the existing hydrodynamics. ...	35

Figure 3.11	SSC plumes during dredging (left) and overflow (right) phases at site C1, C5 and C11 at peak ebb flow during neap tides, at three levels in the water column. These results are obtained using the existing hydrodynamics...	36
Figure 3.12	SSC plumes during dredging (left) and overflow (right) phases at site C1, C5 and C11 at peak flood flow during neap tides, at three levels in the water column. These results are obtained using the existing hydrodynamics...	37
Figure 3.13	SSC plumes during overflow at site C1 at peak flood flow during spring tides, at three levels in the water column, for the existing, Scenario 2, existing with seiche and Scenario 2 with seiche scenarios (top left, top right, bottom left and bottom right, respectively).....	38
Figure 3.14	SSC plumes during overflow at site C5 at peak flood flow during spring tides, at three levels in the water column, for the existing, Scenario 2, existing with seiche and Scenario 2 with seiche scenarios (top left, top right, bottom left and bottom right, respectively).....	39
Figure 3.15	SSC plumes during overflow at site C11 at peak flood flow during spring tides, at three levels in the water column, for the existing, Scenario 2, existing with seiche and Scenario 2 with seiche hydrodynamics (top left, top right, bottom left and bottom right, respectively).	40
Figure 3.16	Probabilistic SSC plumes during dredging (left) and overflow (right) phases at site C1, C5 and C11, at three levels in the water column. These results are obtained using the existing hydrodynamics.....	43
Figure 3.17	Probabilistic SSC plumes during dredging (left) and overflow (right) phases at site C1, C5 and C11, at three levels in the water column. These results are obtained using the Scenario 2 hydrodynamics.....	44
Figure 3.18	Probabilistic SSC plumes during dredging (left) and overflow (right) phases at site C1, C5 and C11, at three levels in the water column. These results are obtained using the existing hydrodynamics with seiche included.	45
Figure 3.19	Probabilistic SSC plumes during dredging (left) and overflow (right) phases at site C1, C5 and C11, at three levels in the water column. These results are obtained using the Scenario 2 hydrodynamics with seiche included.	46
Figure 3.20	Probabilistic SSC plumes during a 10, 20 and 30 minute overflow scenarios (top to bottom) at site C1, over the existing bathymetry, at three levels in the water columns.	47
Figure 3.21	Probabilistic SSC plumes during a 10, 20 and 30 minute overflow scenarios (top to bottom) at site C5, over the existing bathymetry, at three levels in the water columns.	48
Figure 3.22	Probabilistic SSC plumes during a 10, 20 and 30 minute overflow scenarios (top to bottom) at site C11, over the existing bathymetry, at three levels in the water columns.	49
Figure 3.23	Percentage of time SSC thresholds of 10, 50, 100 mg/L (top to bottom) are exceeded during dredging activities at site C1, including dredging (25 min), overflow (10 min) and travel to and from disposal site (85 minutes). The exceedence percentages are computed over a full spring-neap tidal cycle (28 days).	51
Figure 3.24	Percentage of time SSC thresholds of 10, 50, 100 mg/L (top to bottom) are exceeded during dredging activities at site C5, including dredging (25 min), overflow (10 min) and travel to and from disposal site (85 minutes). The exceedence percentages are computed over a full spring-neap tidal cycle (28 days).	52
Figure 3.25	Percentage of time SSC thresholds of 10, 50, 100 mg/L (top to bottom) are exceeded during dredging activities at site C11, including dredging (25 min),	

overflow (10 min) and travel to and from disposal site (85 minutes). The
exceedence percentages are computed over a full spring-neap tidal cycle (28
days).53

LIST OF TABLES

Table 2.1	Representative median grain sizes, settling velocities, and proportions of total volume released for the 4 discrete sediment classes considered.....	16
Table 2.2	Coordinates and depths of release sites along the channel.	17

1. INTRODUCTION

Lyttelton Port Company Limited (LPC) proposes deepening of the harbour shipping channel and turning basin to accommodate vessels with increased draughts, and disposing of the dredged material at an offshore site. A full description of the Channel Deepening Project (CDP) activities, location and methodologies is provided in Section Two (Project Description) of the associated Assessment of Environmental Effects (AEE), while Figure 1.1 provides an outline of the proposed deepened channel and capital disposal ground.

LPC has commissioned MetOcean Solutions Ltd (MSL) to undertake a numerical model study to investigate the far-field dispersion of the passive dredge plume associated with the dredging processes within the main shipping channel and the turning basin. This study take into account the physical entrainment of sediment due to the dredger head, hopper overflow and propeller-wash.

Within the offshore environment, the discharge of dredge spoil occurs over a specific future period of time, but is inherently non-deterministic in that the dispersal and depositional outcomes are influenced by random variables such as currents and turbulence. Conversely, within the confines of the Lyttelton Port tidal velocities are expected to be the salient mechanism for the transport and dispersal of plumes generated during the dredging operations, while velocities associated with harbour seiching are expected to provide a secondary forcing mechanism.

The report presents results of particle tracking simulations undertaken to assess the dispersion of the sediment plumes resulting from the dredging activities in the channel over two complete spring-neap tide cycle (~ 28 days), both with and without the process of harbour seiching being considered. Sediment releases were simulated at multiple positions within the channel to allow characterising spatial variations of sediment dispersion processes expected throughout the progression of the CDP. A sediment distribution using four different sediment classes was used in simulations to reproduce the nature of the material to be dredged (see MetOcean Solutions Ltd., 2016).

The report is structured as follows. Section 2 details the numerical dispersal modelling methods that have been employed. The results are provided in Section 3 and a summary of the work is provided in Section 4. References cited are listed in the final Section 5. Details of the hydrodynamic modelling, including validation are presented elsewhere (Goring, 2014).

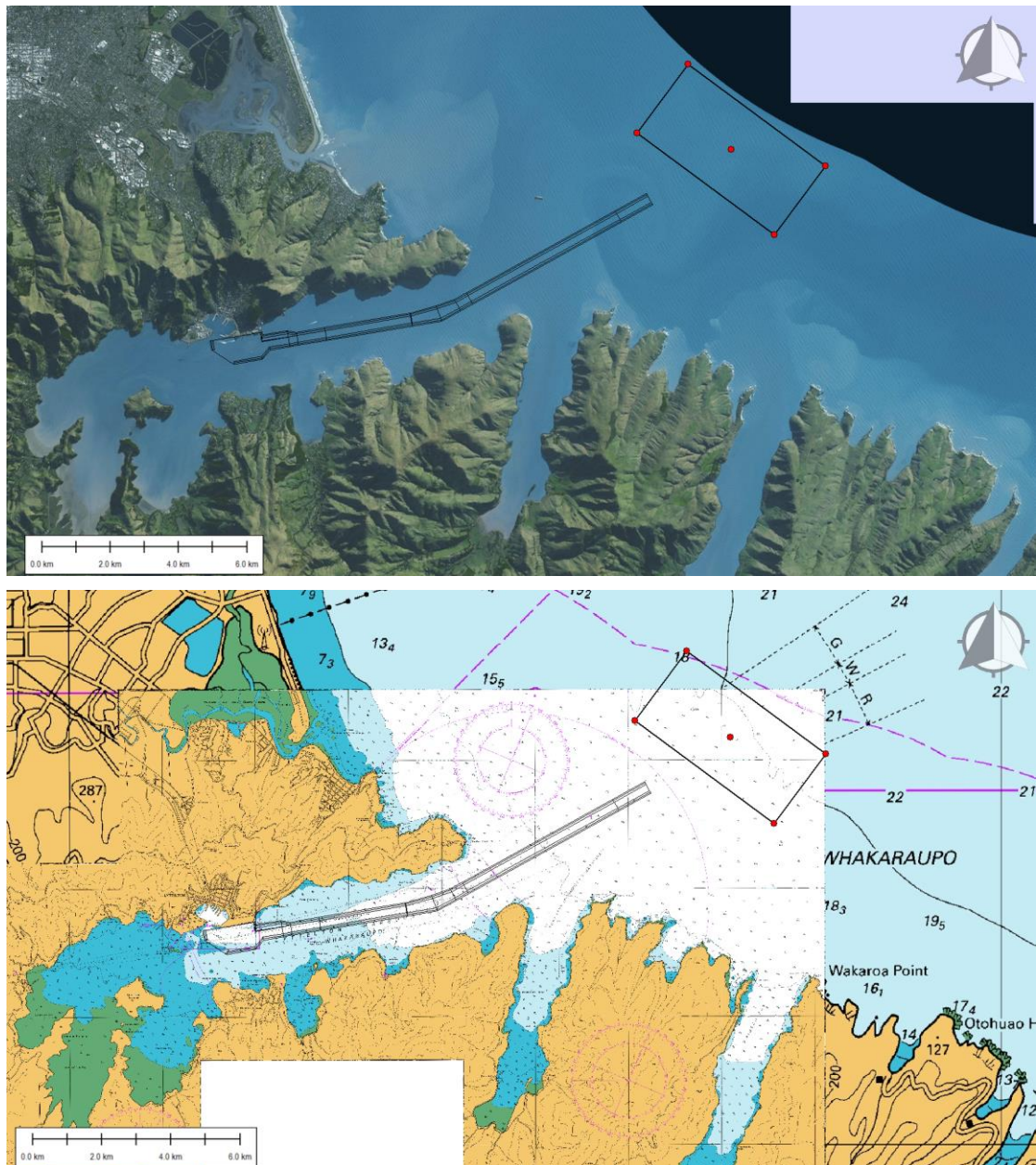


Figure 1.1 Footprints of the new proposed shipping channel and offshore disposal ground.

2. METHODS

2.1. Approach

An actual release of sediment in the oceanic environment is a process that is finite in time (i.e. occurring at a specific time, over a finite period) and inherently non-deterministic (i.e. controlled by a range of random and unpredictable variables such as currents and turbulences). However, unlike the offshore sediment disposal for which a range of forcing may be significant (i.e. wind, wave, residual currents), the present study focuses on dredging activities inside the Harbour where tidal forcing dominates.

The cyclic nature of tides, as well as the ability to confidently predict tidal hydrodynamics, notably with numerical modelling, simplifies the approach to obtain robust estimations of the sediment dispersion patterns. To ensure the expected variability in plume dispersions is captured; simulations are undertaken over two complete spring-neap tidal cycles (~ 28 days) both with and without including the recognised seiche within Lyttelton Harbour/Whakaraupō (Goring and Henry, 1998).

Patterns of the dredging plume dispersion are initially investigated at key tidal stages including peak flows during ebb and flood phases of neap and spring tides. The full spring-neap tidal cycle simulations capture the entire range of hydrodynamic forcing encountered during a cycle; model outputs were combined and further post-processed into probabilistic suspended sediment concentration (SSC) fields which provide valuable guidance on the extents and magnitudes of dredging-related plumes.

2.2. Hydrodynamics

The particle tracking simulations were undertaken using 2D hindcasts of the tidal hydrodynamics, which were simulated using the SELFE model. SELFE is a prognostic finite-element unstructured-grid model designed to simulate 3D baroclinic, 3D barotropic or 2D barotropic circulation. The barotropic mode equations employ a semi-implicit finite-element Eulerian-Lagrangian algorithm to solve the shallow-water equations, forced by relevant physical processes (atmospheric, oceanic and fluvial forcing). A detailed description of the SELFE model formulation, governing equations and numerics can be found in Zhang and Baptista, 2008.

For the purposes of this study, SELFE was run in full 2D barotropic mode and the domain was nested within the MetOcean Solutions New Zealand tidal model which was run using an implementation of POM (Princeton Ocean Model) and has been validated at numerous locations throughout New Zealand. Both tidal surface elevation and current velocities were prescribed along the open hemispheric boundary.

The model domain is shown in Figure 2.1. The finite element mesh was refined in shallow regions and around complex features, with mesh sizes ranging from 20 to 200 m.

In order to bracket the expected plume dispersion through all stages of the proposed dredging, simulations were undertaken using hydrodynamic flows predicted for the existing bathymetry and the bathymetry following dredging (Scenario 2).

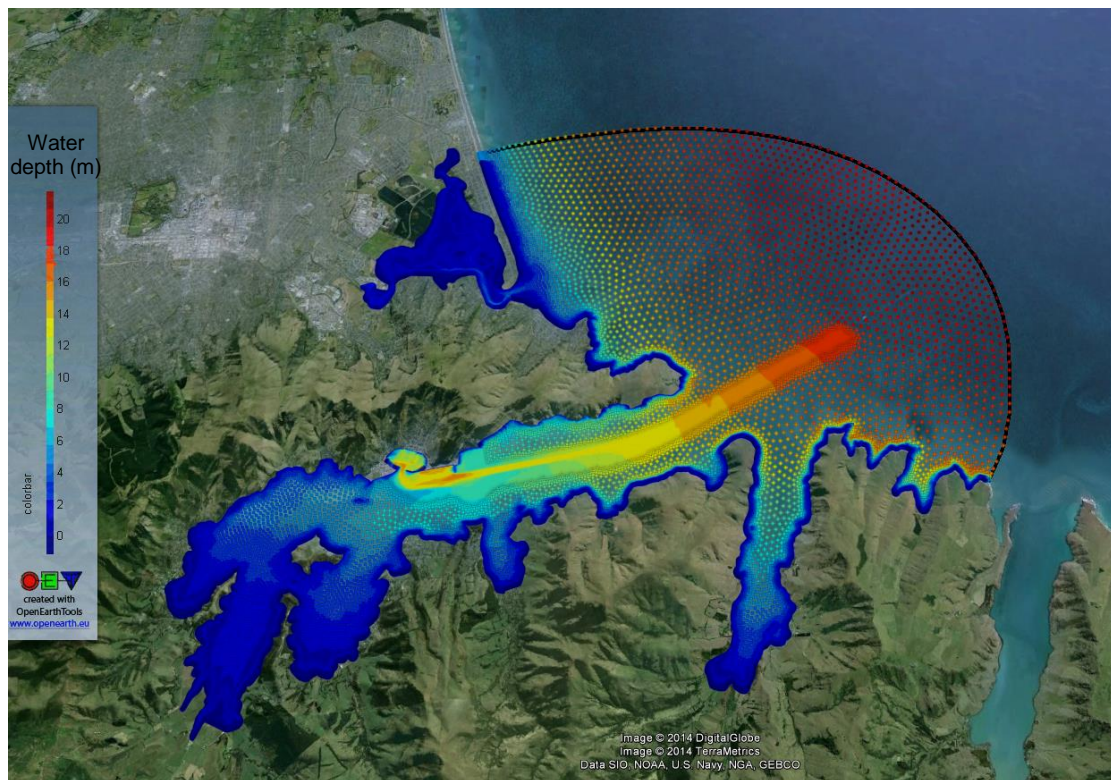


Figure 2.1 SELFE model mesh and bathymetry.

2.3. Trajectory Modelling

A Lagrangian model developed by MSL was used to simulate the trajectories of particles released at the various dredging sites within the channel and turning basin. The model consists of trajectory scheme applied to the existing 2D Eulerian current field (\tilde{u}, \tilde{v}) (see section 2.2), solving for the motion of discrete particles.

$$\begin{aligned}\frac{dx_p}{dt} &= \tilde{u}(x, y, z, t) + u_t \\ \frac{dy_p}{dt} &= \tilde{v}(x, y, z, t) + v_t \\ \frac{dz_p}{dt} &= -w_s + w_g + w_t\end{aligned}\tag{2.1 a,b,c}$$

where (x_p, y_p, z_p) are the particle coordinates, (u_t, v_t, w_t) are the diffusion components representing turbulent motions, w_s is the particle settling velocity and w_g is a vertical velocity component accounting for bathymetric gradients.

In the horizontal plane, the model uses an Ordinary Differential Equations (ODE) solver, including a 4th order Runge-Kutta method, to calculate the trajectory of a given particle (x_p, y_p) in the time-varying derivative field.

Diffusion is treated with the following equation, shown for the u_t component:

$$\int_t^{t+\Delta t} u_t \cdot dt = \sqrt{6 \cdot k_{u,v} \cdot \Delta t} \cdot \theta(-1,1)\tag{2.2}$$

where $\theta(-1,1)$ is a random number from a uniform distribution between -1 and 1, Δt is the time-step of the model in seconds and $k_{u,v}$ is the horizontal eddy diffusivity coefficient in $\text{m}^2 \cdot \text{s}^{-1}$.

In absence of specific field data on diffusive processes, the determination of the diffusion coefficient $k_{u,v}$ is generally based on guidance from empirical relationships. Several relationships are summarized in Fischer et al., 1979 including that of Elder, J.W., 1956 for simple unidirectional shear flows that estimates the longitudinal diffusion coefficient as a function of the water depth and current velocity of the form,

$$k_{u,v} = 5.93 \cdot H \cdot u^*\tag{2.3}$$

where H and u^* are the water depth and friction velocity respectively.

Transverse mixing can be estimated using a relationship of the same form but with reduced proportionality factor (with 50 % error bound).

$$k_{\text{transverse}} \sim 0.6 \cdot H \cdot u^*\tag{2.4}$$

The vertical diffusion is generally expected to be at least one order or magnitude smaller. Elder's formula suggests a vertically averaged value of :

$$k_{\text{vertical}} \sim 0.067 \cdot H \cdot u^*\tag{2.5}$$

Here, both depth and mean current velocities vary along the channel but these equations can still be used to provide a bracketing of reasonable diffusion coefficient values for the present application.

Assuming a generic water depth of 13 metres in the channel and a mean current velocity of 0.1 to 0.2 m².s⁻¹, the above equations yields coefficient of ~[0.3-0.5] m².s⁻¹, [0.03-0.05] m².s⁻¹, and ~[0.003-0.005] m².s⁻¹ for the longitudinal, transverse and vertical diffusivities respectively.

Furthermore, in numerical models, the role of the horizontal diffusion coefficient is also to implicitly account for sub-grid scale turbulent processes such as eddies that are not explicitly resolved in the model due to the limited resolution. This means that horizontal diffusion must generally increase as grid size increases since eddies of increasing scale are unrepresented. On the contrary, the reduction of grid size allows explicit resolution of flow patterns and eddies at finer scales which thereby reduce the required amount of added diffusion.

For dispersion at oceanic scales, (Okubo, A., 1971) notably showed that $k_{u,v}$ varies approximately (with wide scatter) as :

$$k_{u,v} = \alpha.L^{4/3} \quad (2.6)$$

where L is the horizontal scale of the mixing phenomena and α is an empirical proportionality factor.

The hydrodynamic model of Lyttelton Harbour/Whakaraupō was significantly refined in the channel region with resolution of order 20 m. This yields small horizontal diffusivities of order 0.01 m².s⁻¹. This is because the high resolution allows resolving an important fraction of the turbulent processes and therefore requires less added diffusion. Resolution elsewhere in the Harbour is generally less than 100 m which yields diffusion coefficient of order 0.1 m².s⁻¹.

Here, the average of the longitudinal and lateral diffusivities obtained with the Elder formula which yields coefficients of order ~0.1-0.2 m².s⁻¹. Given results provided by the Okubo Equations, a generic diffusion coefficient of 0.1 m².s⁻¹ was eventually selected. Vertical diffusion is not expected to be the dominant process during the descent of the disposed sediment and a small generic value of 0.0001 m².s⁻¹ was used.

The trajectory of particles in the vertical plane is controlled by the particle's settling velocity w_s , the vertical diffusion component w_t as defined in equation 2.1c, and a component w_g related to the bathymetric gradients to ensure that the trajectory of a particle close to the sea-floor is parallel to it (before settling and diffusion components are applied):

$$w_g = \frac{(h-z)}{h} \left(\tilde{u}(x, y, z, t) \times \frac{dh}{dx} + \tilde{v}(x, y, z, t) \times \frac{dh}{dy} \right) \quad (2.7)$$

where z is the particle elevation above the seabed, h is the water-column height at the particles' horizontal location (x,y), (\tilde{u}, \tilde{v}) is the current field

from equation 2.1 and $\left(\frac{dh}{dx}, \frac{dh}{dy} \right)$ are the bathymetry gradients in the x and y directions, respectively.

Note a logarithmic profile was used to extrapolate the 2D depth-averaged current magnitudes to any water column level, with a roughness length of 0.001 m (Smart et al., 2002).

In the present model implementation, any particle reaching the shoreline, the seabed or the outside domain boundaries remained at the position of intersection (*i.e.* 'sticky' boundaries), thus allowing no sediment re-suspension.

2.4. Particle Size Distribution and Settling Velocity

The particle size distribution of the sediment to be dredged and disposed was estimated from sample data from the outer harbour presented in McLaren (2012). The surficial sediment consists of predominant fine material in the clay-silt range (0-63 μm) with a small fraction of fine sand (63 μm < d50 < 256 μm) (see distribution in Figure 2.2).

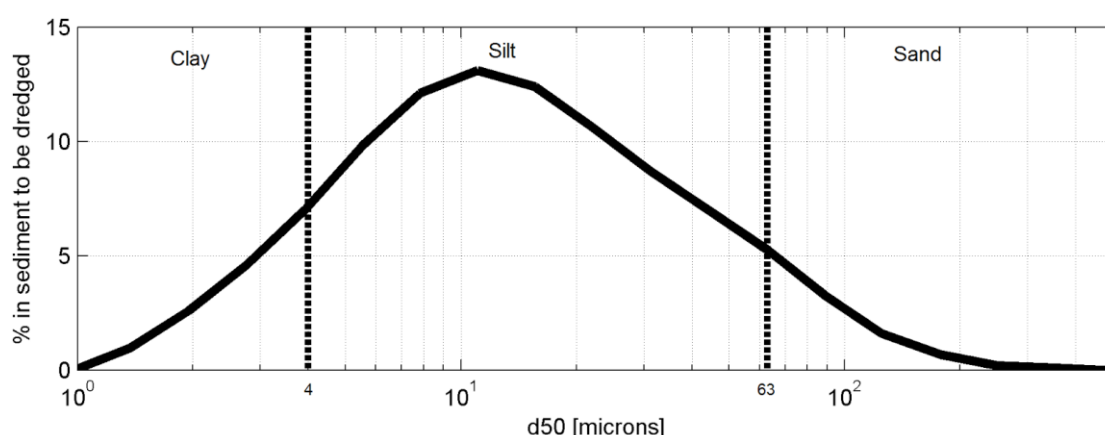


Figure 2.2 Particle size distribution of sediment to be dredged in the Lyttelton Harbour/Whakaraupō. The vertical dashed lines indicate the clay, silt, and sand size ranges.

For the simulations, the continuous sediment distribution was split into 4 discrete classes, each with a representative median grain size and dry sediment densities.

Although general equations are available to compute the settling velocity of individual particles of given sizes (e.g. Stokes Law), it is unrealistic to assume that the sediment consists in single particles in the fine silt range (~40 μm or smaller) because of the cohesive nature of material and associated flocculation effects (e.g. Van Rijn, 2007).

In the present application sediment smaller than 44 μm are assumed to belong to a single sediment class. In the absence of in-situ measurements on the settling of such flocculated cohesive sediment at the site, a generic settling rate of 1 mm.s^{-1} was used, which is appropriate for such flocculated particles (Whitehouse et al, 2000), and commonly used in the context of sediment disposal (e.g. Smith and Friedrichs, 2011) to represent the finest sediment grain size fraction. The remaining sediment distribution was split into three additional classes with similar proportions, each with a representative median grain size computed as a weighted average from the continuous distribution. For these classes, particle settling velocities were computed using the standard equation of Van Rijn, (1984) for non-cohesive sediment. Dry densities for the silt and sand material were set to 300 kg.m^{-3} .

and 1600 kg.m⁻³, respectively (Spearman, pers. comm.). The characteristics of the 4 representative classes and relative proportion of the total volumes are summarized in Table 2.1

Table 2.1 Representative median grain sizes, settling velocities, and proportions of total volume released for the 4 discrete sediment classes considered.

	Representative d50 [microns]	Settling velocity [m/s]	Percentage of total volume [%]
Class 1	Smaller than 44	0.0010	81.8
Class 2	44.0	0.0014	7.0
Class 3	62.5	0.0028	5.3
Class 4	118.0	0.0085	5.9

Appropriate simulation time steps were chosen to correctly capture the horizontal trajectories due to the ambient tidal and residual flows. Time steps were also adjusted according to the particle settling velocities to ensure sufficient resolution of the vertical settling, and ranged from 60 to 600 seconds. The total number of particles released per time-step varied for each of the different size classes according to the different settling rates. This ensured a sufficient number of particles remained in suspension, taking into account the diffusion processes and allowing statistically representative concentrations to be derived. For example, a larger number of coarse silt particles were released per discharge event compared to the fine silts since a greater proportion of the coarse silt would settle over a given time period due to the higher settling velocities. Each sediment fraction is simulated separately and all results are combined afterwards to produce total suspended sediment concentration (SSC) fields.

2.5. Disposal scenarios

The effects of the varying hydrodynamic forcing throughout the Harbour on the dredging plumes patterns was assessed by simulating sediment releases at 12 representative locations along the channel (Figure 2.3, Table 2.2).

These simulations were reproduced for the existing hydrodynamics and the completed Scenario 2 scenarios, representative of the bathymetry expected at the completion of the dredging program.

Besides tides, Lyttelton Harbour/Whakaraupō can be subject to seicheing with periods of order 3-4 hours that are present in the Pegasus Bay (see Goring and Henry, 1998). The effect of this forcing on plume dispersion patterns was also investigated by including a generic forcing signal in both the existing and Scenario 2 hydrodynamics.

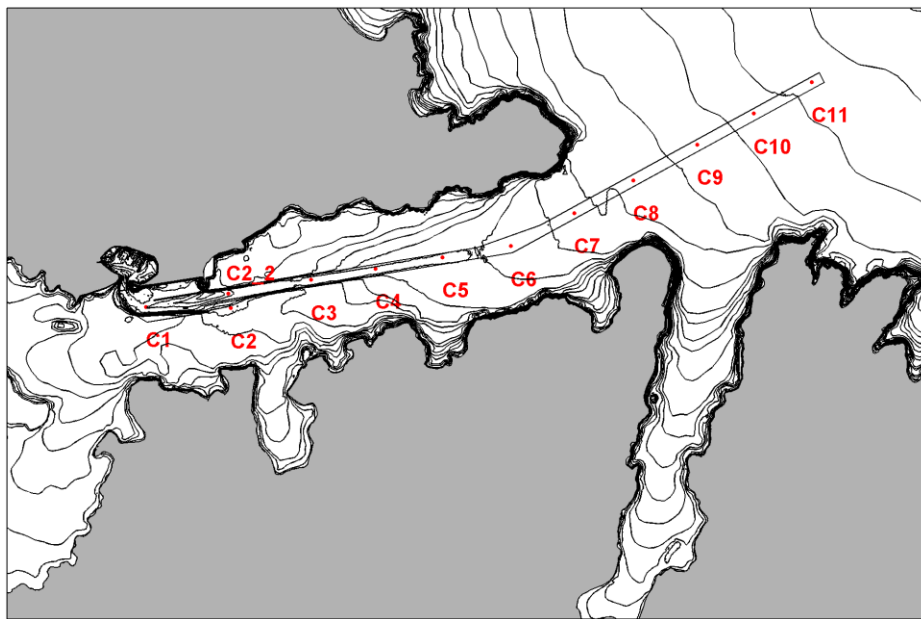


Figure 2.3 Simulated release sites along the proposed channel (see Table 2.2 for actual positions).

Table 2.2 Coordinates and depths of release sites along the channel.

	Longitude	Latitude	Depth[m]
C1	172.7211	-43.6131	13.7
C2	172.7388	-43.6133	9.3
C2_2	172.7383	-43.6111	14.5
C3	172.7555	-43.609	13.6
C4	172.769	-43.6073	13.2
C5	172.7829	-43.6056	13.2
C6	172.7972	-43.6039	13.3
C7	172.8104	-43.5989	14.6
C8	172.8227	-43.5939	15.4
C9	172.8361	-43.5885	16.4
C10	172.8478	-43.5838	17.4
C11	172.8599	-43.579	18.4

The processes by which sediment is released and suspended in the water column during dredging operations are briefly outlined in the context of the choice of the source term magnitudes and release depths for the particle tracking simulations undertaken in this study.

The dredging method likely to be used in the present case involves the use of large Trailing Suction Hopper Dredger (TSHD). These vessels operate following two modes, i.e. dredging and overflow modes.

During the dredging phase, sediment is sucked into the hopper using a drag head; a fraction of the sediment disturbed by the drag head is not pumped into the hopper and remains suspended in the water column. Sediment suspension is also expected due to the action of propeller wash (Source 1 and 3 respectively in Figure 2.4). These two sources of sediment suspension form a passive plume that is expected to be contained in the bottom part of the water column. In the present study the following release depths have been used:

- Drag head source: bottom 2 meters of water column.
- Propeller wash source: bottom 4 m of the water column.

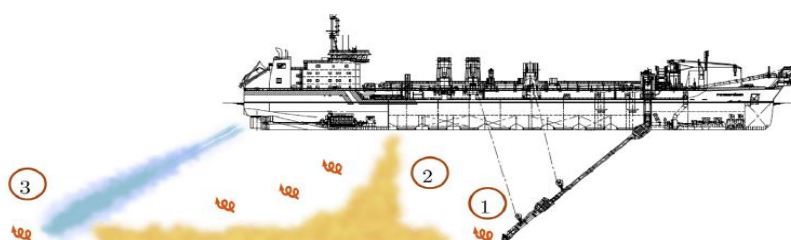


Figure 2.4 Sources of a dredge plume for a Trailing Suction Hopper Dredger: 1- Drag Head, 2-Overflow, 3-Propeller wash (after Becker J. et al., 2015).

Release rates of 25 kg.s^{-1} were used for both the Drag head and propeller wash source terms following recommendations by Spearman (pers. comm.). This initial “dredging phase” will continue until the hopper is full and is expected to last up to 25 minutes in the present application.

After the initial hopper infilling, the actual content of the hopper is a sediment/water mixture which is expected to contain ~20 % solids by volume (Spearman, J. et al., 2007). To maximize the amount of sediment in the hopper, it can be decided to continue to pump sediment and water from the seabed; this will result in the hopper “overflowing” and thereby releasing some sediment in the water column. This phase will be referred to as “overflow phase”, and is shown as the source “2” in Figure 2.4.

The typical overflow sediment loading is significant, typically of order $1400\text{-}2000 \text{ kg.s}^{-1}$ (Spearman pers. comm.) and can create evident sediment plumes.

The overflow load consists of a highly concentrated mixture of sediment and water and the bulk behavior of that sediment mixture becomes dominant over the individual particle settling processes (Winterwerp, J.C., 2002). As a result, it is expected that the overflow release will be followed by a dynamic

plume phase where the sediment mixture descends to bottom as a jet-like feature, and impacts the seabed, suspending sediment and forming an initial density driven near-field plume.

A fraction of the sediment load will also be de-entrained from the dynamic plume during descent and become suspended in the water column. As illustrated in Figure 2.5, this is comparable to processes involved during the offshore disposal, i.e.:

1. Convective descent,
2. Dynamic Collapse, and
3. Passive dispersion

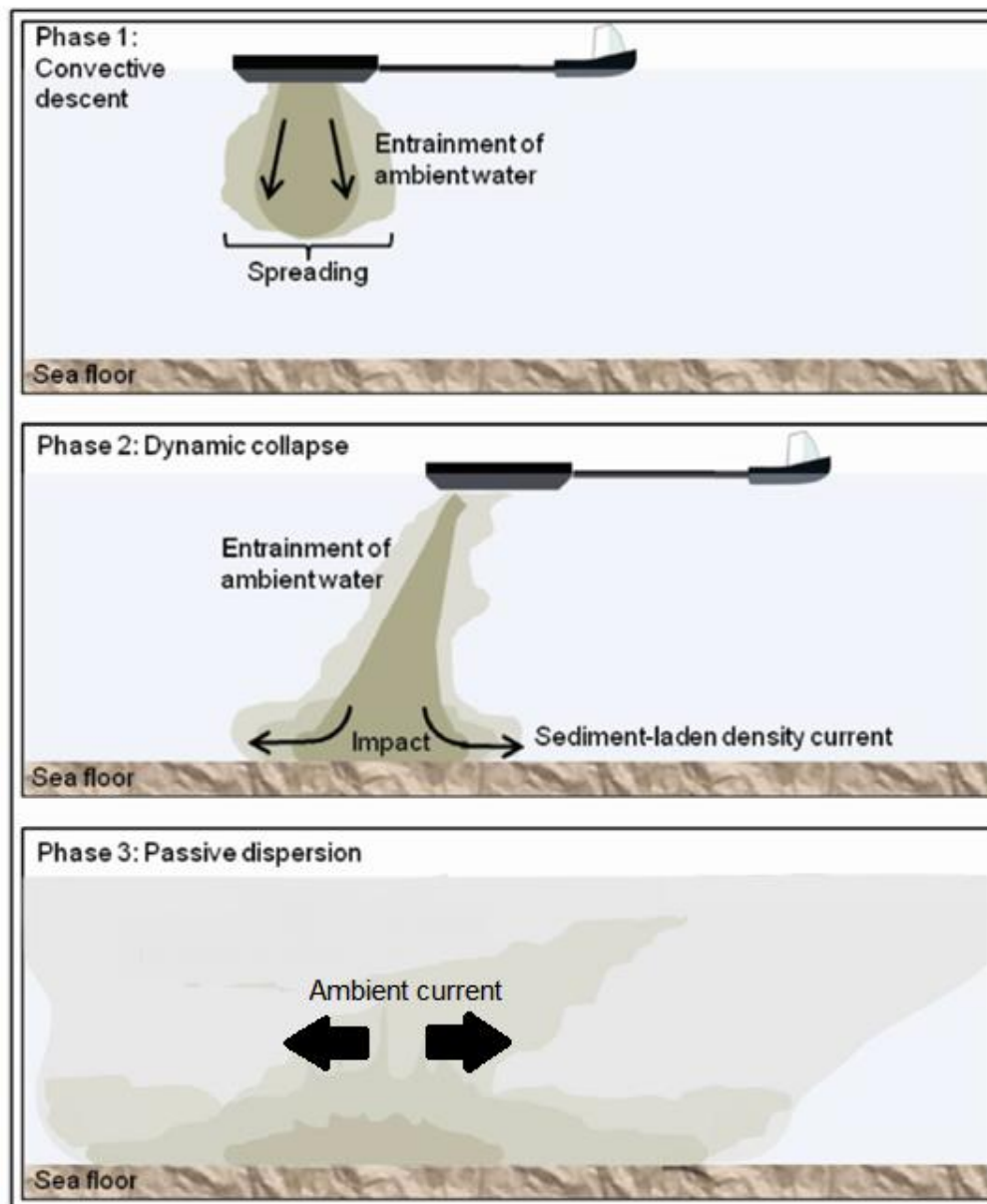


Figure 2.5 Three main phases occurring during the disposal of dredged material: 1) Convective descent, 2) Dynamic Collapse, and 3) Passive plume dispersion.

The general length scales expected for the overflow process are an order of magnitude smaller than the discharge of sediment at the offshore disposal ground. Additionally, the overflow sediment mixture is less concentrated than in a offshore sediment disposal context.

In the present study, this overflow phase was modelled considering two sources of sediment to the passive plume:

- Suspension of sediment de-entrained from the dynamic plume descent uniform release within the entire water column, and
- Passive plume generated following the dynamic plume impact: release within a cylinder of 2 m height and 60 m radius on the seabed.

The release rate of the initial total raw overflow was taken as 1600 kg.s^{-1} (Spearman pers. comm.).

The processes governing the proportions of the total overflow load that is effectively transferred to the passive plume are complex and generally not well described (EcoShape, 2010).

In the absence of *in-situ* measurement, appropriate values were estimated from the available literature. The typical fraction transferred in the water column is generally expected to be in the order of 20 % (e.g. Becker et al., 2015). Fields measurement in water depths greater than 20 m suggest that fraction may go down to ~ 5-15 % (HR Wallingford, 2010), which is the default range used in the TASS model (EcoShape, 2010). However, field measurement and modelling undertaken in depths of 10-18 m suggest that the proportion can be larger (up to ~50 %) in shallower depths (HR Wallingford, 2012).

In the present application, a fraction of 25% was considered for the sediment source term released within the entire column (i.e. sediment suspension due to dynamic plume descent). A similar proportion of 25% was used for the amount of the overflow load found in the bottom source release, i.e. resulting from the density current following the dynamic plume impact (see Figure 2.6).

The impact of that overflow phase was tested considering overflow period times of 10, 20, and 30 minutes.

Finally, when dredging stops between loads the suction pipes are pumped clean to prevent settling of the dredged material during the hoisting of the pipes causing extra load for the winches and to prepare the dredge for transit to the disposal site. This can result in a very limited localised near bed plume that is not expected to be significant compared with the other plume sources.

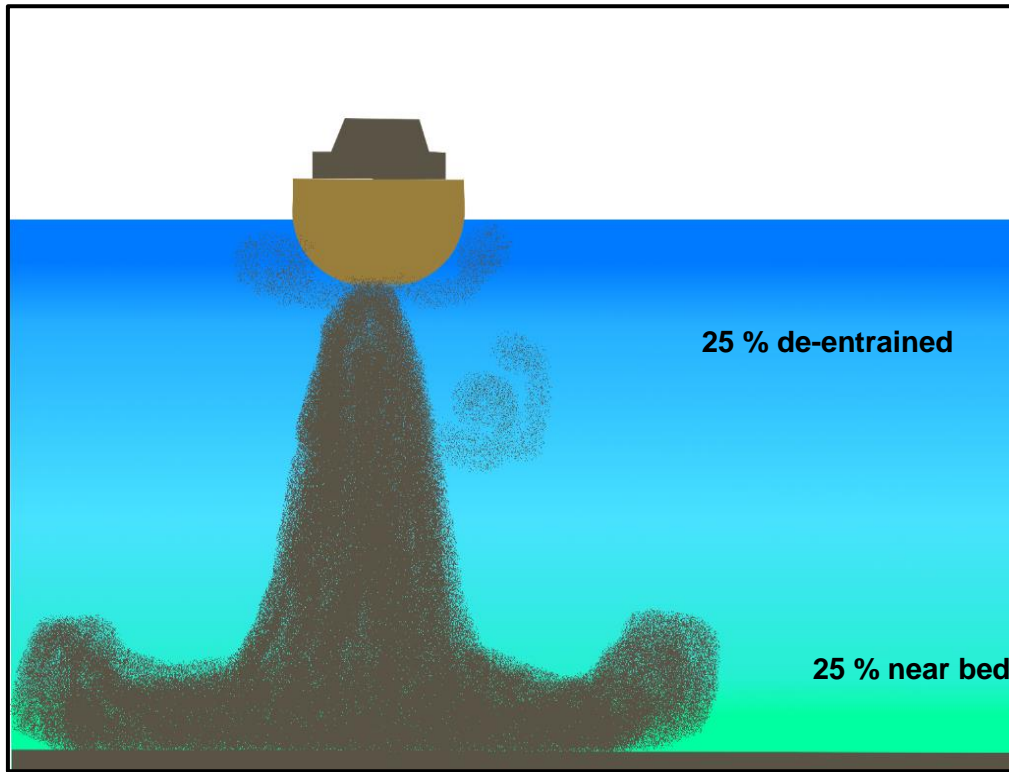


Figure 2.6 Percentages of sediment transferred from the near-field density driven plume to the far-field plume during overflowing

2.6. Post-Processing

The results of the 28-day particle tracking simulations were post-processed to produce maps of the instantaneous and probabilistic suspended sediment concentrations fields. The general methods employed to reconstruct concentration fields from the particle tracking model outputs are outlined below.

2.6.1. Concentration and depositional thickness computation

To reconstruct concentrations from the particle tracking simulations at chosen receptors, a kernel method with variable bandwidth was used. The use of a variable bandwidth (kernel size) attempts to represent true variability of spatial concentration, while minimizing statistical variability that inevitably occurs away from the source due to a necessarily finite number of particles. A small kernel is used in regions gathering a high number of particles, where it is statistically appropriate to infer relatively small scale changes in concentration. Conversely, a larger kernel is used in regions presenting a low number of particles, so as to prevent unrealistically high concentrations around the precise (but partially random) locations of a few isolated particles.

In practice, the concentration C at a given receptor location (x,y) is computed as:

$$C(x, y) = \sum_{i=1}^n \frac{m_i}{\lambda_x(x, y)\lambda_y(x, y)} K\left(\left|\frac{x_i - x}{\lambda_x}\right|\right) K\left(\left|\frac{y_i - y}{\lambda_y}\right|\right) \quad (2.8)$$

where (x_i, y_i) is the location of each particle i , n is the total number of particles, m_i is the loading for each particle, λ_x and λ_y are the kernel bandwidth in the x and y directions for location (x, y) and K is the kernel function.

Following Vitali et al. (2006), an Epanechnikov kernel function was used:

$$K(q) = \begin{cases} 0.75(1 - q^2), & |q| \leq 1 \\ 0, & |q| > 1 \end{cases} \quad (2.9)$$

where q is the ratio of the particle distance from receptor to bandwidth ($q_x = d_x / \lambda_x$, or $q_y = d_y / \lambda_y$).

A receptor-based method derived from the RL3 method in Vitali et al. (2006) was used to define the bandwidths λ_x and λ_y .

For each receptor location, a neighbourhood was defined as the region enclosing the 1/20th closest particles. Then, for each direction x and y , the bandwidths λ_x and λ_y were defined as the minimum value between the maximum projected distance of the particles within the neighbourhood and twice the standard deviation of the projected distances within the neighbourhood. Finally, in order to prevent unrealistically elongated kernels, the aspect ratio λ_x / λ_y was limited to be no greater than 5:1, with the smaller value increased.

The loading of each particle m_i directly depends on the quantity being modeled. Here, each discrete particle was attributed a certain sediment mass which was determined as the ratio from the total true sediment volume of a given class released per step, to the total number of particles of that class introduced in the model at each release.

2.6.2. Application to the present study

In the present study, these methods were applied to compute snapshots of SSC plumes during peak tidal flows as well as probabilistic SSC fields over a complete spring-neap tidal cycle (~28 days).

These results are based on the sediment concentration fields computed following the methods presented above on the suspended particle clouds of each sediment class. These were then combined to produce total “true” SSC magnitudes. The receptor grid used for the SSC computations is provided in Figure 2.7, and is refined within the channel region.

The particle load m_i governs the concentration magnitudes, and directly depends on the amount of sediment released in the environment as well as the actual number of particles released in the model (see Eqn. 2.8).

The predicted suspended sediment concentrations should be interpreted as dredging-related SSC only, and would add to any ambient SSC from other sources, such as river inputs or catchment run-offs.

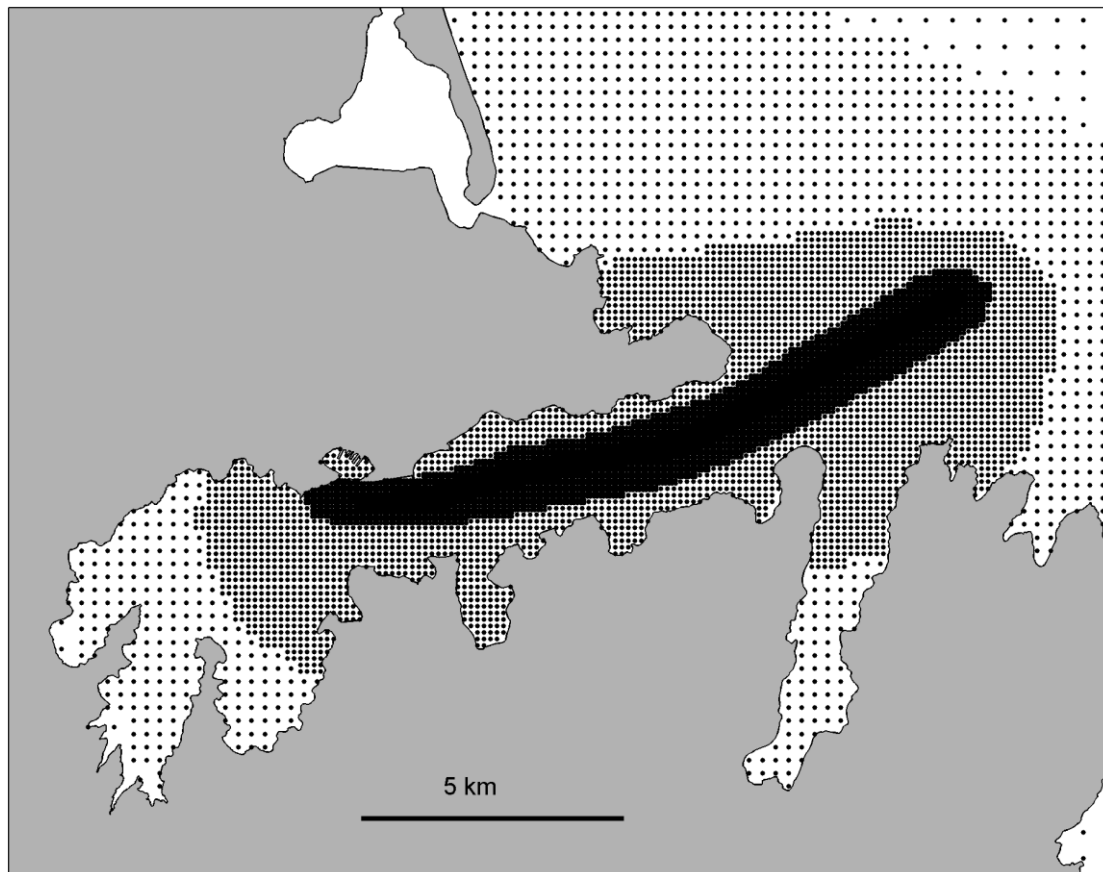


Figure 2.7 Receptor grid for the SSC plumes. The resolution ranges from 30 m in the channel to ~500 m offshore.

3. RESULTS

This section presents the results of the various particle-tracking simulations undertaken for the present study.

- The hydrodynamic fields used to drive the particle-tracking simulations are presented and variations between the existing and Scenario 2 scenarios are described in the first section (3.1).
- The dispersion characteristics of the suspended sediment concentration (SSC) plumes resulting from the dredging activities are investigated using snapshots of SSC fields developing at key tidal stages in the second section (3.2).
- Probabilistic SSC plumes derived from the 28-day simulations (spring-neap tidal cycle) are included in the third section (3.3).

Exceedence time associated with relevant SSC thresholds are estimated based on the expected dredging work cycle in a final section (3.4).

In all cases, SSC fields are shown at three levels in the water column, namely surface, mid-water, and bottom. Each of the fields are computed considering a 4-m thick layer of the water column and presented SSC should be interpreted as mean SSC levels within these layers.

Given the large number of runs (i.e. 12 sites, 4 hydrodynamic forcing scenarios, two dredging modes), results are presented for the sites C1, C5 and C11 to capture the key variations throughout the channel. Additional results are provided in Appendix 1 when relevant.

3.1. Existing and post-dredging hydrodynamics

The projected bathymetric changes resulting from channel deepening and reclamation are shown in Figure 3.1

The key changes of the tidal hydrodynamics between the existing and Scenario 2, representative of the bathymetry expected at the completion of the dredging program, are illustrated in Figure 3.2 to Figure 3.5 comparing tidal flow fields during peak flows of spring and neap tide phases. These hydrodynamics allow bracketing of the likely plume extents during the proposed dredging program.

The significant deepening of the area just off the Port entrance (i.e. start of channel) results in a clear reduction of the tidal current magnitude for the Scenario 2 scenario. The reclaimed area west of Gollans Bay obstructs the existing flows and forces a slightly different flow bifurcation pattern in the reclamations vicinity. Differences are less evident moving further east along the channel. Tidal flows are slightly more focused within the deeper channel in the Scenario 2 bathymetry and relatively weaker elsewhere, notably on the spring tide snapshots.

Compass rose plots of the tidal flows at the study sites along the shipping channel (see Figure 2.3) over a complete spring-neap cycle are provided in Figure 3.6 and Figure 3.7 for both the existing and Scenario 2 scenarios.

The reduction of tidal current magnitudes throughout the deeper region off the Port entrance is clearly seen at site C1. The reclaimed area results in a modification of the tidal flow axis in the vicinity of the reclamation that is apparent at sites C2 and C2_2.

Current magnitudes are generally similar but there is a reduction of the tidal flow asymmetry at site C2_2. Tidal roses are generally very similar for both existing and Scenario 2 cases further east along the channel (sites C3 to C11). There is a strong bi-directionality in tidal flows at sites C1 to C8 which progressively transitions to tidal flow roses that are more homogenous direction-wise at sites C9 to C11, with smaller current magnitudes (Figure 3.6 and Figure 3.7).

In addition to the tidal forcing, Goring and Henry (1998) found that Pegasus Bay can be subject to sea-level fluctuations with periods of order 3-4 hours, which can then propagate into the Lyttelton Harbour/Whakaraupō as a seiche; with resultant water level and velocity fluctuations (of the order 0.1 m.s-1)

The effect of the potential forcing from the seiche super-imposed over the pure tidal signal is investigated by introducing an additional sea level fluctuation in the hydrodynamic simulations and reproducing the particle-tracking simulations for the combined tidal and seiche signal. The magnitude of the simulated seiche oscillation at the model boundaries was calibrated to match the mean 3-4 h band-pass filtered measured ADCP data available within the Bay.

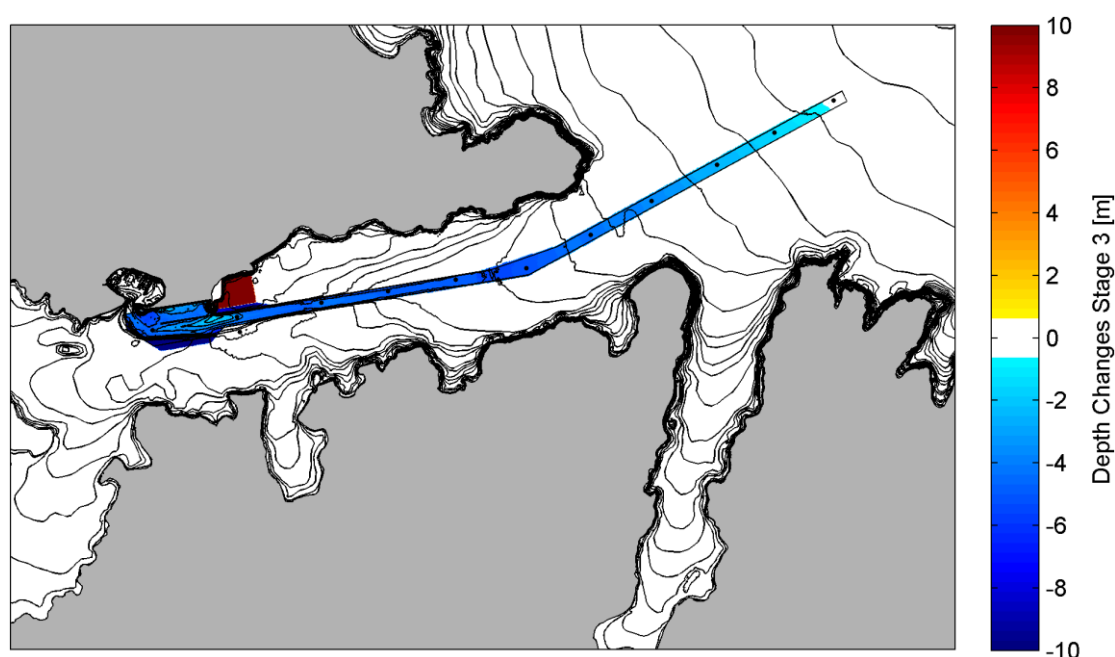


Figure 3.1 Bathymetric changes associated with the Scenario 2 scenario including an extended and deeper channel and reclaimed land east of Gollans Bay. Negative depth changes indicate a deepening relative to the existing bathymetry.

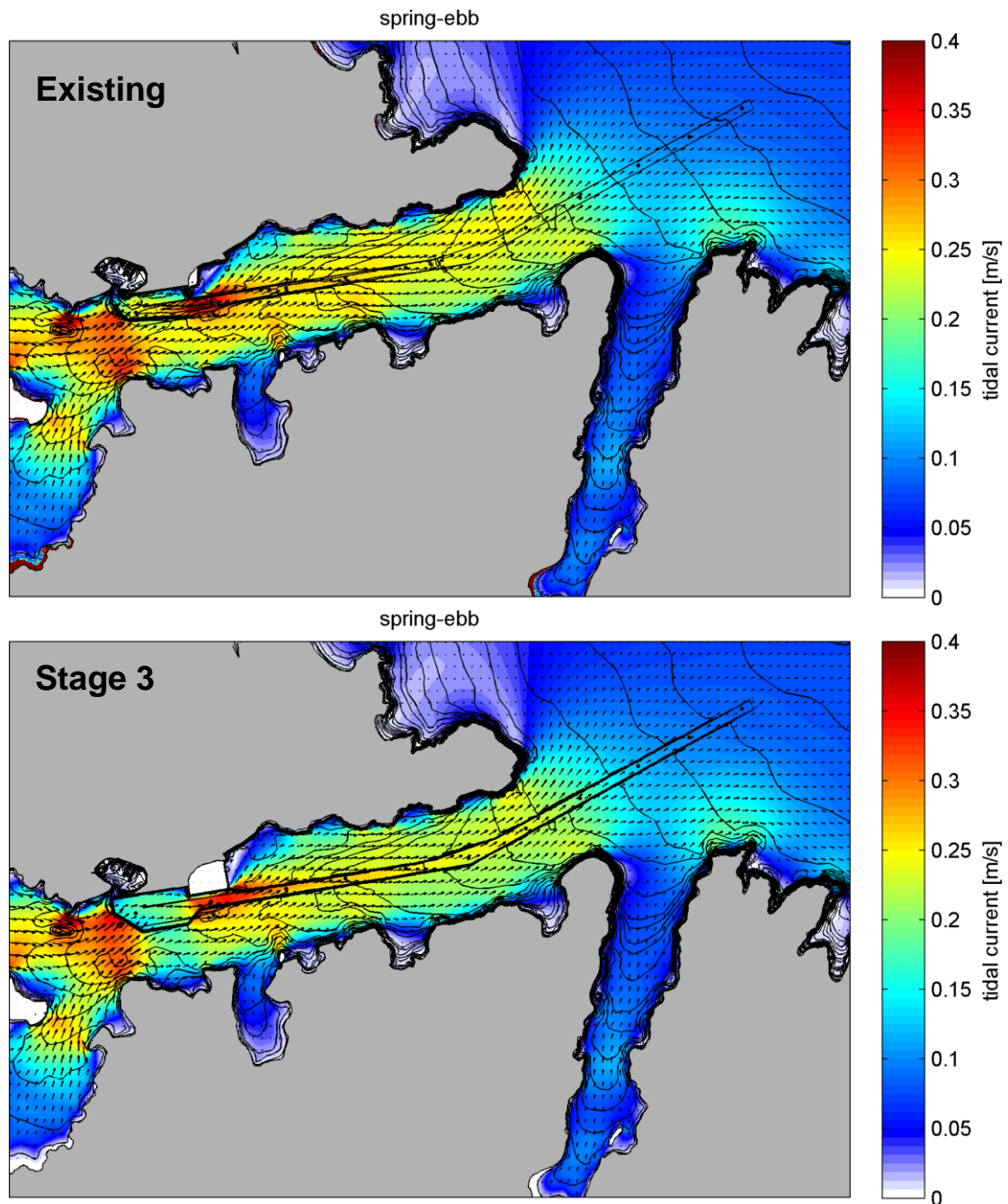


Figure 3.2 Snapshots of peak ebb flows during spring tides over the existing and Scenario 2 bathymetries, representative of the bathymetry expected at the completion of the dredging program. The proposed channel polygon is show in black.

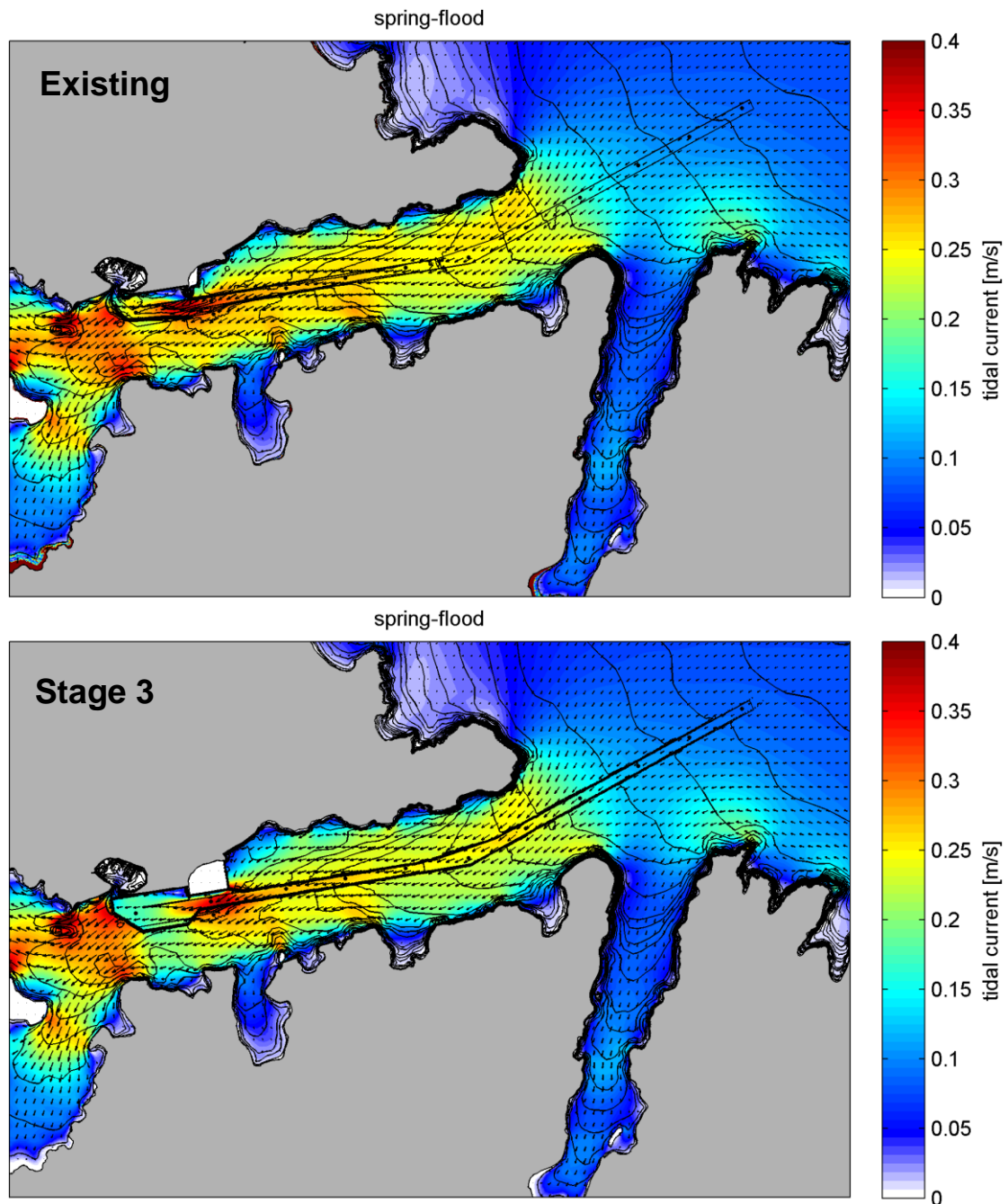


Figure 3.3 Snapshots of peak flood flows during spring tides over the existing and Scenario 2 bathymetries, representative of the bathymetry expected at the completion of the dredging program. The proposed channel polygon is show in black.

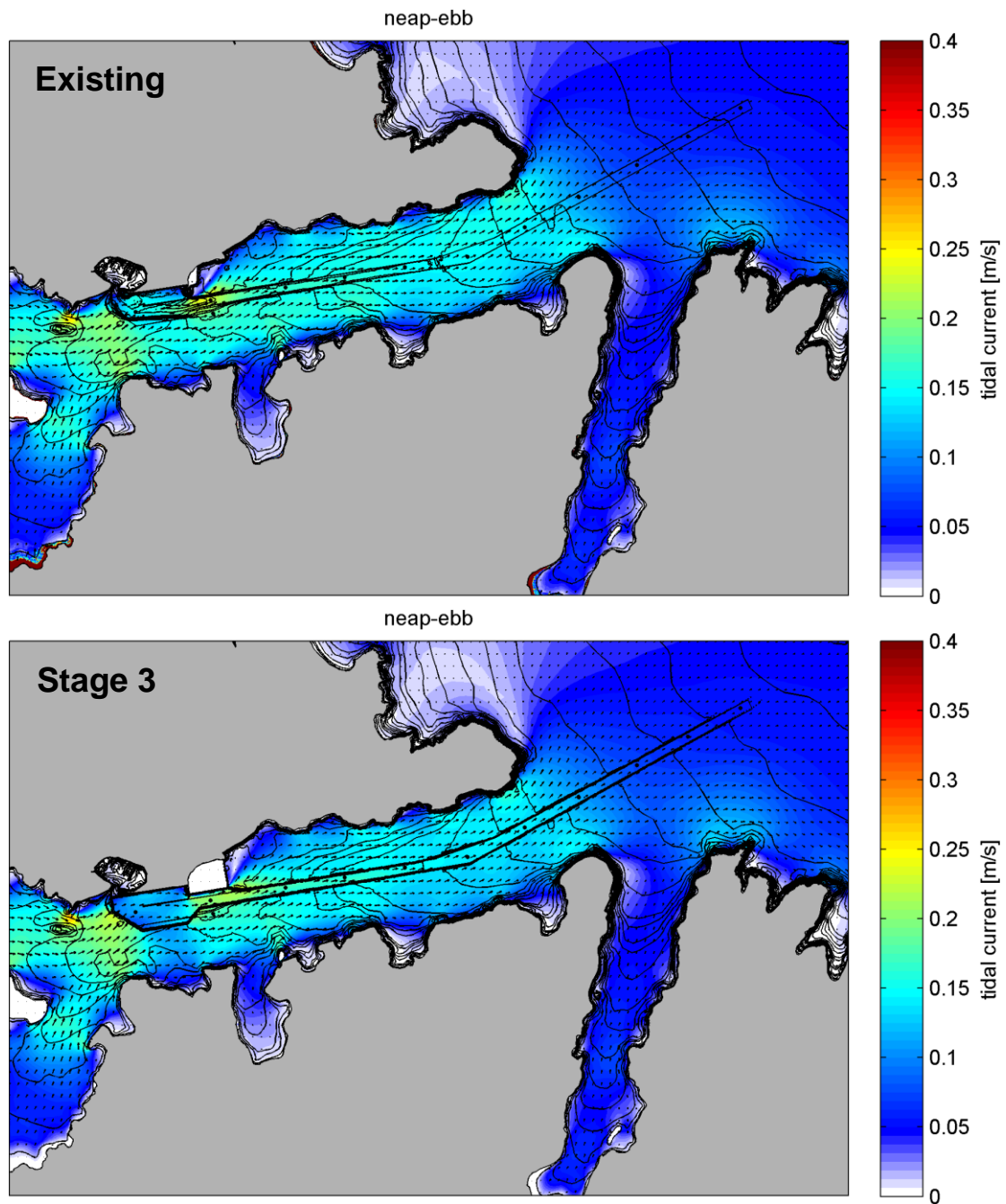


Figure 3.4 Snapshots of peak ebb flows during neap tides over the existing and Scenario 2 bathymetries, representative of the bathymetry expected at the completion of the dredging program. The proposed channel polygon is show in black.

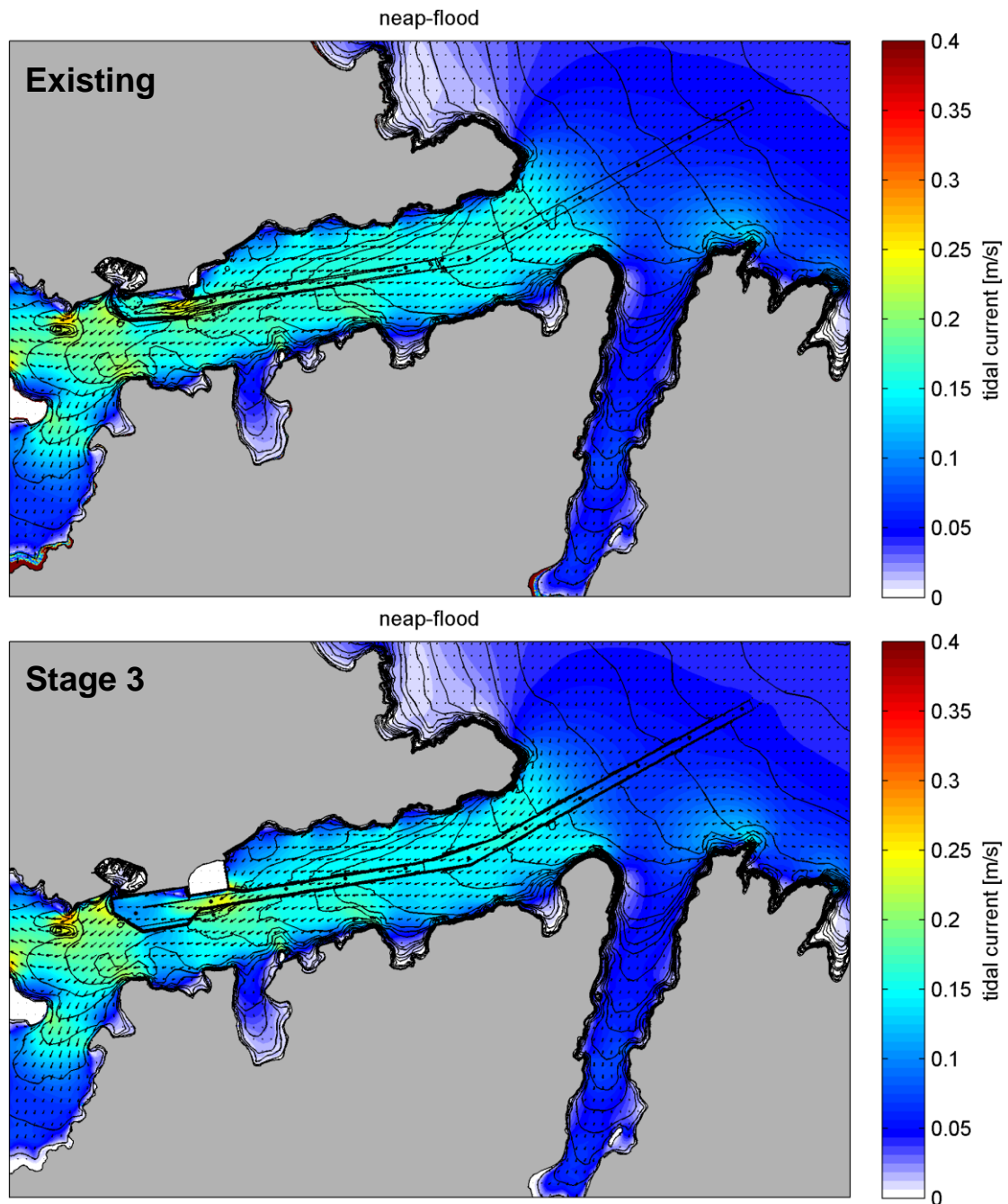


Figure 3.5 Snapshots of peak flood flows during neap tides over the existing and Scenario 2 bathymetries, representative of the bathymetry expected at the completion of the dredging program. The proposed channel polygon is show in black.

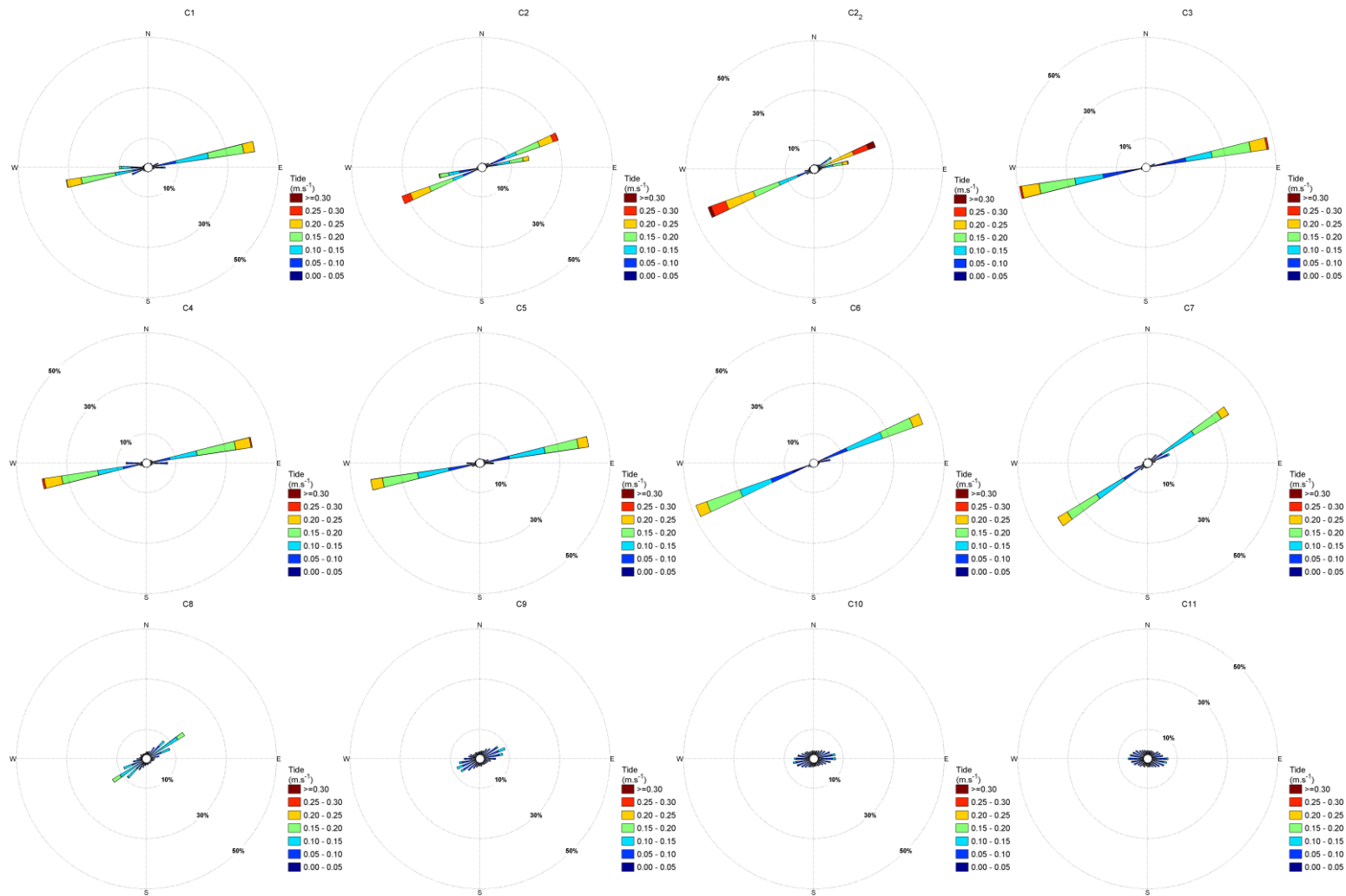


Figure 3.6 Rose of existing tidal currents at study sites C1 to C11 (see Figure 2.3 for site position).

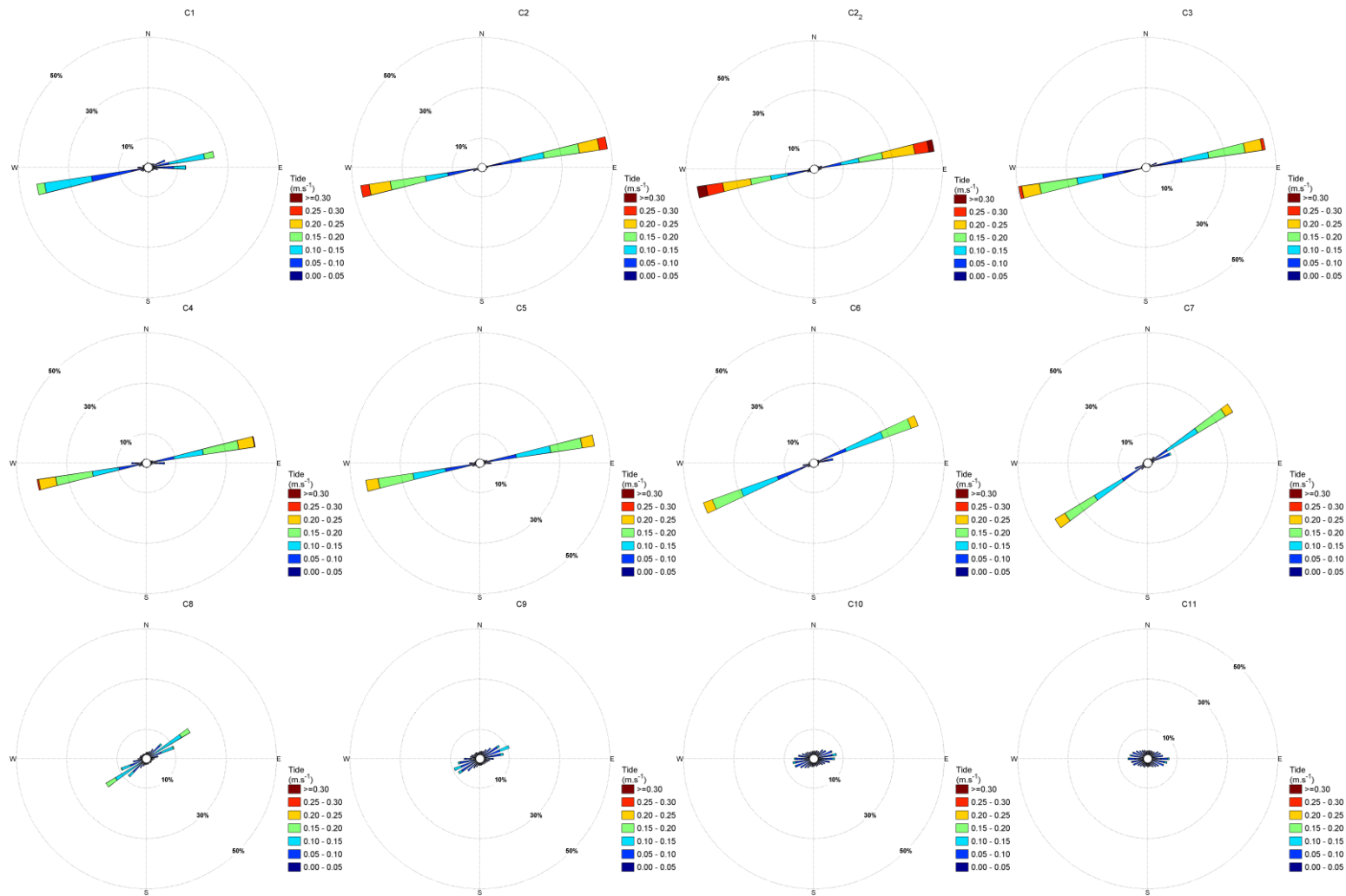


Figure 3.7 Rose of tidal currents for the Scenario 2 bathymetry at study sites C1 to C11 (see Figure 2.3 for site position).

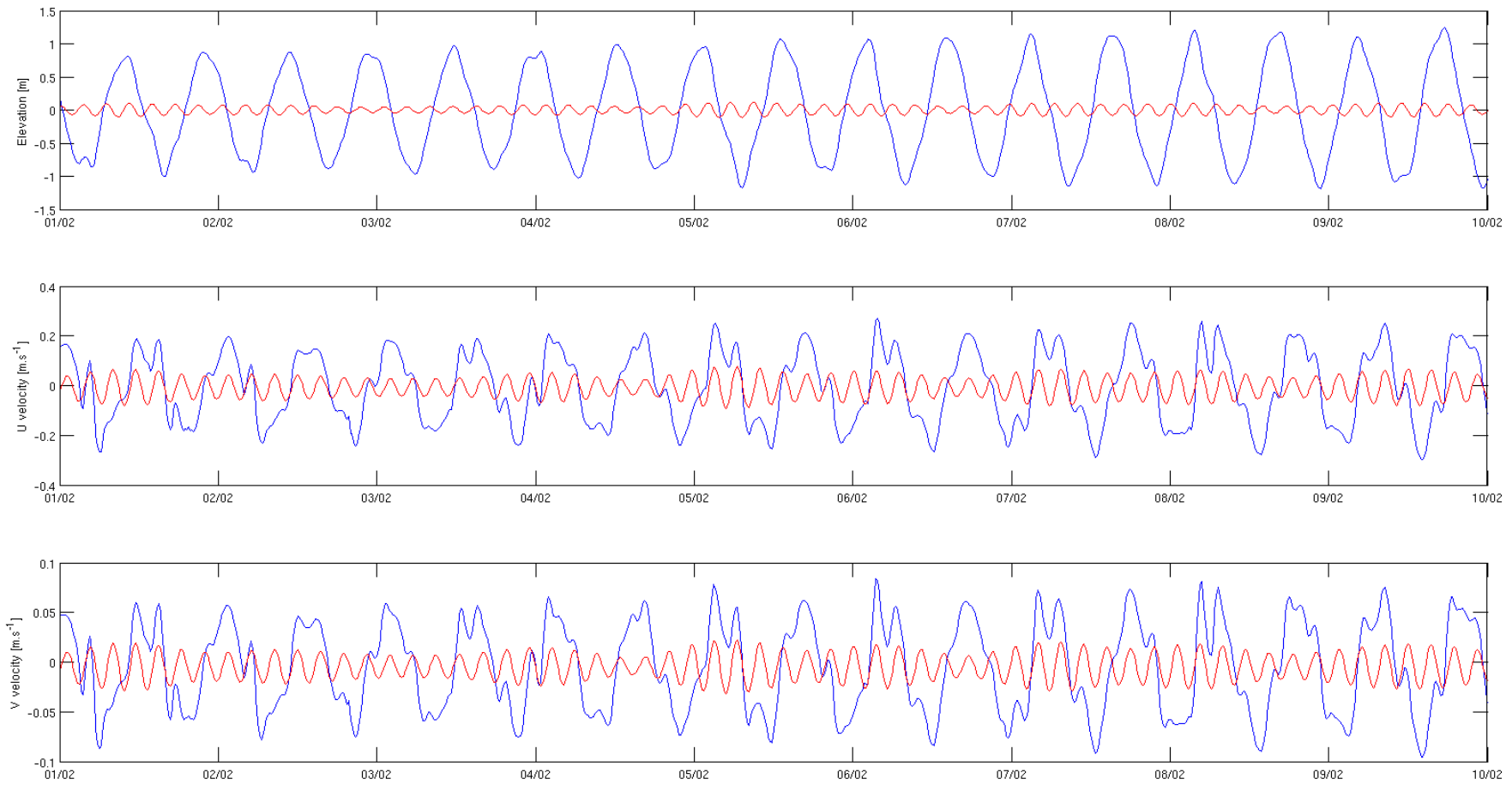


Figure 3.8 Seiche signal super-imposed over tidal signal. The blue line represents the combined tidal and seiche signal, while the red line represents the seiche component only.

3.2. Dredging plumes during peak tidal flows

3.2.1. Dredging and overflow modes

Snapshot of SSC dredging plumes at sites C1, C5 and C11 during peak neap and spring tidal flows for both the dredging (i.e. infilling of hopper by the drag head) and 10-minute overflow (release of water sediment mixture to maximize hopper load) phases are given in Figure 3.9 to Figure 3.12.

General plume dispersion patterns follow the ambient hydrodynamic forcing. SSC plumes have relatively larger excursion during spring tides but are also relatively more diluted, with comparatively smaller SSC levels in the vicinity of the release site (see Figure 3.9 to Figure 3.12).

Results show limited development of SSC plumes while in dredging only mode (see Figure 3.9 to Figure 3.12). In this operating mode sediment is entrained by a drag head, with some additional suspension resulting from the propeller disturbance. SSC plumes are essentially contained within the bottom layer of the water column.

In contrast, while in overflow mode, a highly concentrated (~1600 kg.s⁻¹) mixture of water and sediment is released directly from the hopper which generates elevated SSC plumes within the entire water column (see Figure 3.9 to Figure 3.12).

3.2.1. Existing, Scenario 2 and seiche hydrodynamics

The modulation of the SSC plumes associated with the modification of the hydrodynamic regime due to channel deepening (i.e. Scenario 2) or due to the presence of the inclusion of seiche velocities are illustrated in Figure 3.13 to Figure 3.15 for sites C1, C5, and C11 respectively.

Results are shown only for overflow mode (10 minute overflow period), for which SSC are most significant at peak flood flows during spring tides. Additional figures are presented in Appendix 1 for the dredging mode only and other tidal stages.

General dispersion patterns are consistent between the existing and Scenario 2 scenarios. The most evident variations are seen at site C1 (Figure 3.13 - top) where SSC plumes have slightly reduced excursions for the Scenario 2 hydrodynamics, consistent with the tidal flow change (see Figure 3.6 and Figure 3.7). The reduced excursions result in relatively higher SSC within the plume.

Inclusion of sea level fluctuation or “seiche” generally results in a slightly more compact SSC plume at site C1, and a relatively higher SSC within the plume (Figure 3.13).

At site C5, the inclusion of the seiche acts to concentrate the plume, resulting in an extended area with higher concentrations (Figure 3.14).

Modulations of the predicted SSC plumes with respect to the deepened channel of the Scenario 2 scenario, or inclusion of a seiche velocities are generally very limited at site C11.

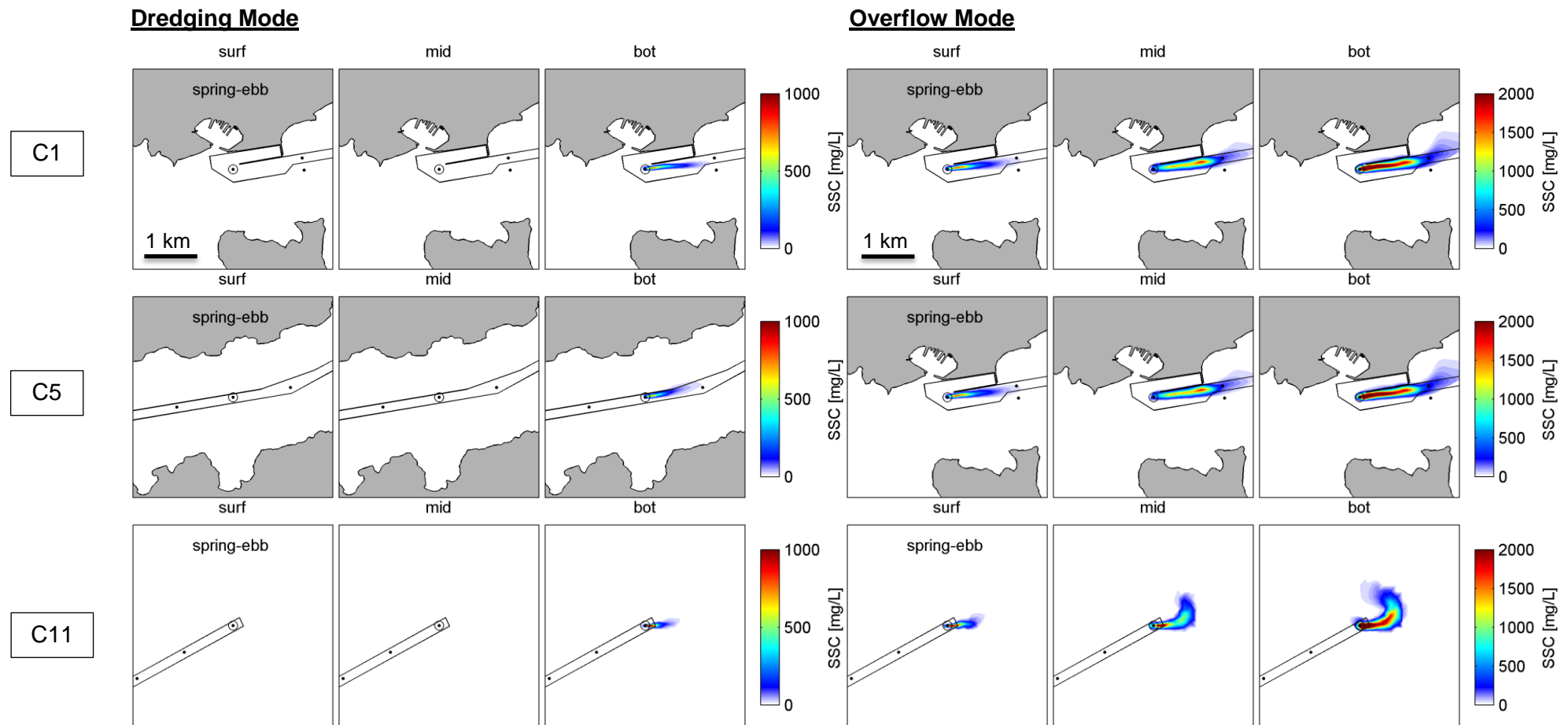


Figure 3.9 SSC plumes during dredging (left) and overflow (right) phases at site C1, C5 and C11 at peak ebb flow during spring tides, at three levels in the water column. These results are obtained using the existing hydrodynamics.

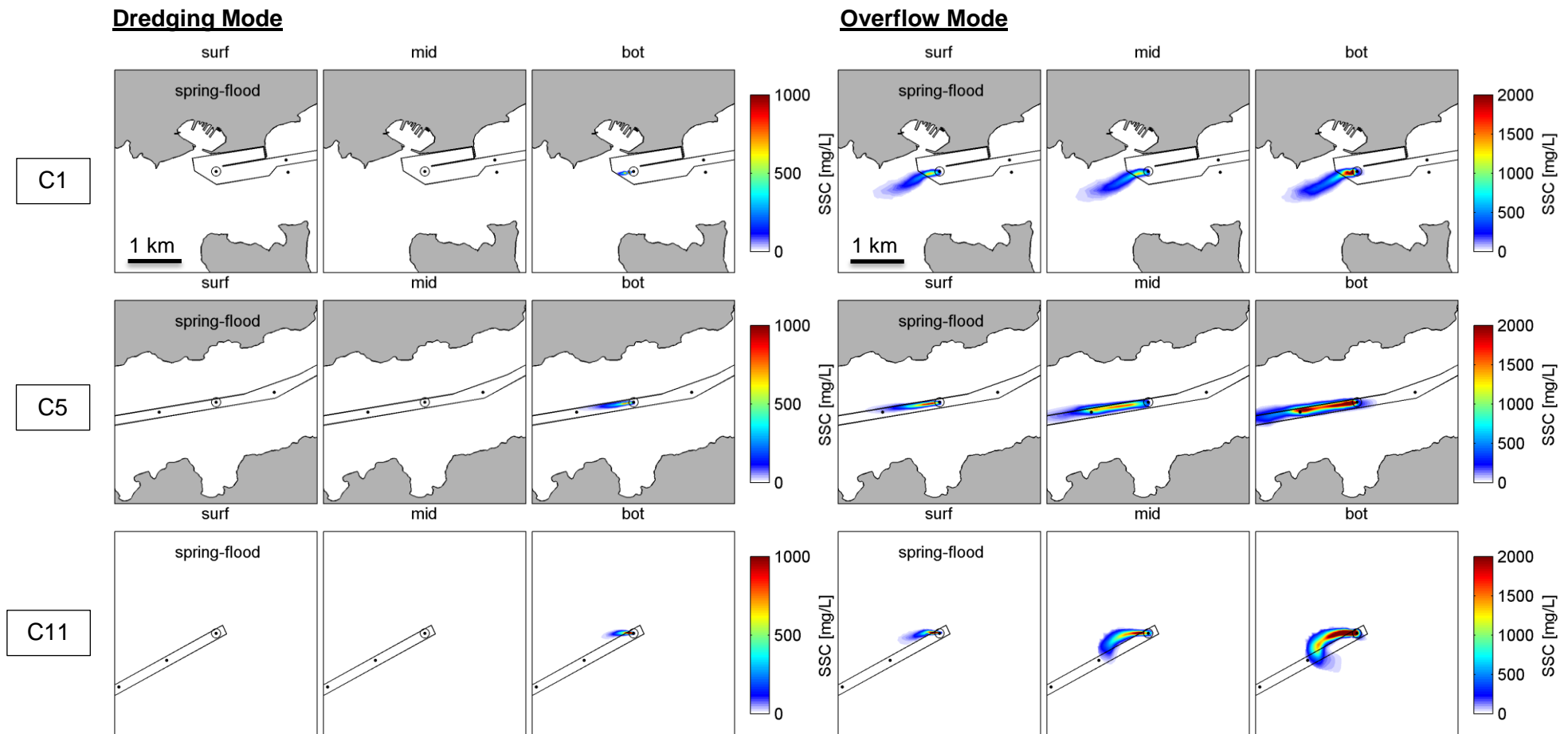


Figure 3.10 SSC plumes during dredging (left) and overflow (right) phases at site C1, C5 and C11 at peak flood flow during spring tides, at three levels in the water column. These results are obtained using the existing hydrodynamics.

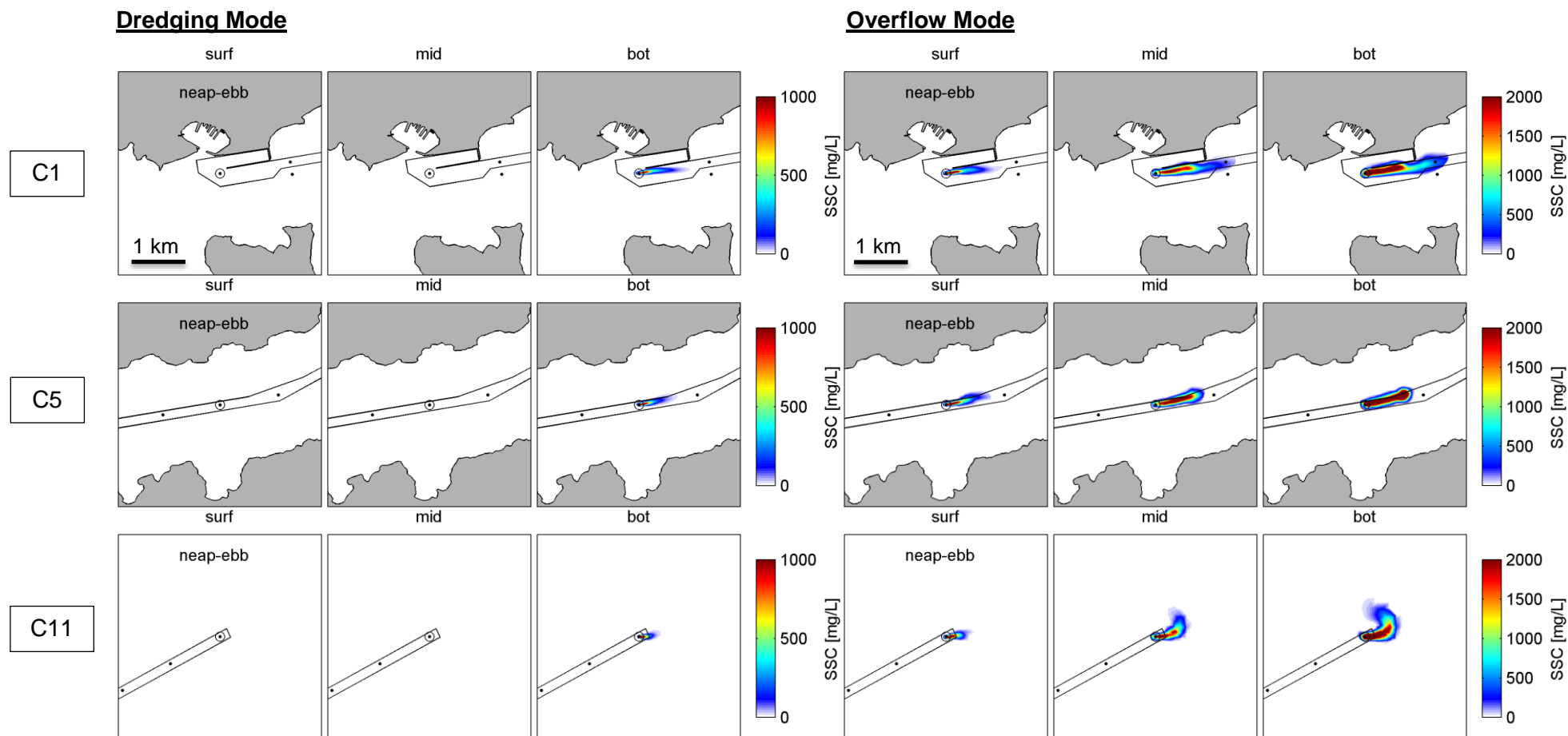


Figure 3.11 SSC plumes during dredging (left) and overflow (right) phases at site C1, C5 and C11 at peak ebb flow during neap tides, at three levels in the water column. These results are obtained using the existing hydrodynamics.

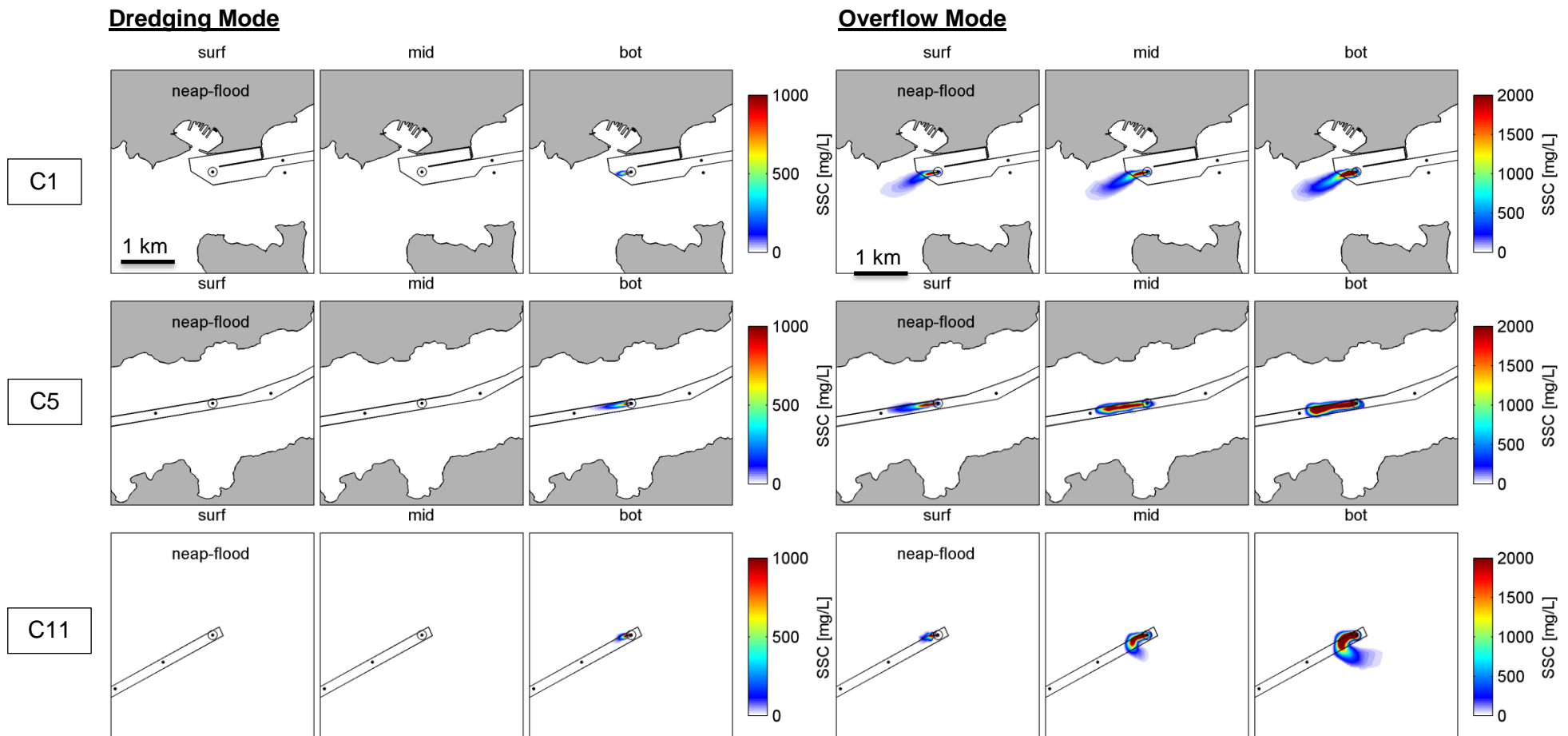
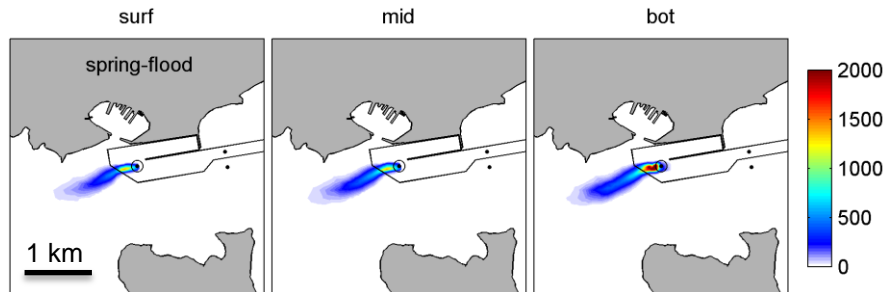
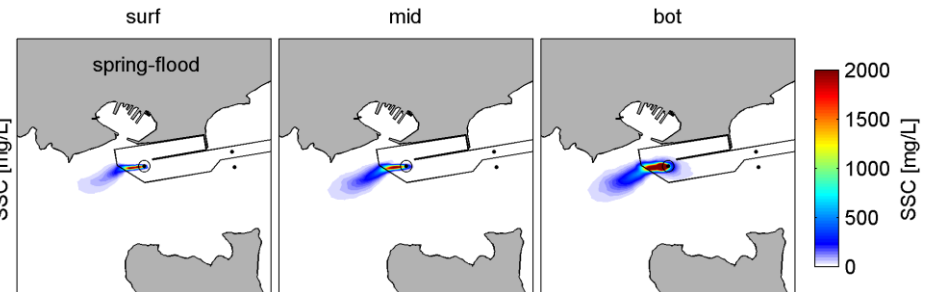


Figure 3.12 SSC plumes during dredging (left) and overflow (right) phases at site C1, C5 and C11 at peak flood flow during neap tides, at three levels in the water column. These results are obtained using the existing hydrodynamics.

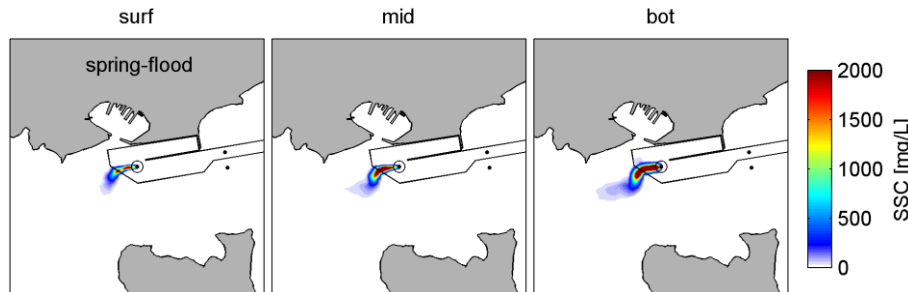
Existing



Scenario 2



Existing with seiche



Scenario 2 with seiche

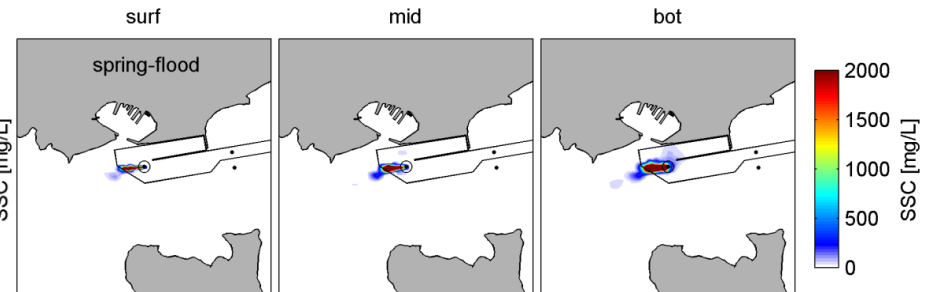


Figure 3.13 SSC plumes during overflow at site C1 at peak flood flow during spring tides, at three levels in the water column, for the existing, Scenario 2, existing with seiche and Scenario 2 with seiche scenarios (top left, top right, bottom left and bottom right, respectively).

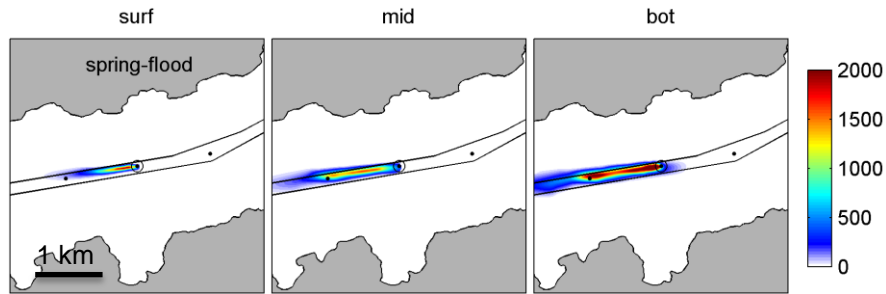
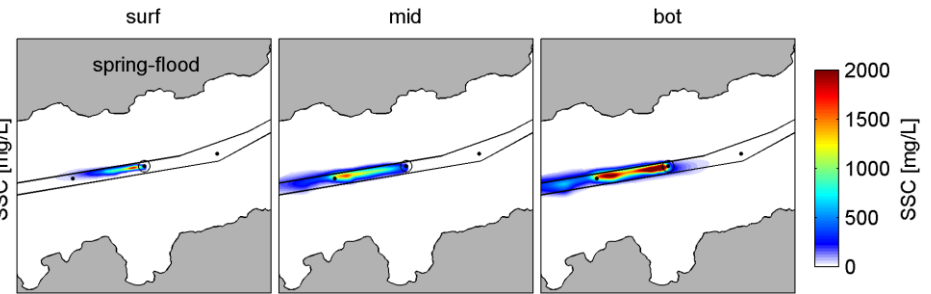
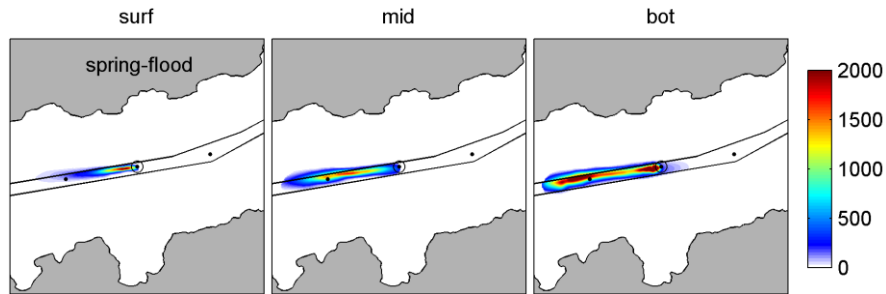
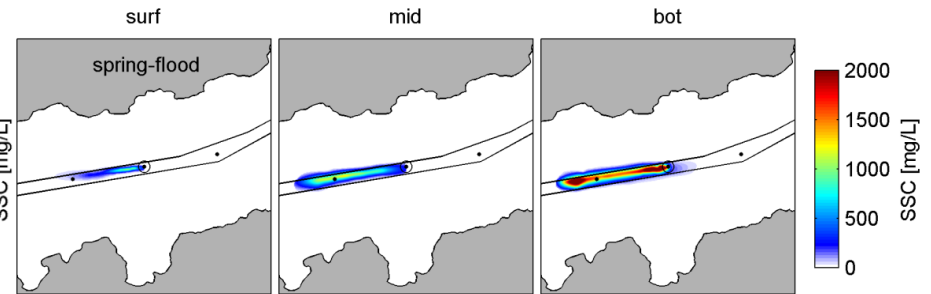
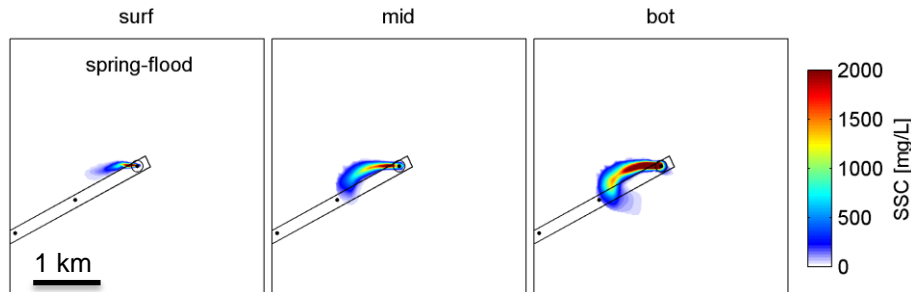
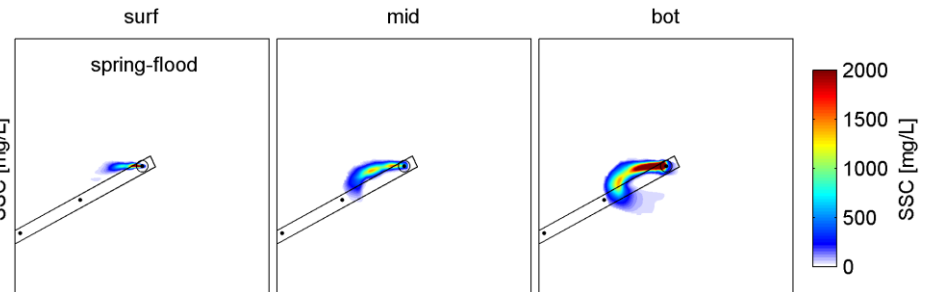
Existing**Scenario 2****Existing with seiche****Scenario 2 with seiche**

Figure 3.14 SSC plumes during overflow at site C5 at peak flood flow during spring tides, at three levels in the water column, for the existing, Scenario 2, existing with seiche and Scenario 2 with seiche scenarios (top left, top right, bottom left and bottom right, respectively).

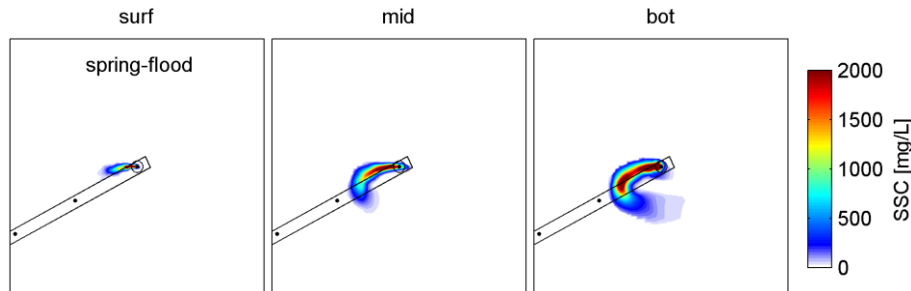
Existing



Scenario 2



Existing with seiche



Scenario 2 with seiche

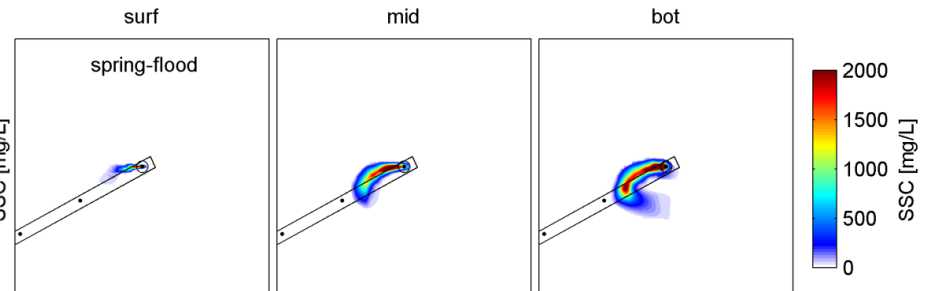


Figure 3.15 SSC plumes during overflow at site C11 at peak flood flow during spring tides, at three levels in the water column, for the existing, Scenario 2, existing with seiche and Scenario 2 with seiche hydrodynamics (top left, top right, bottom left and bottom right, respectively).

3.3. Probabilistic dredging plumes

The exact timing of the dredging work to be undertaken is unknown and will typically be dependent on a range of factors such as weather conditions, tides, or other time dependant factors (e.g. travel to and from disposal site, technical issues etc.). In that sense it is not necessarily relevant to try and predict the actual SSC field history over a certain period. Instead, it is more informative to consider a probabilistic approach whereby the entire range of hydrodynamic forcing conditions are considered to produce robust description of the SSC plumes expected at a given site, for a given task.

In the present application where the tidal forcing dominates, two complete spring-neap tidal cycle were used as a reference period to produce probabilistic SSC plumes associated with the dredging and overflow phases.

The probabilistic SSC plumes are obtained by overlaying the successive particle clouds throughout the 28-day period and computing the SSC fields based on the combined particle clouds. These were computed for the dredging only phase (i.e. no overflow) and three overflow durations, i.e. 10, 20, and 30 minutes.

Probabilistic SSC plumes associated with dredging and 10-minute overflow at sites C1, C5 and C11, for the existing hydrodynamics, are given in Figure 3.16.

The SSC plumes during the dredging phase are contained in the bottom of the water column with negligible SSC levels predicted in the mid-water and surface levels. In contrast, SSC plumes spread across the entire water column during overflow, due to the shallower release point and large sediment quantities involved (see section 2.5).

There is an evident variation of the general SSC plumes patterns at different positions along the channel which is consistent with the expected tidal regime (see Figure 3.6 and Figure 3.7). The SSC plumes clearly follow the channel orientations at sites C1 and C5 while the patterns becomes more elliptical at site C11 where the tidal currents are less bi-directional.

These SSC plumes were computed for all study sites (see Figure 2.3); results are included in Appendix 1 for completeness.

Difference between the existing (Figure 3.16) and Scenario 2 (Figure 3.17) results are minimal. The overflow plumes are slightly skewed more to the east at site C1. At site C5, SSC plumes of Scenario 2 are slightly more elongated (~ 100 m) but also relatively more diluted. SSC plumes are very similar in both cases at site C11.

Modulation of the predicted SSC plumes when the additional short period fluctuations of the sea level and associated seiche velocities suggests seiching velocities likewise have a minimal effect of the plume extents, i.e. Figure 3.16 and Figure 3.18 for the existing hydrodynamics and Figure 3.17 and Figure 3.19 for the Scenario 2 hydrodynamics.

The overflow duration has a significant effect on the magnitude and extent of the SSC plumes associated with the dredging activities. The overflow phase

consists in releasing a highly concentrated mixture of water-sediment to maximize the amount of sediment stored in the hopper (see section 2.5). The process is generally highly turbulent and will result in suspended sediment within the entire water column.

The predicted SSC plumes associated with three overflow phase durations of 10, 20, and 30 minutes are compared in Figure 3.20 to Figure 3.22 for sites C1, C5 and C11 respectively. Increasing the overflow durations expectedly results in more elongated SSC plume extents with larger zones subject to high SSC levels of order 1000 mg.L⁻¹, at all levels of the water columns.

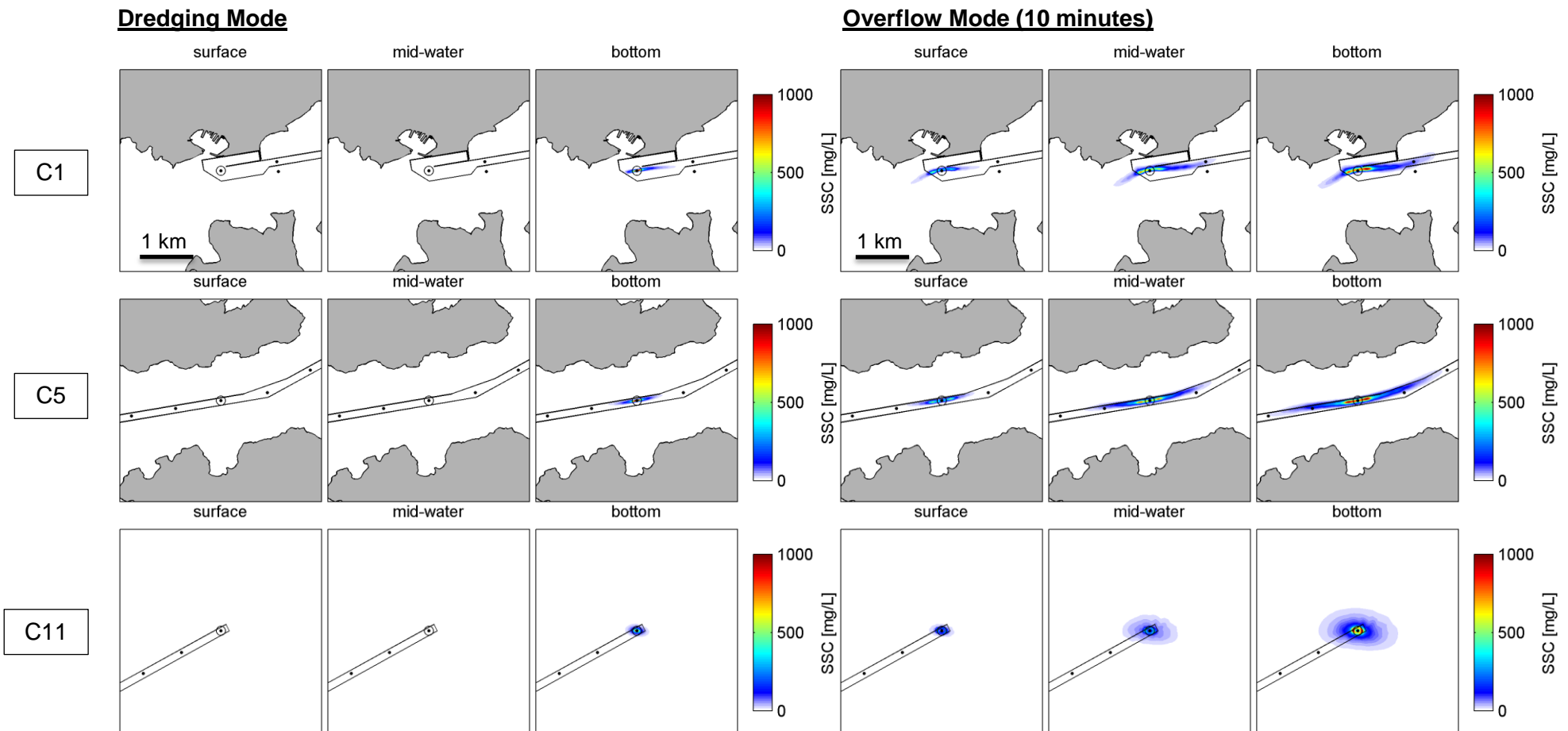


Figure 3.16 Probabilistic SSC plumes during dredging (left) and overflow (right) phases at site C1, C5 and C11, at three levels in the water column. These results are obtained using the existing hydrodynamics.

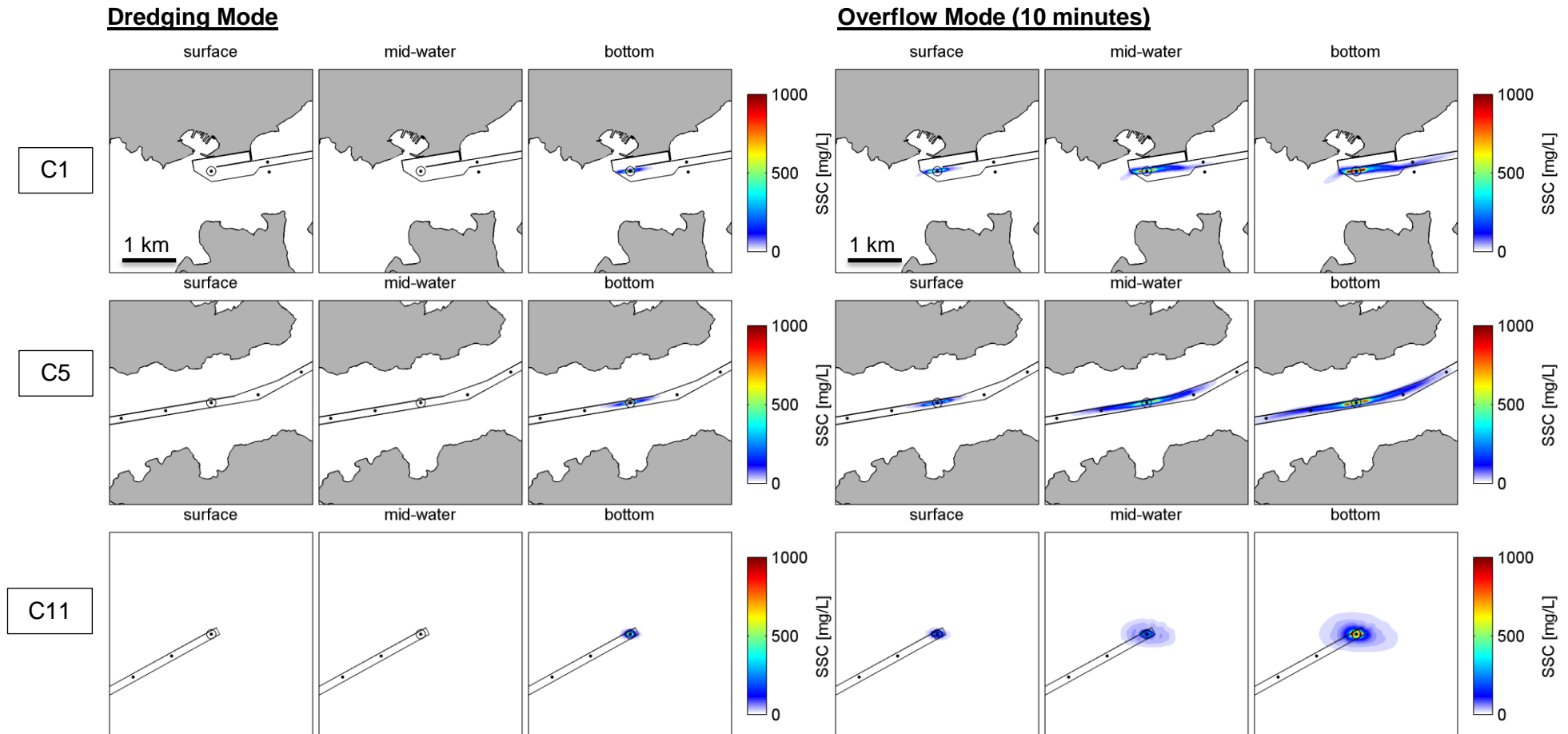


Figure 3.17 Probabilistic SSC plumes during dredging (left) and overflow (right) phases at site C1, C5 and C11, at three levels in the water column. These results are obtained using the Scenario 2 hydrodynamics.

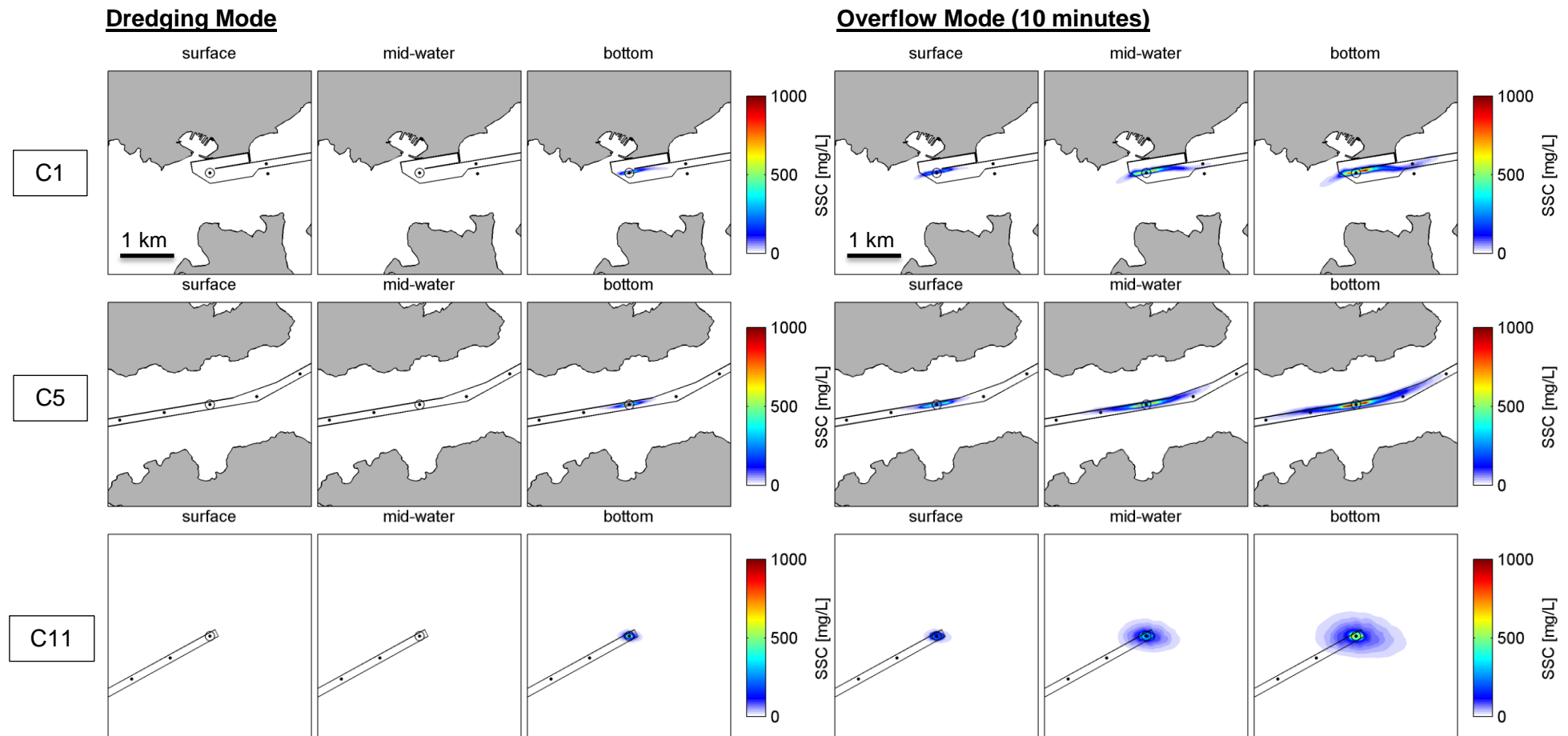


Figure 3.18 Probabilistic SSC plumes during dredging (left) and overflow (right) phases at site C1, C5 and C11, at three levels in the water column. These results are obtained using the existing hydrodynamics with seiche included.

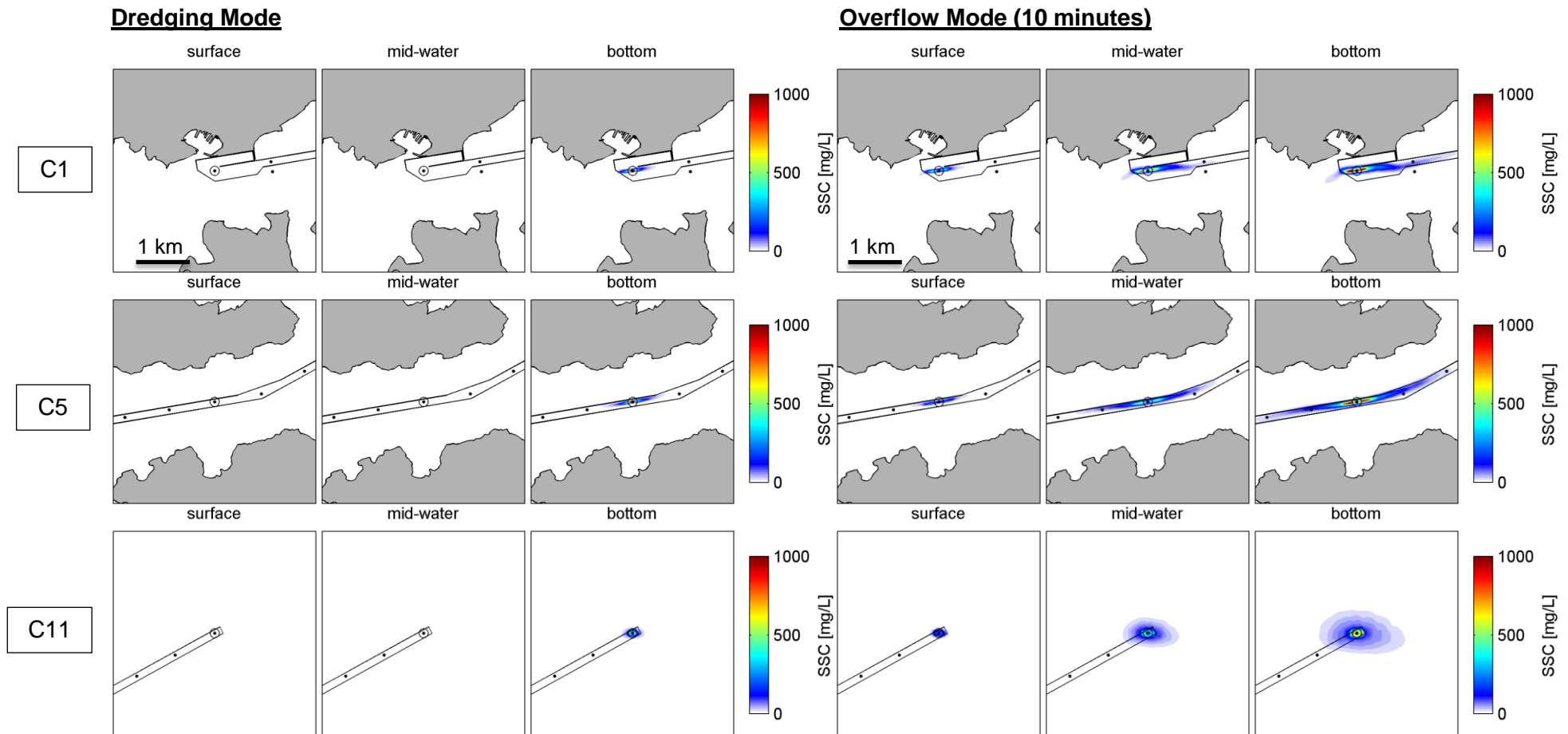


Figure 3.19 Probabilistic SSC plumes during dredging (left) and overflow (right) phases at site C1, C5 and C11, at three levels in the water column. These results are obtained using the Scenario 2 hydrodynamics with seiche included.

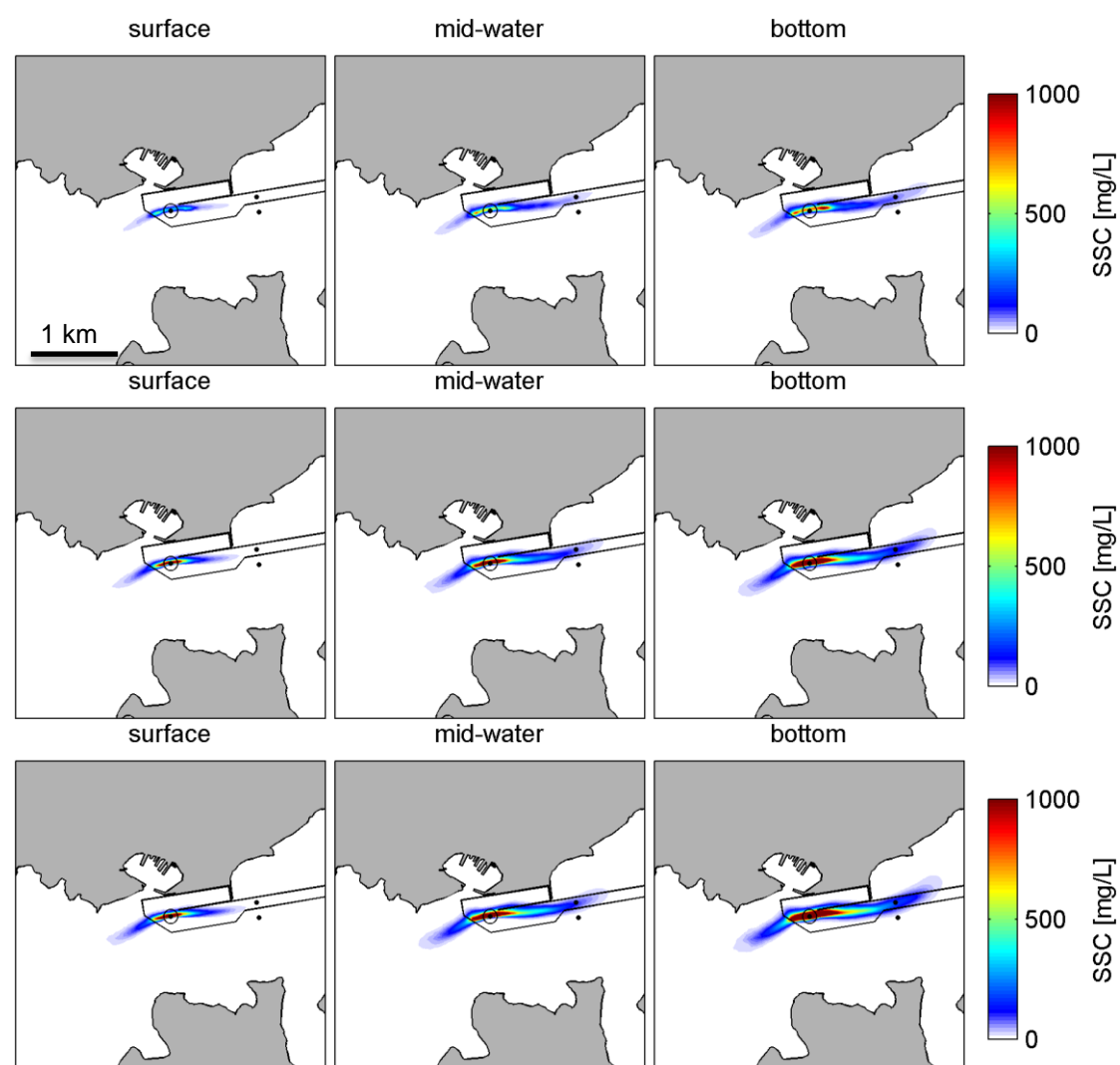


Figure 3.20 Probabilistic SSC plumes during a 10, 20 and 30 minute overflow scenarios (top to bottom) at site C1, over the existing bathymetry, at three levels in the water columns.

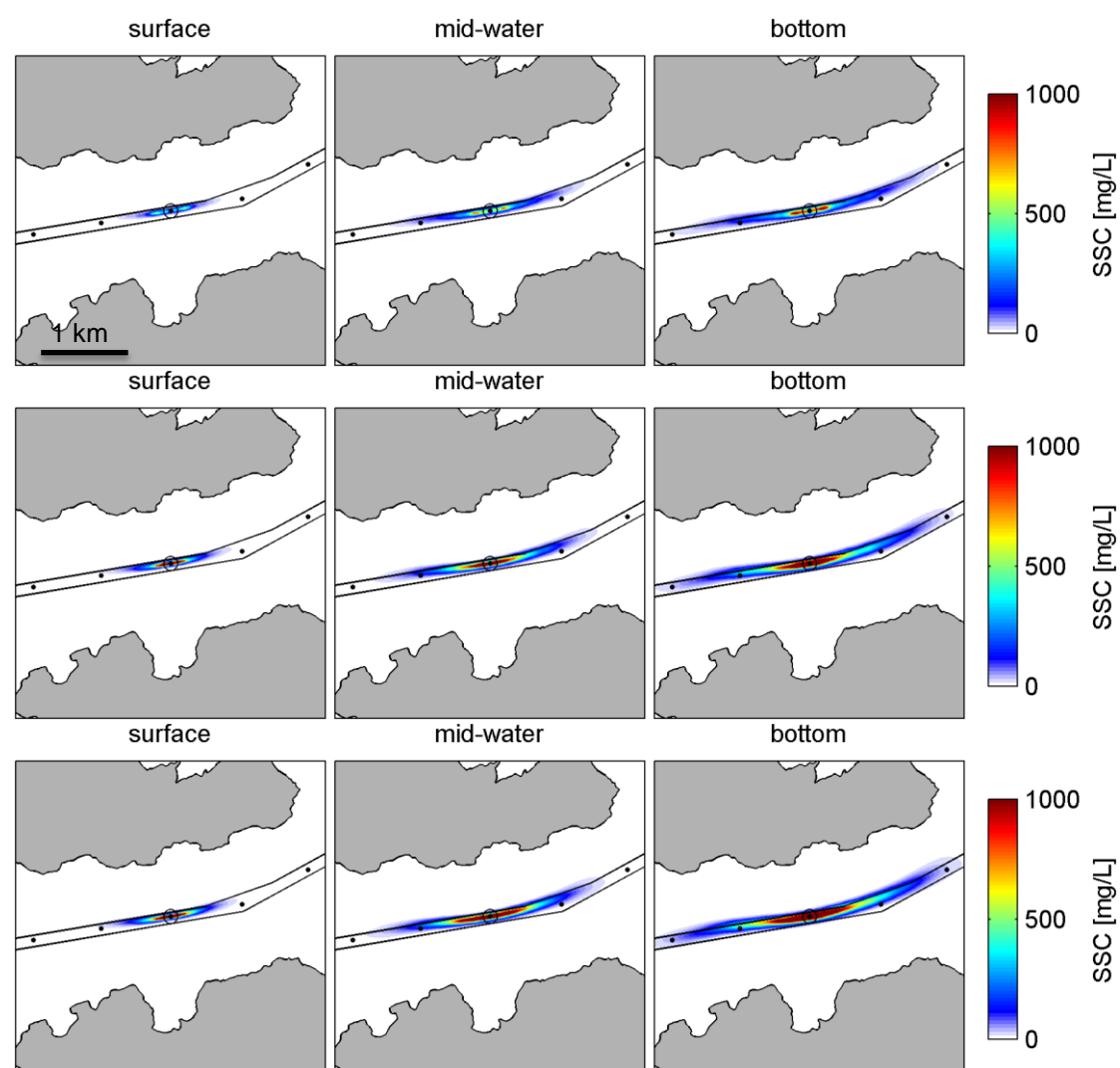


Figure 3.21 Probabilistic SSC plumes during a 10, 20 and 30 minute overflow scenarios (top to bottom) at site C5, over the existing bathymetry, at three levels in the water columns.

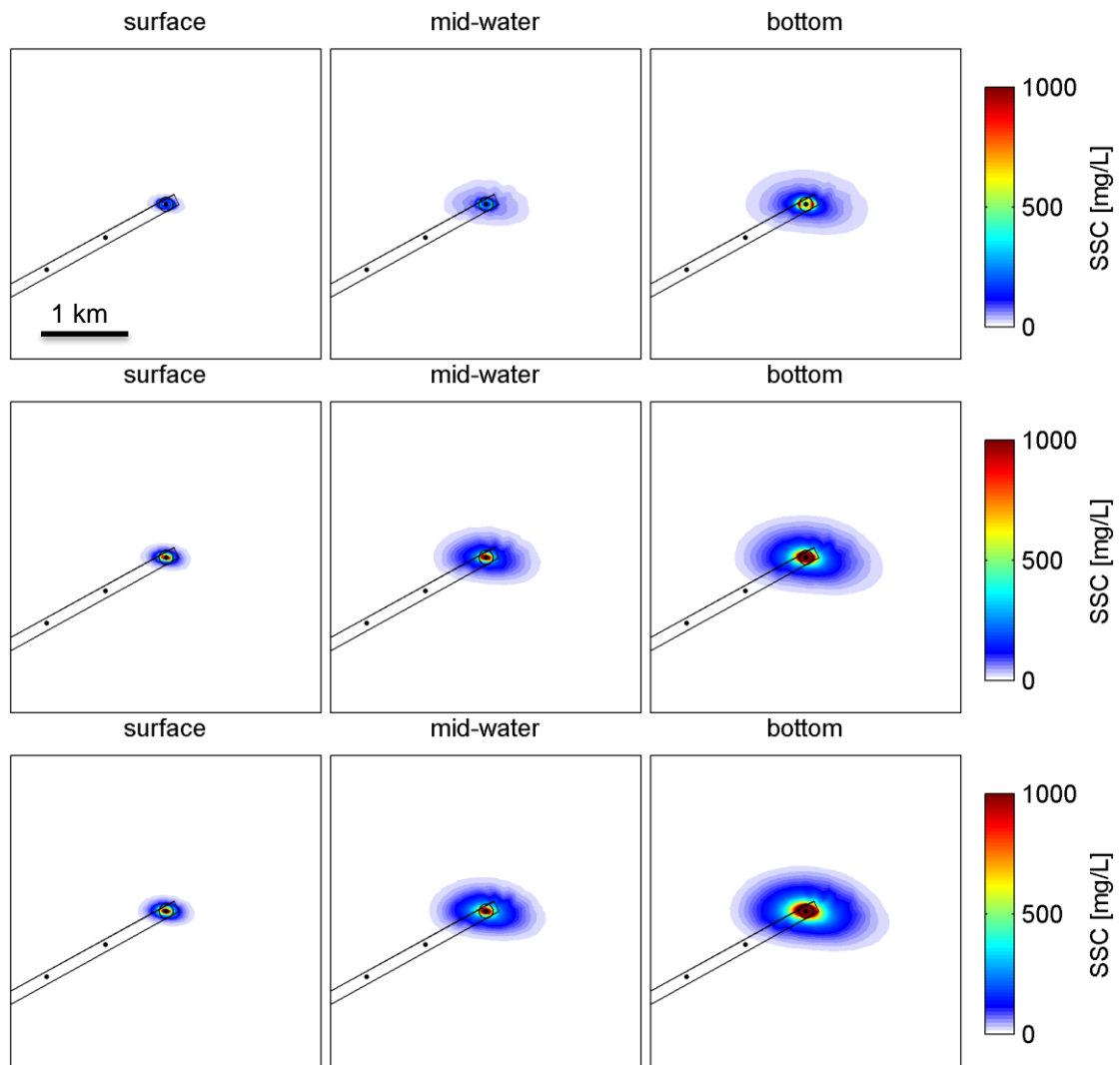


Figure 3.22 Probabilistic SSC plumes during a 10, 20 and 30 minute overflow scenarios (top to bottom) at site C11, over the existing bathymetry, at three levels in the water columns.

3.4. Dredging plume concentration exceedence maps

Another useful metric for assessing the SSC plumes resulting from the dredging operations is the percentage of time a certain SSC level is exceeded.

Exceedence time estimations were undertaken relative to the typical ambient SSC levels that are naturally found within Pegasus Bay, namely 10, 50 and 100 mg.L-1 (see MetOcean Solutions Ltd., 2016).

The dredging cycle was assumed to be of 25 minutes dredging, 10 minutes overflow and 85 minutes travel to and from disposal sites (i.e. consistent with a 2 hour disposal cycle). The dredging cycle was reproduced continuously over the 28 day spring-neap tidal cycle (i.e. day and night).

SSC exceedence time maps associated with the dredging at C1, C5 and C11 are presented in Figure 3.23 to Figure 3.25 respectively. Results illustrate that although the surface SSC levels can be significant at times during overflow phases (e.g. Figure 3.23), this represents a very small percentage of time (~1-2 %) in a realistic dredging cycle context.

At sites C1 and C5, the considered SSC thresholds are exceeded 5-10 % of the time in the mid-water layer. This increases to 30-40 % of the time in the bottom layers. Note these maximum percentages of time are of the same order of magnitude for the three SSC thresholds levels tested. However, the general areas within which these SSC levels are exceeded progressively decrease as the threshold SSC magnitude increases. The regions subject to the largest exceedence times typically extend up to 500-1000 m from the release sites C1 and C5 depending on the considered thresholds (i.e. 10, 50 or 100 mg.L-1, Figure 3.23 and Figure 3.24 for site C1 and C5, respectively)

General patterns of the exceedence maps obtained for the site C11 have more elliptical shape which is consistent with the tidal flows at the site (Figure 3.25). The more elliptical nature of the tidal currents at site C11 result in the greater spatial dispersion of the dredging plume, and hence the considered SSC thresholds are exceeded relatively less frequently than for sites C1-C5, where the dispersion patterns are strongly bi-directional. Maximum exceedence times are of ~15 % in the bottom layer, reducing to 0-5 % in the mid-water level. Extents of the most significant exceedence times are reduced relative to sites C1-C5 (500 m or less) and are distributed more homogeneously around the release site.

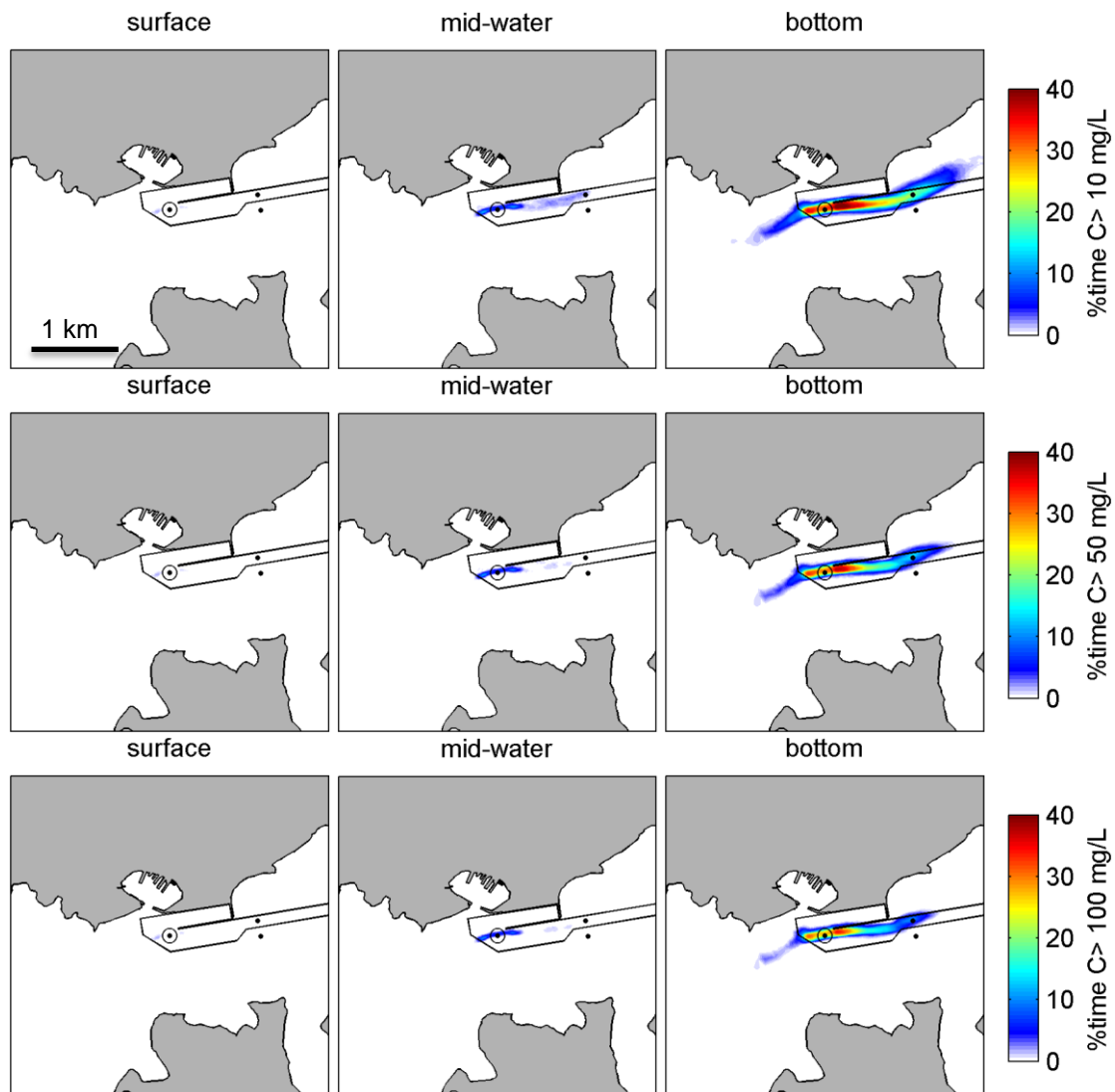


Figure 3.23 Percentage of time SSC thresholds of 10, 50, 100 mg/L (top to bottom) are exceeded during dredging activities at site C1, including dredging (25 min), overflow (10 min) and travel to and from disposal site (85 minutes). The exceedence percentages are computed over a full spring-neap tidal cycle (28 days).

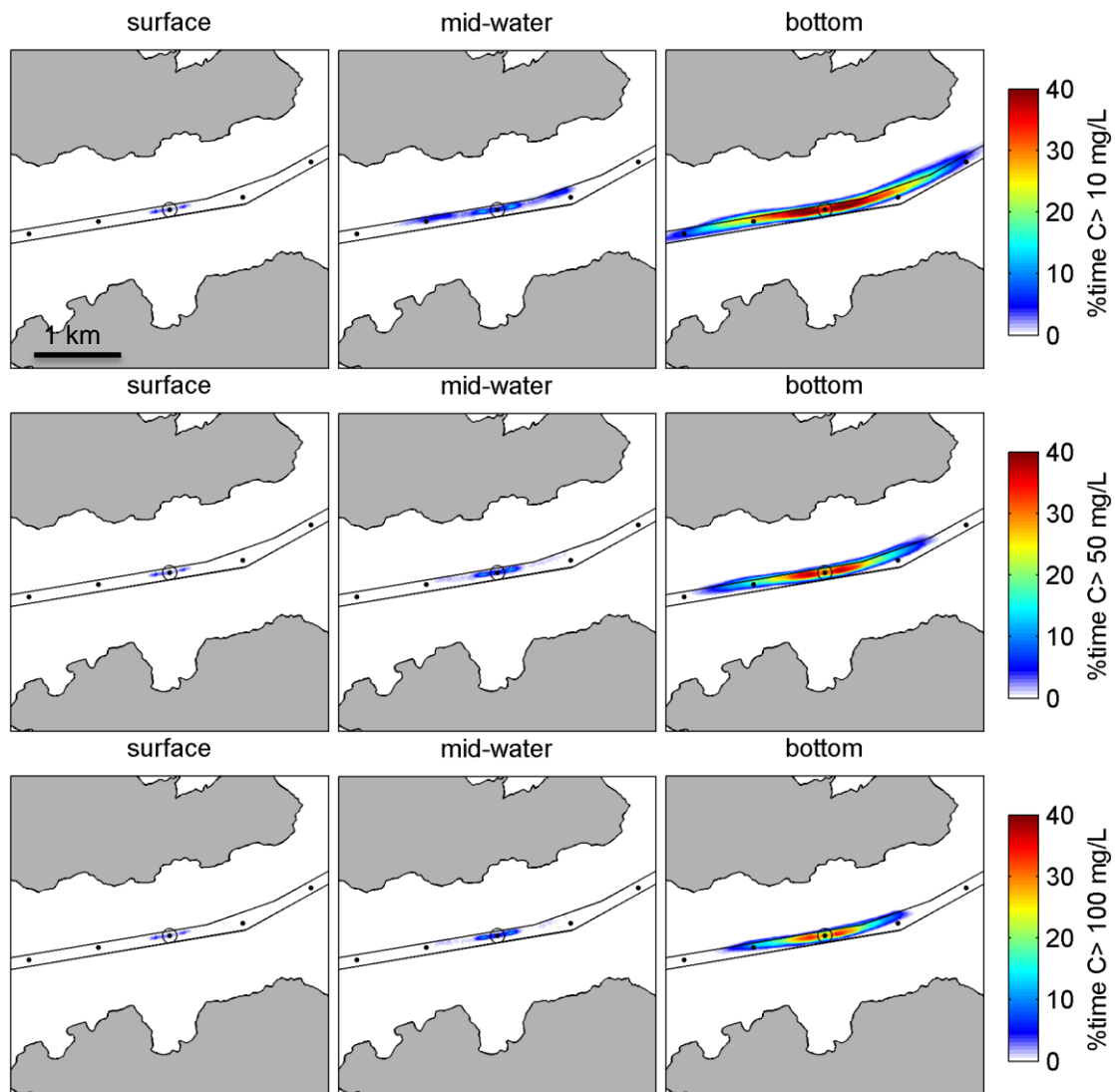


Figure 3.24 Percentage of time SSC thresholds of 10, 50, 100 mg/L (top to bottom) are exceeded during dredging activities at site C5, including dredging (25 min), overflow (10 min) and travel to and from disposal site (85 minutes). The exceedence percentages are computed over a full spring-neap tidal cycle (28 days).

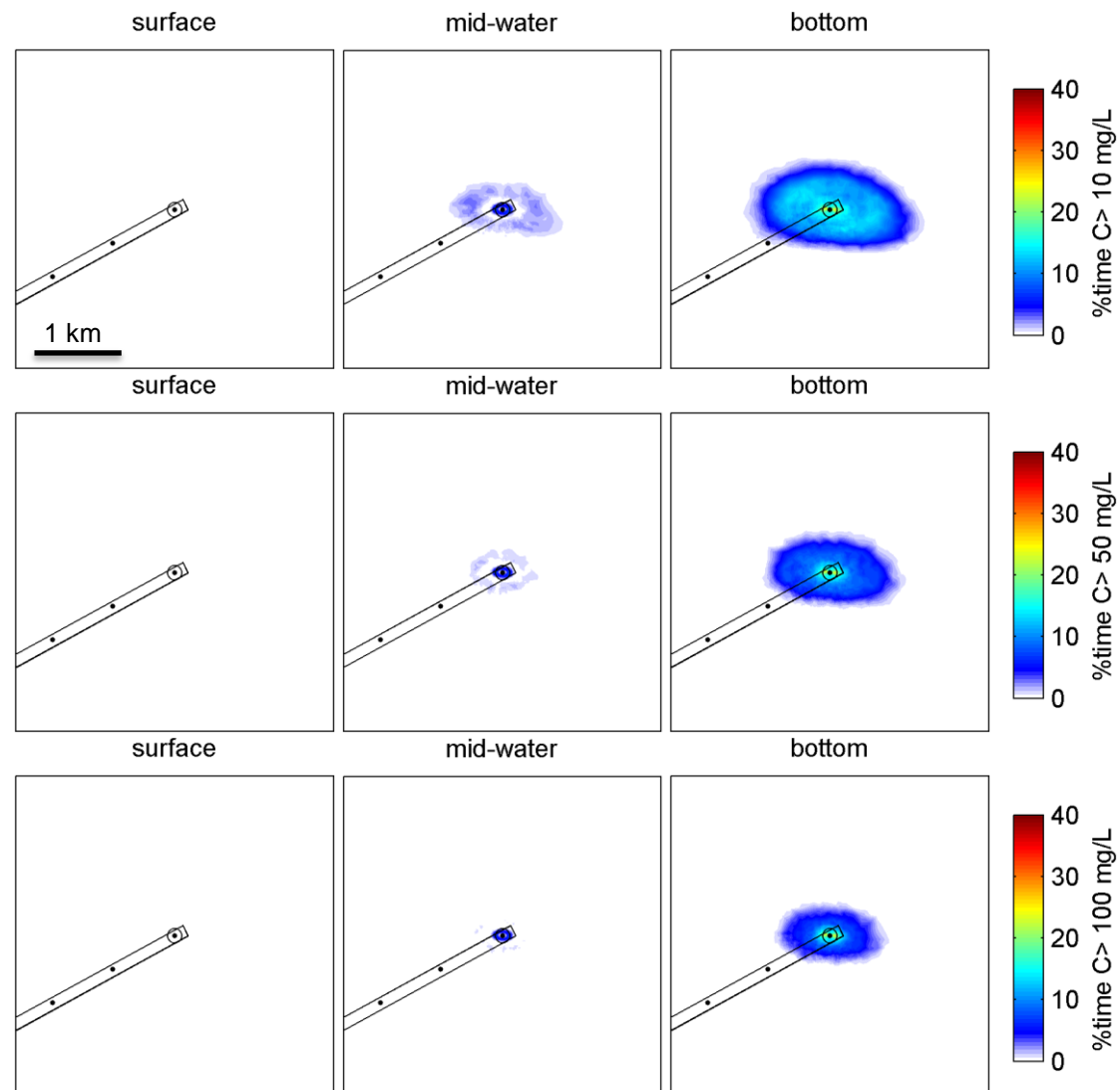


Figure 3.25 Percentage of time SSC thresholds of 10, 50, 100 mg/L (top to bottom) are exceeded during dredging activities at site C11, including dredging (25 min), overflow (10 min) and travel to and from disposal site (85 minutes). The exceedence percentages are computed over a full spring-neap tidal cycle (28 days).

4. SUMMARY

Characteristics of the suspended sediment plumes associated with the dredging works to be undertaken in the Lyttelton Harbour in the context of the channel deepening project have been examined.

The existing and post-dredging tidal hydrodynamics (Scenario 2) of the Harbour were simulated both with and without seiche velocities. A range of particle-tracking simulations reproducing the projected dredging activities were undertaken at 12 locations along the channel.

Key findings are summarized below.

- The modification of the Harbour consists in an extension and deepening of the shipping channel and land reclamation west of Gollans Bay. The key changes in hydrodynamics include a reduction of the tidal current magnitudes throughout the dredged zone due to the deeper water depths as well as a modification of the flow bifurcation patterns in the vicinity of the reclaimed area. Variations are more limited further east towards the Harbour Entrance where general tidal current axes and magnitudes are conserved.
- Patterns of the suspended sediment concentration (SSC) plumes are strongly bi-directional within the Harbour, following the channel orientation, and become more elliptical close to the entrance. This is consistent with the tidal flow regime.
- The dredging phase (initial infilling of the hopper) produces SSC plumes that are contained within the bottom part of the water column. In contrast, the overflow phase produces significant sediment plumes through the entire water column, including near the surface, with high SSC levels.
- A key factor governing the overall extents and concentration magnitudes of the sediment plumes resulting from the dredging activities is the overflow duration.
- A range of hydrodynamic forcing scenarios were tested including existing and post-dredging (Scenario 2) bathymetry states, with or without the inclusion of short period sea level fluctuations that can be experienced in Pegasus Bay and into Lyttelton Harbour/Whakaraupō, and the resultant seiche velocities. Although some slight modulation of the predicted SSC plumes patterns are present, key plume dispersion characteristics are generally conserved.
- The percentages of time background SSC levels are exceeded were estimated based on the expected dredging cycle. Background SSC levels are exceeded up to 30-40 % of the time within ~500-1000 m of the dredging site in the bottom layers, and 5 to 10 % of the time in the mid-water layers over similar extents. In the surface level, although SSC can be relatively large (e.g. during overflow), effective exceedence times are very limited (i.e. in the order of 1 % or less).

5. REFERENCES

- Becker J., van Eekelen E., van Wiechen J., de Lange W., Damsma T., Smolders T., van Koningsveld M., 2015. Estimating source terms for far field dredge plume modelling. *J. Environ. Manage.* 149, 282–293.
- EcoShape, 2010. TASS Software – Trailer suction hopper dredger, User guide for TASS version 3.2.1 (Report prepared by HR Wallingford for the EcoShape Project No. EX 6134 Revision 7). HR Wallingford.
- Elder, J.W., 1956. The dispersion of marked fluid in turbulent shear flow. *J. Fluid Mech.* 5, 544–560.
- Fischer, H.B., Koh, R.C.Y., Imberger, J., Brooks, N.H., 1979. *Mixing in Inland and Coastal Waters*. Academic Press, San Diego, California USA.
- Goring, D.G., 2014. Implications of the Lyttelton Port Recovery Plan on Waves and Tidal Currents in Lyttelton Harbour (No. 2014/2).
- Goring and Henry, 1998. Short period (1–4 h) sea level fluctuations on the Canterbury coast, New Zealand, New Zealand. *J. Mar. Freshw. Res.* 32:1, 119–134.
- HR Wallingford, 2012. TASS Validation 2011, HR Wallingford report EX 6747.
- HR Wallingford, 2010. Validation of the TASS System for Trailer Suction Hopper Dredging - HR Wallingford Technical Note DDR4237-01.
- McLaren, 2012. A sediment trend analysis of the Outer Lyttelton Harbour. Technical report prepared for Lyttelton Port of Christchurch. SedTrends Analysis Ltd.
- MetOcean Solutions Ltd., 2016. LYTTTELTON HARBOUR DREDGING PROJECT - Simulations of suspended sediment plumes and associated deposition from offshore disposal. (Technical report prepared for Lyttelton Port of Christchurch.).
- Okubo, A., 1971. Oceanic diffusion diagrams. *Deep-Sea Res.* 18, 789–802.
- Smart, G.M., Duncan, M.J., Walsh, J.M., 2002. Relatively rough flow resistance equations. *J. Hydraul. Eng.* 128, 568–578.
- Smith, S.J., Friedrichs, C.T., 2011. Size and settling velocities of cohesive flocs and suspended sediment aggregates in a trailing suction hopper dredge plume. *Cont. Shelf Res.* 10.
- Spearman, J., Bray, R.N., Land, J., Burt, T.N., Mead, C.T., Scott, D., 2007. *Estuarine and Coastal Fin Sediments Dyanmics*.
- Van Rijn, L.C., 2007. A unified view of sediment transport by current and waves, Part II: Suspended transport. *J. Hydraul. Eng. ASCE* 22.
- Van Rijn, L.C., 1984. Sediment Transport Part II: Suspended Load Transport. *J. Hydraul. Eng.* 110, 1613–1641.
- Vitali, L., Monforti, F., Bellasio, R., Bianconi, R., Sachero, V., Mosca, S., Zanini, G., 2006. Validation of a Lagrangian dispersion model implementing different kernel methods for density reconstruction. *Atmos. Environ.* 40, 8020–8033.
- Whitehouse R., et al, 2000. *Dynamics of estuarine muds*, Thomas Telford, London. ed.
- Winterwerp, J.C., 2002. Near-field behavior of dredging spill in shallow water. *J. Waterw. Port Coast. Ocean Eng.* 128, 96–98.
- Zhang, Y.L., Baptista, A.M., 2008. A semi-implicit Eulerian-Lagrangian finite element model for cross-scale ocean circulation. *Ocean Model.* 21, 71–96.

APPENDIX – SUPPLERMENTARY FIGURES

A1. DREDGING PLUMES DURING PEAK TIDAL FLOWS

A1.1 Dredging Mode

A1.1.1 Existing bathymetry

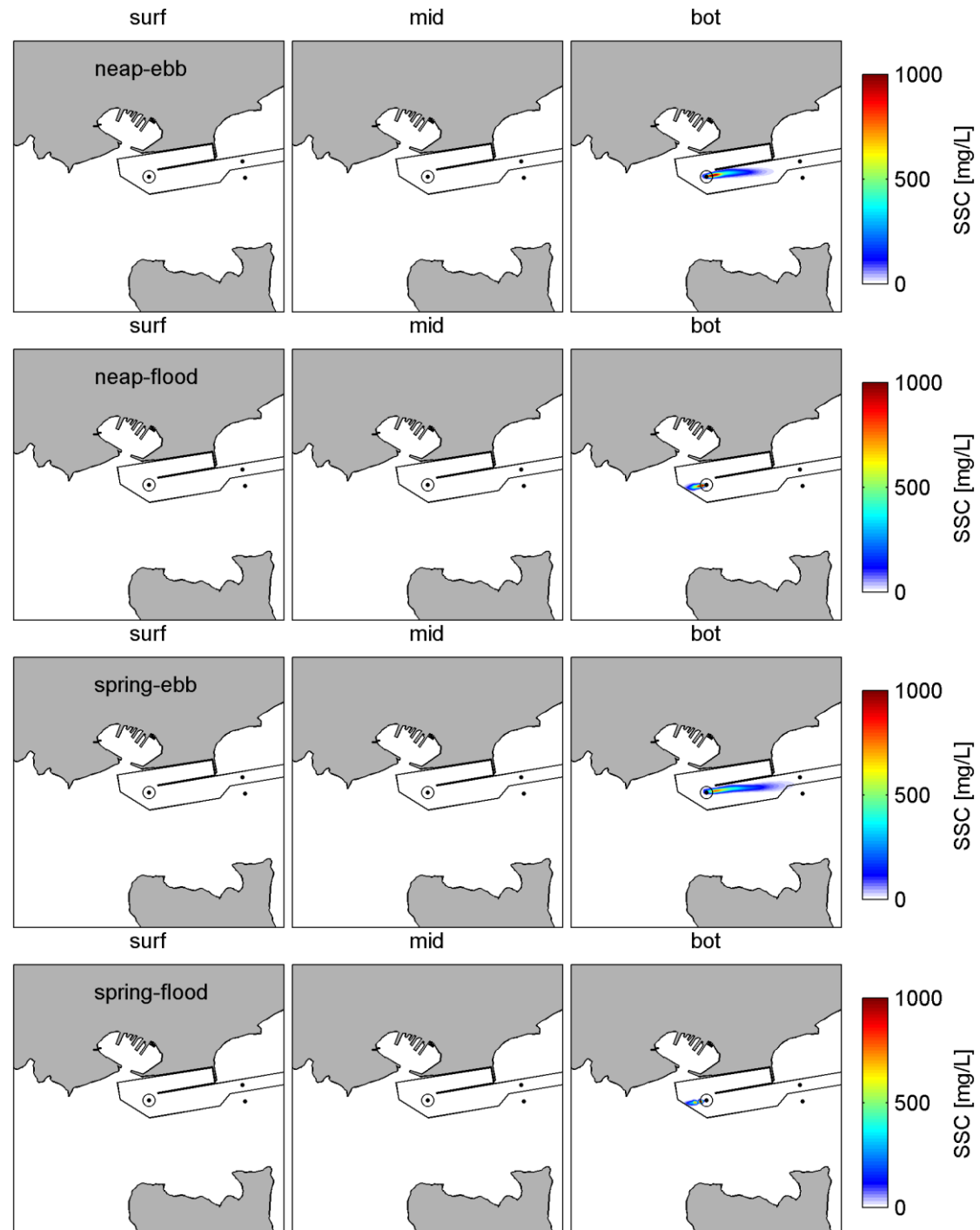


Figure A 1.1 Snapshots of suspended sediment concentrations plumes during dredging at site C1 during peak tidal flows (top to bottom) over the existing bathymetry, at three levels in the water column (left to right).

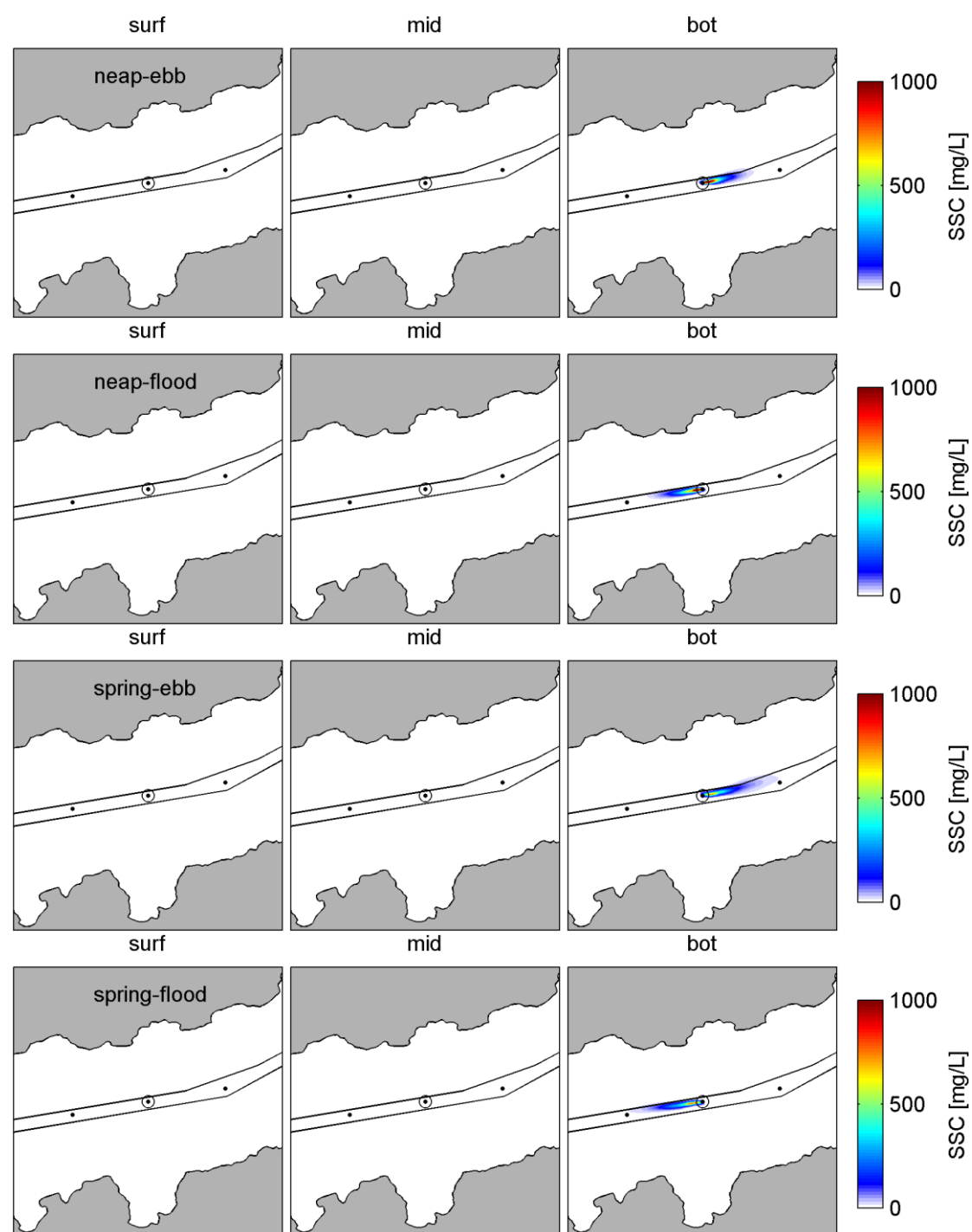


Figure A 1.2 Snapshots of suspended sediment concentrations plumes during dredging at site C5 during peak tidal flows (top to bottom) over the existing bathymetry, at three levels in the water column (left to right).

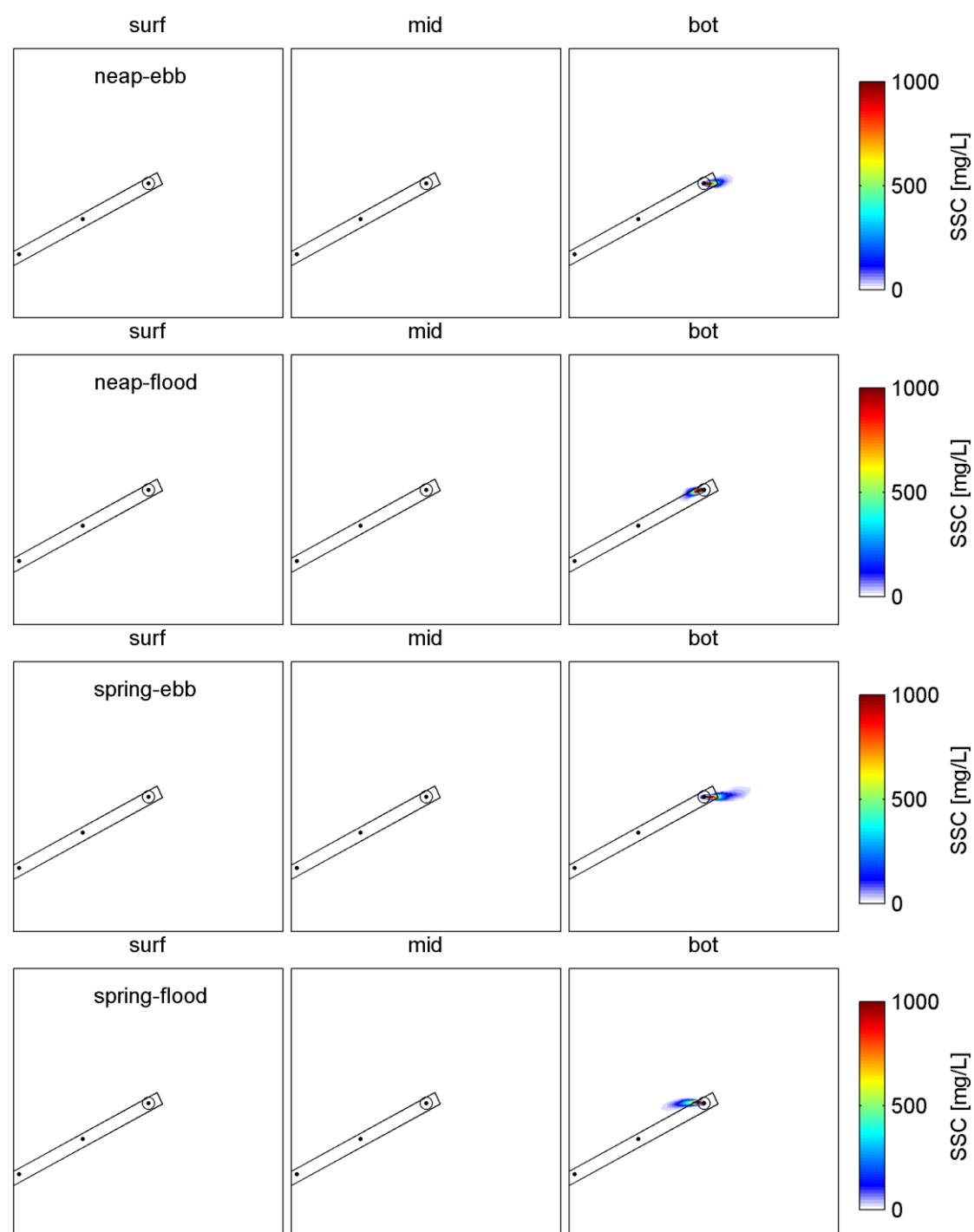


Figure A 1.3 Snapshots of suspended sediment concentrations plumes during dredging at site C11 during peak tidal flows (top to bottom) over the existing bathymetry, at three levels in the water column (left to right).

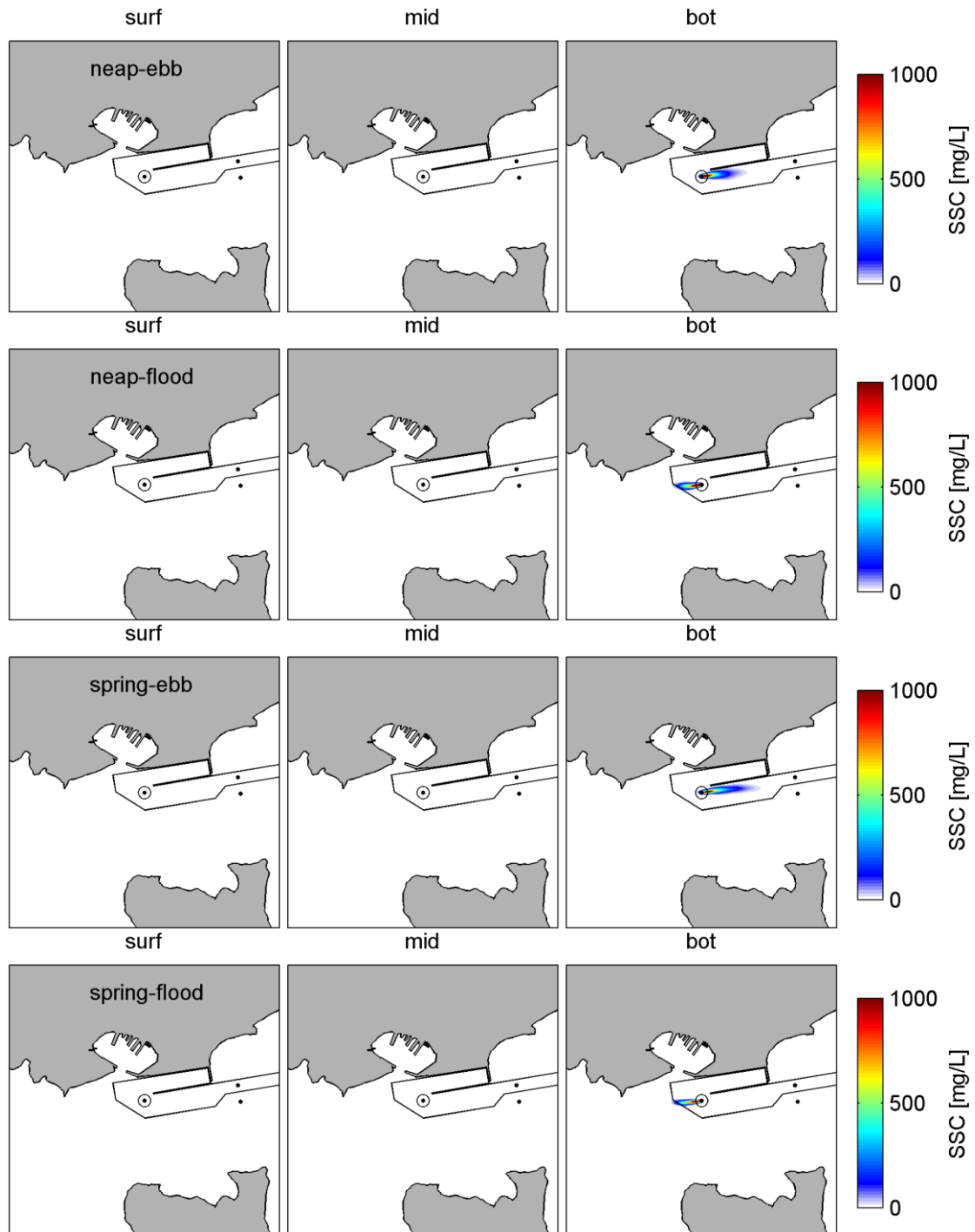
A1.1.2 Stage3 bathymetry

Figure A 1.4 Snapshots of suspended sediment concentrations plumes during dredging at site C1 during peak tidal flows (top to bottom) over the Scenario 2 bathymetry, at three levels in the water column (left to right).

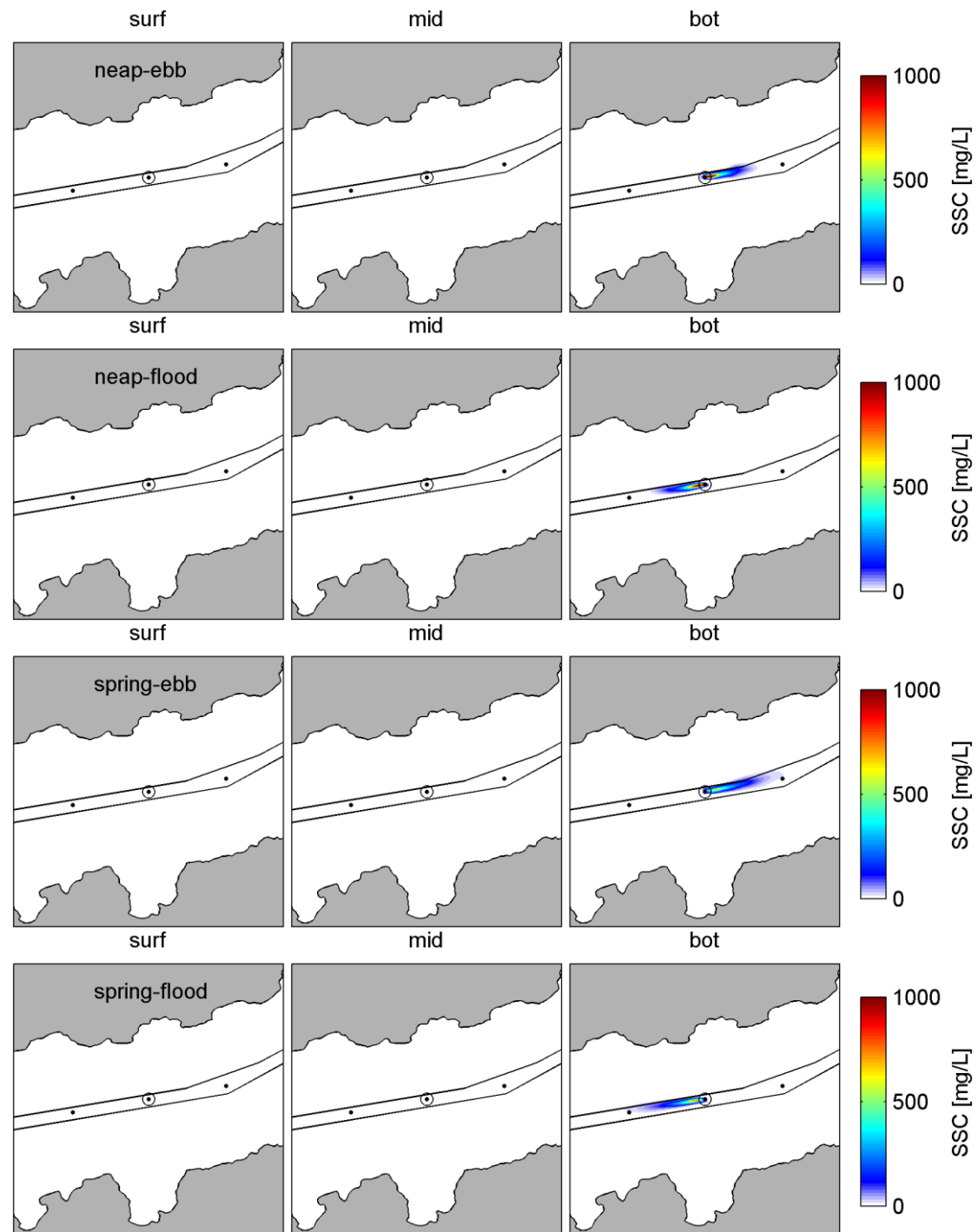


Figure A 1.5 Snapshots of suspended sediment concentrations plumes during dredging at site C5 during peak tidal flows (top to bottom) over the Scenario 2 bathymetry, at three levels in the water column (left to right).

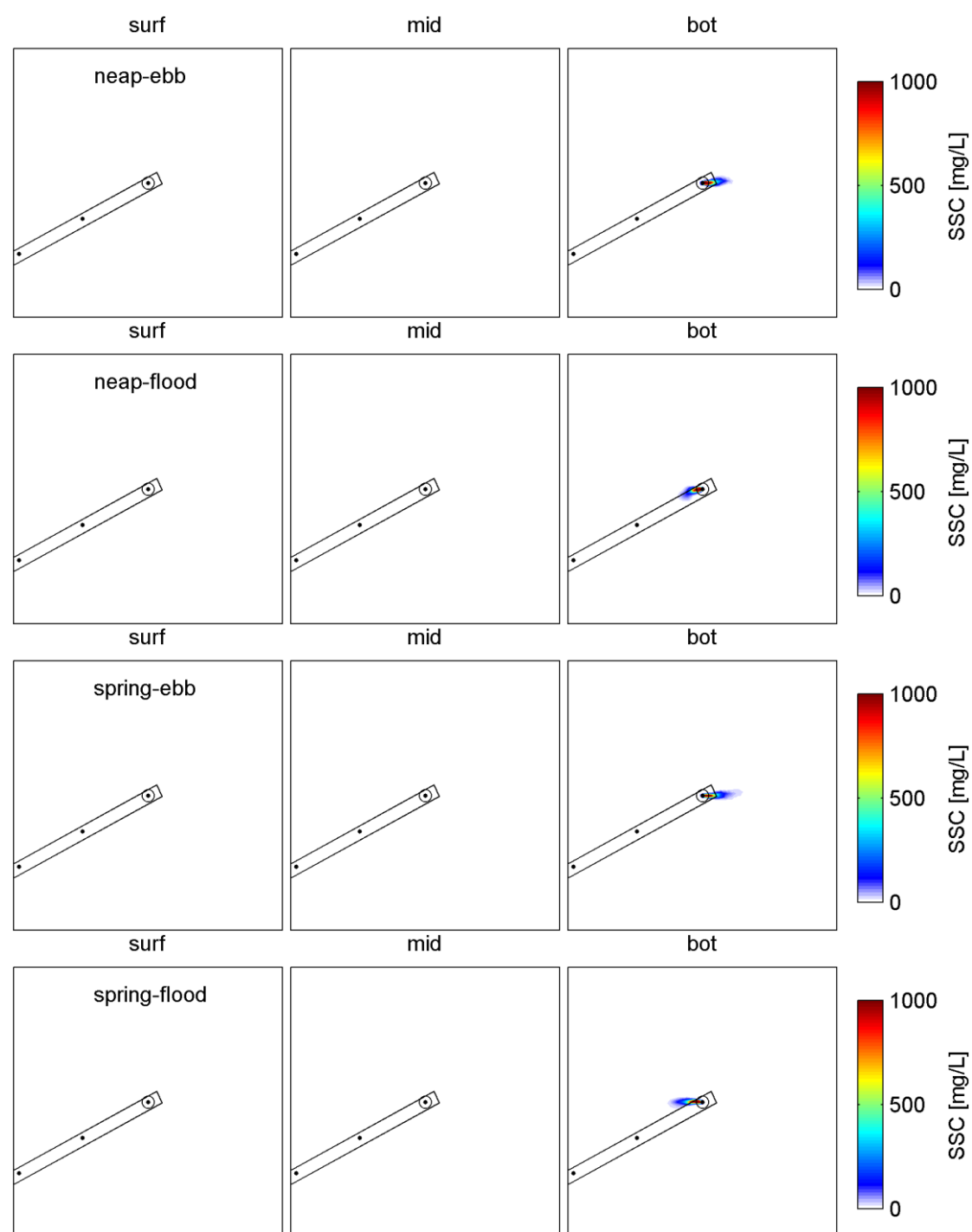


Figure A 1.6 Snapshots of suspended sediment concentrations plumes during dredging at site C11 during peak tidal flows (top to bottom) over the Scenario 2 bathymetry, at three levels in the water column (left to right).

A1.1.3 Existing bathymetry with surge signal

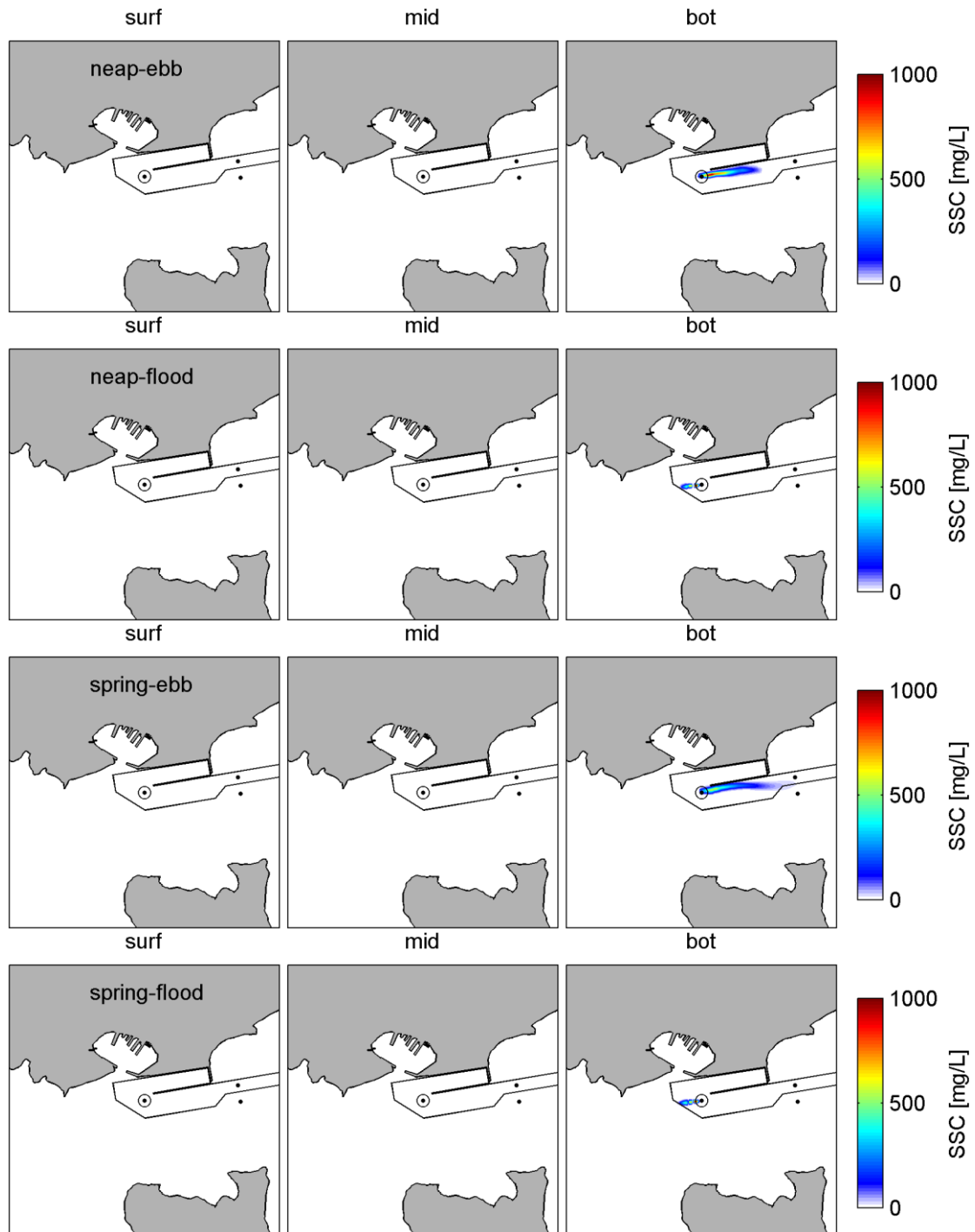


Figure A 1.7 Snapshots of suspended sediment concentrations plumes during dredging at site C1 during peak tidal flows (top to bottom) over the existing bathymetry, including a surge signal, at three levels in the water column (left to right).

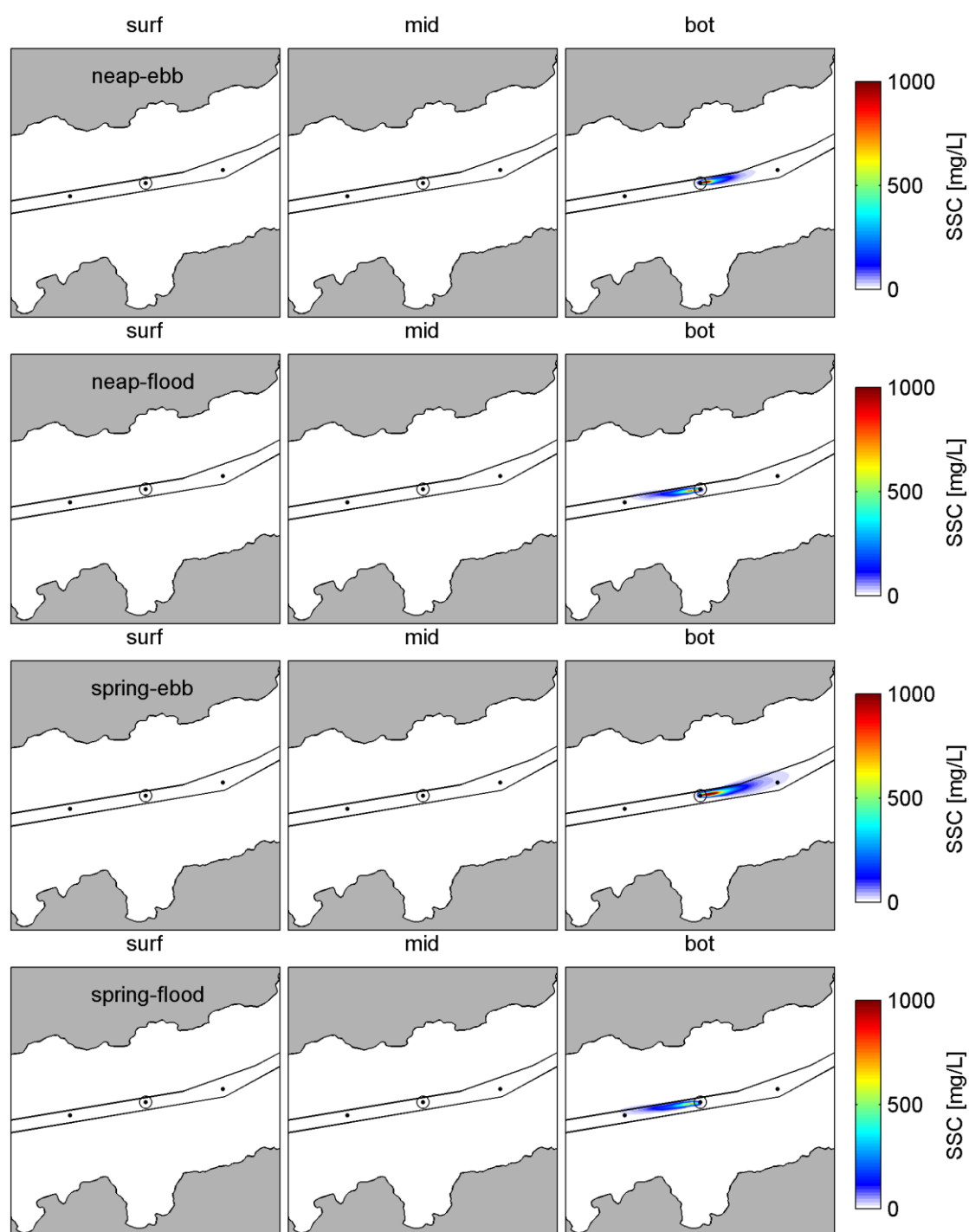


Figure A 1.8 Snapshots of suspended sediment concentrations plumes during dredging at site C5 during peak tidal flows (top to bottom) over the existing bathymetry, including a surge signal, at three levels in the water column (left to right).

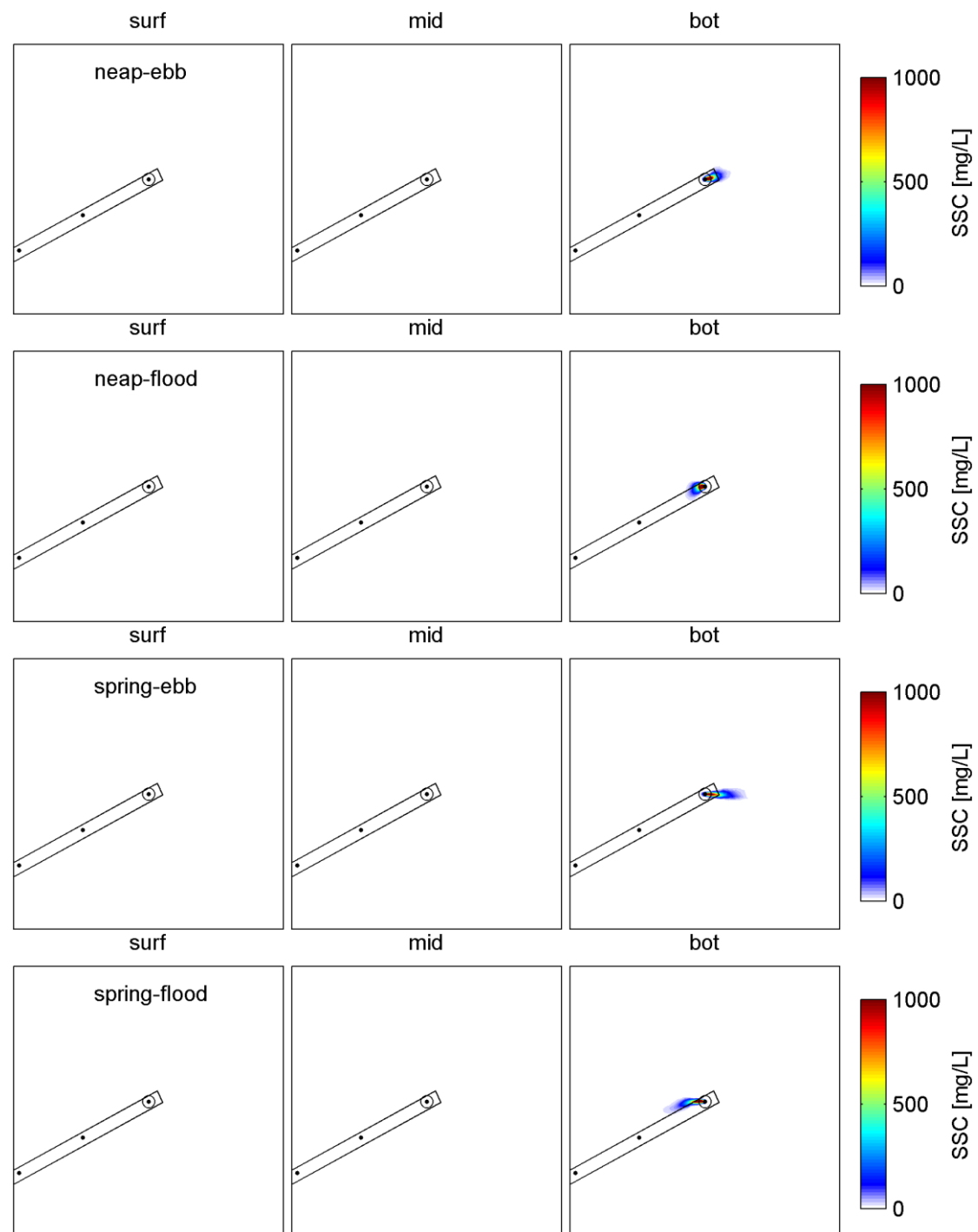


Figure A 1.9 Snapshots of suspended sediment concentrations plumes during dredging at site C11 during peak tidal flows (top to bottom) over the existing bathymetry, including a surge signal, at three levels in the water column (left to right).

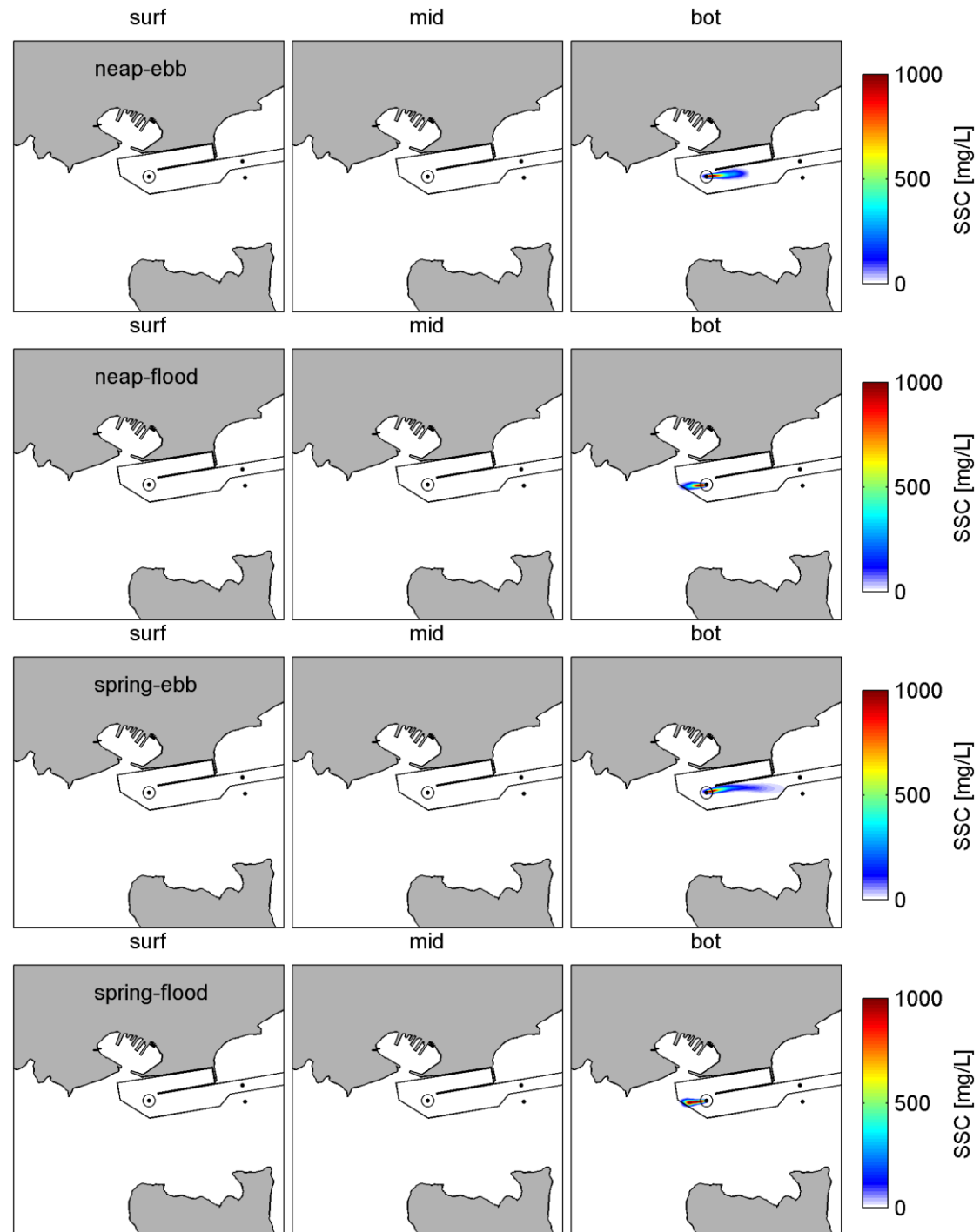
A1.1.4 Scenario 2 bathymetry with surge signal

Figure A 1.10 Snapshots of suspended sediment concentrations plumes during dredging at site C1 during peak tidal flows (top to bottom) over the Scenario 2 bathymetry, including a surge signal, at three levels in the water column (left to right).

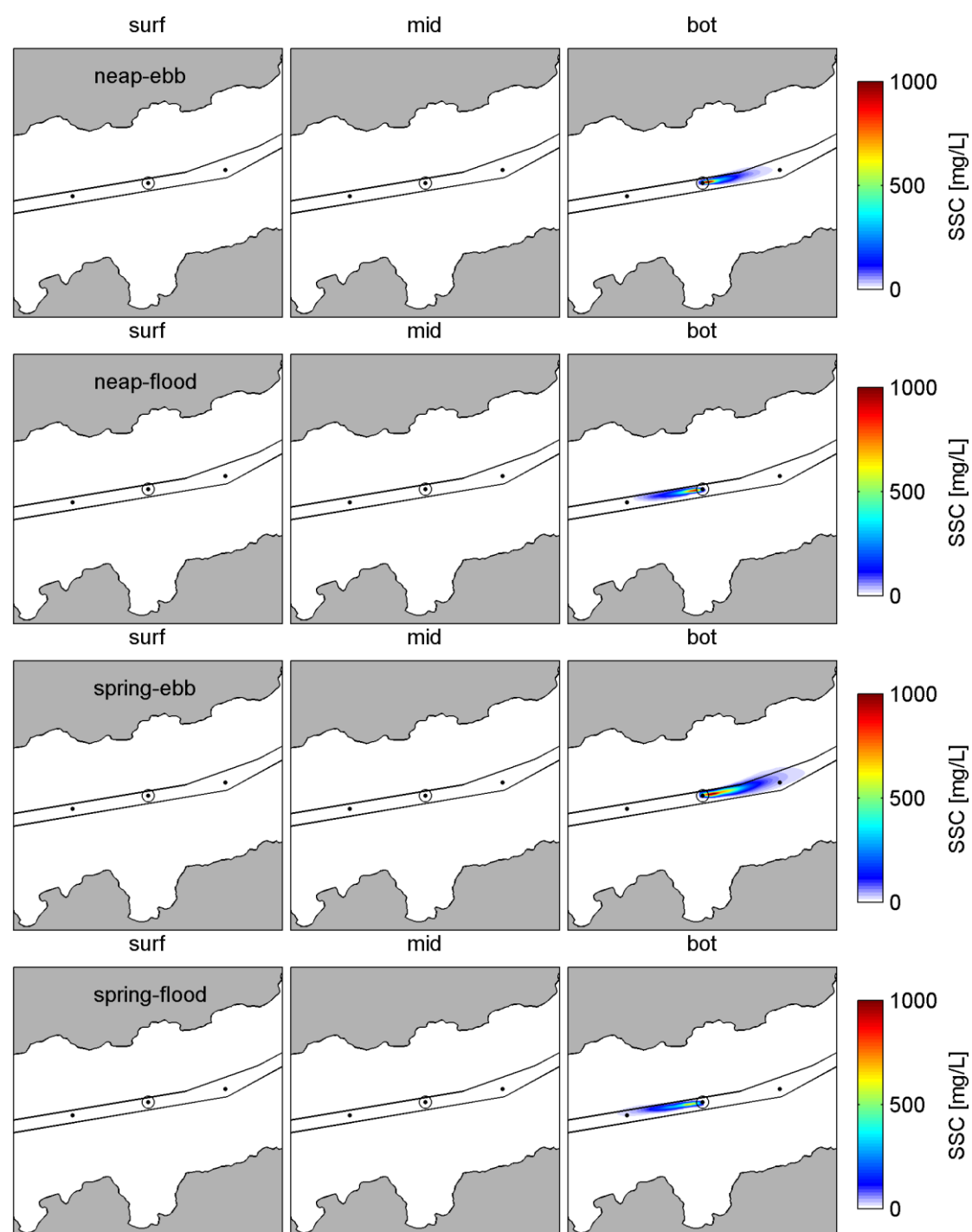


Figure A 1.11 Snapshots of suspended sediment concentrations plumes during dredging at site C5 during peak tidal flows (top to bottom) over the Scenario 2 bathymetry, including a surge signal, at three levels in the water column (left to right).

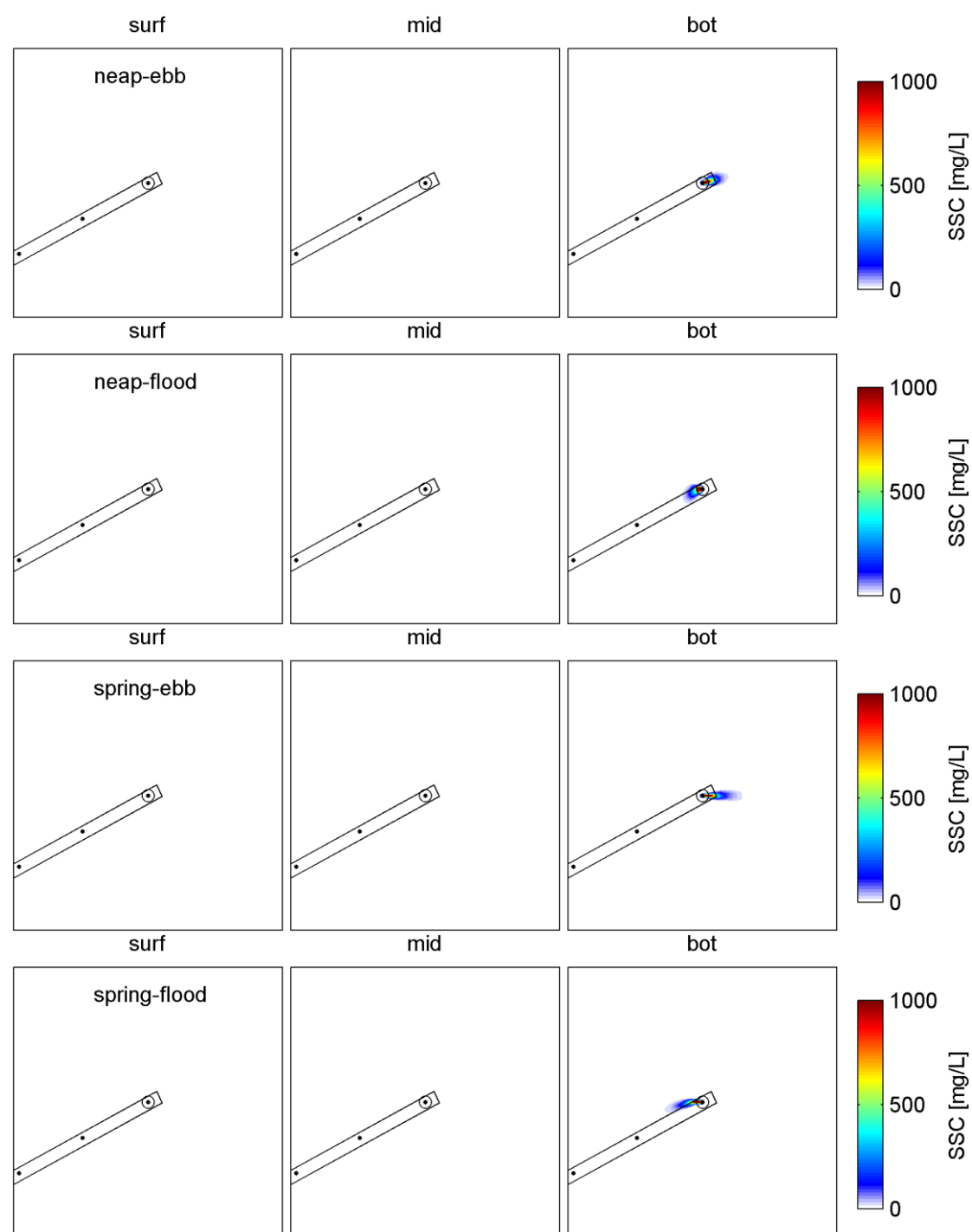


Figure A 1.12 Snapshots of suspended sediment concentrations plumes during dredging at site C11 during peak tidal flows (top to bottom) over the Scenario 2 bathymetry, including a surge signal, at three levels in the water column (left to right).

A1.2 Overflow Mode

A1.2.1 Existing bathymetry

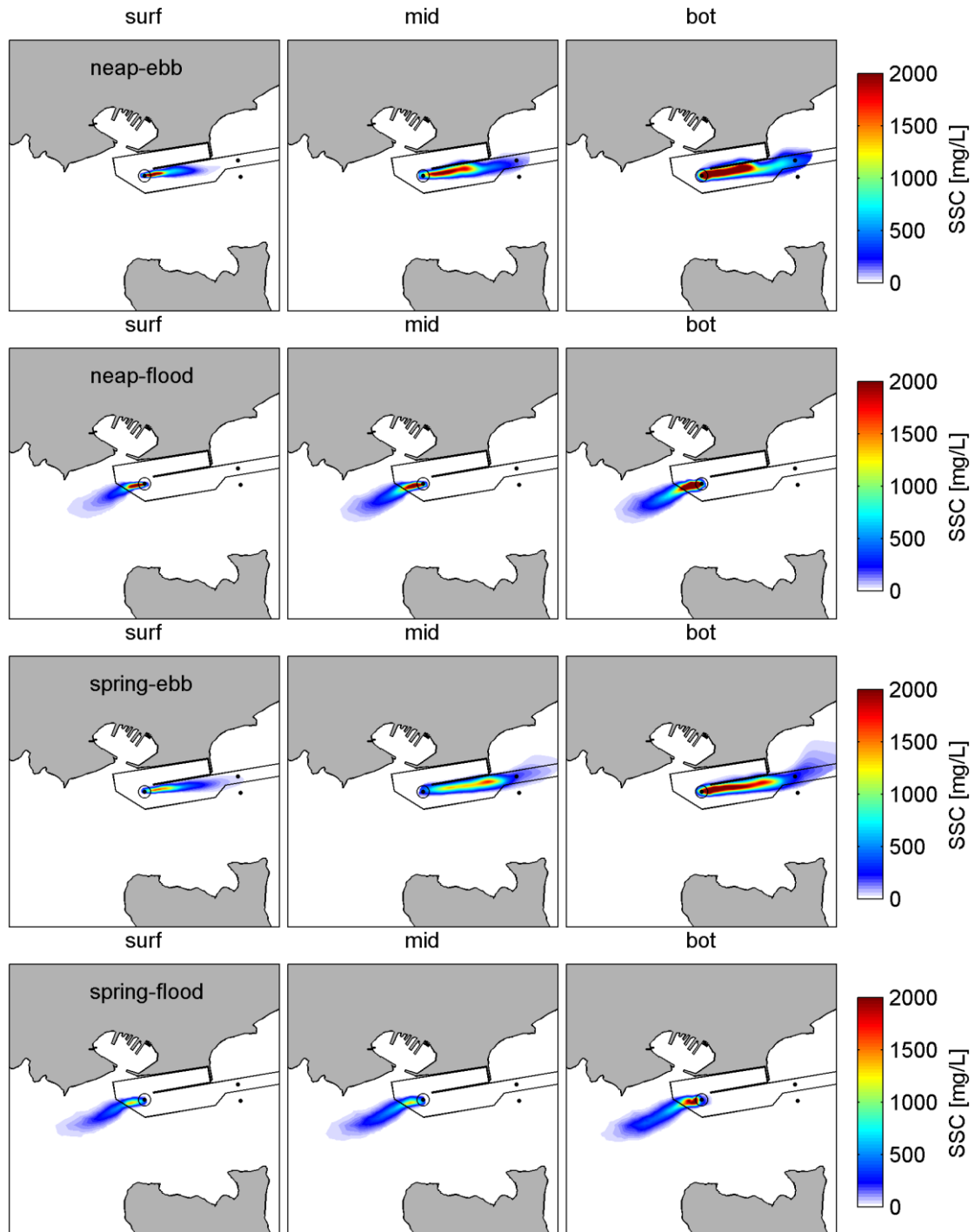


Figure A 1.13 Snapshots of suspended sediment concentrations plumes during overflow at site C1 during peak tidal flows (top to bottom) over the existing bathymetry, at three levels in the water column (left to right).

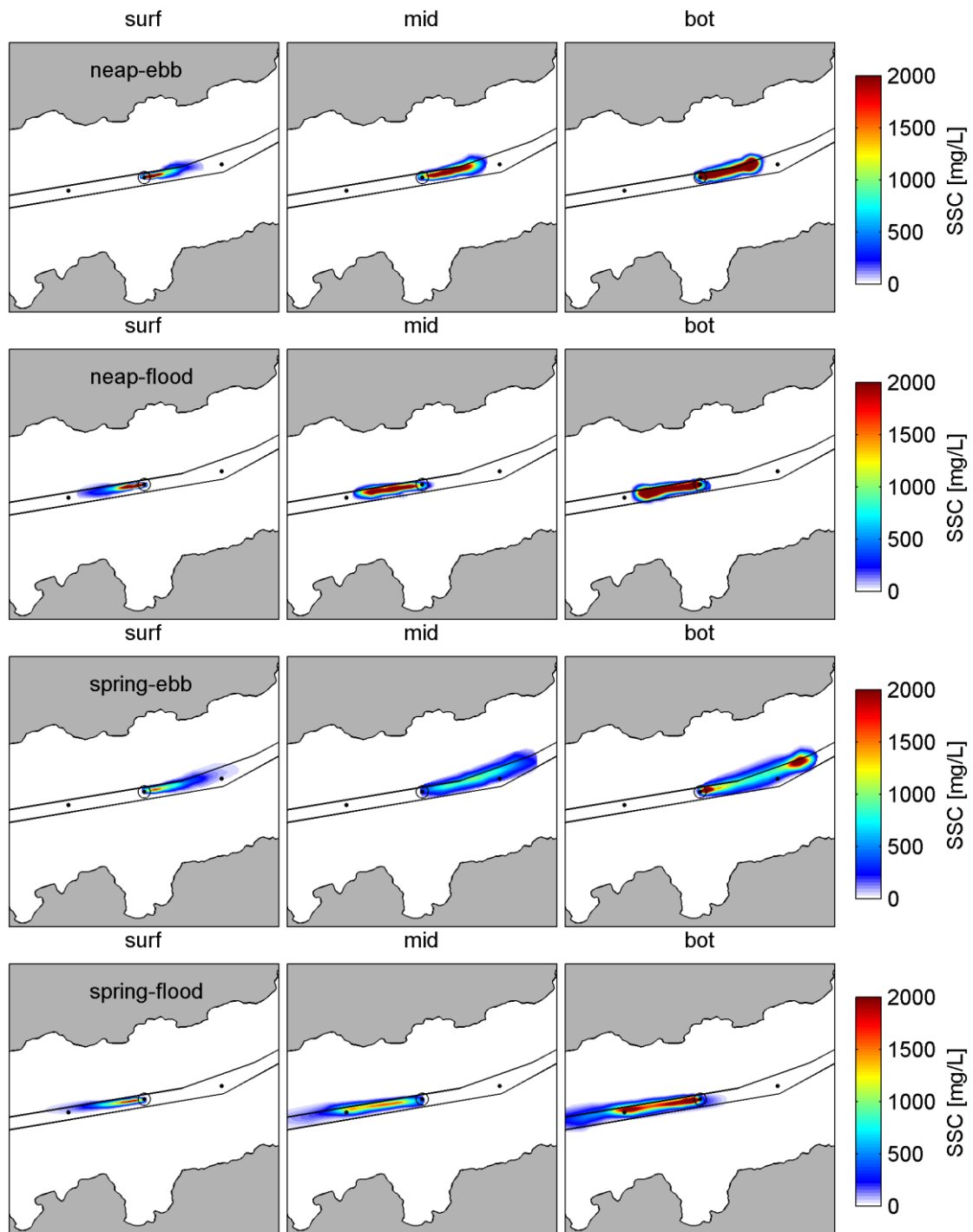


Figure A 1.14 Snapshots of suspended sediment concentrations plumes during overflow at site C5 during peak tidal flows (top to bottom) over the existing bathymetry, at three levels in the water column (left to right).

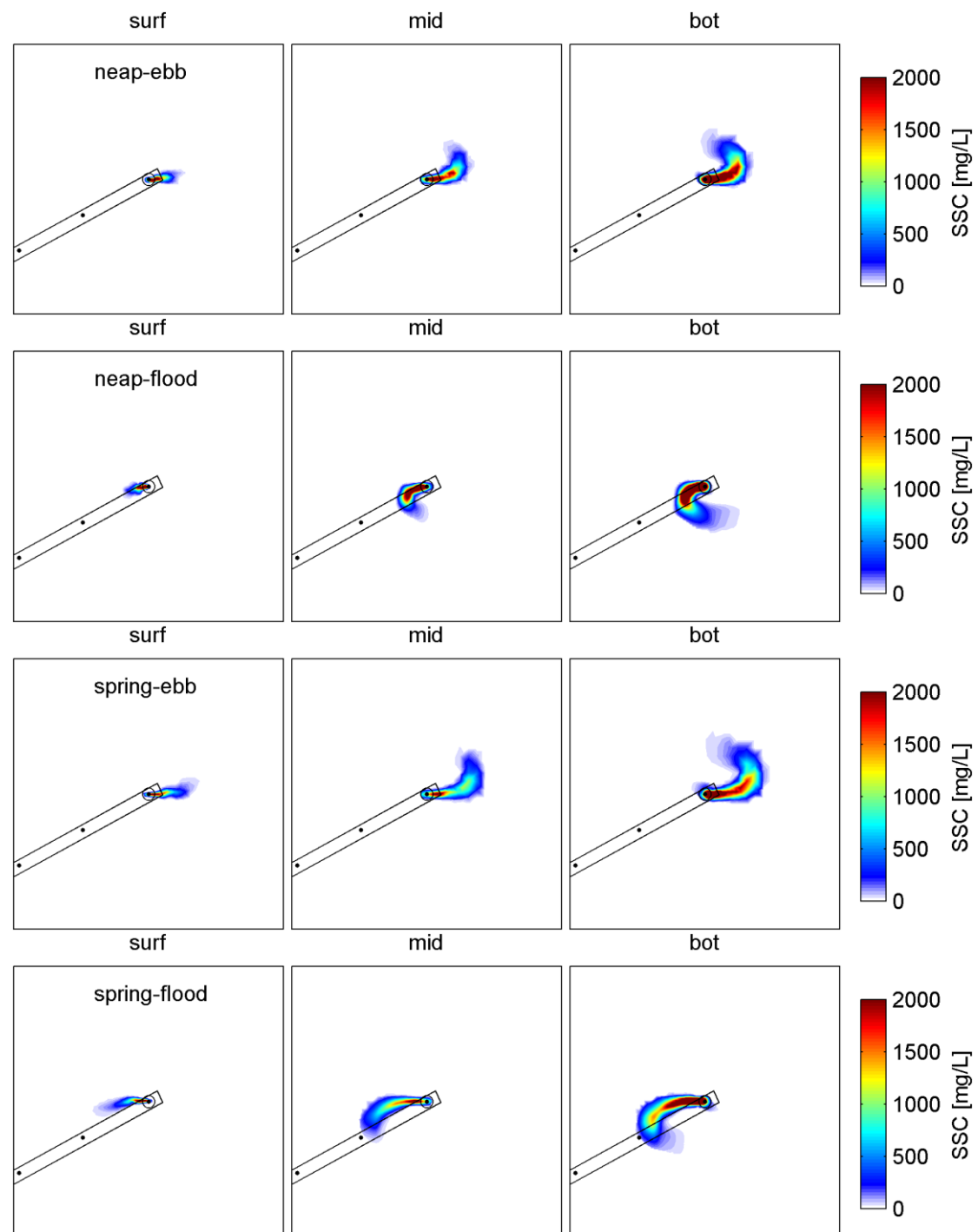


Figure A 1.15 Snapshots of suspended sediment concentrations plumes during overflow at site C11 during peak tidal flows (top to bottom) over the existing bathymetry, at three levels in the water column (left to right).

A1.2.2 Stage3 bathymetry

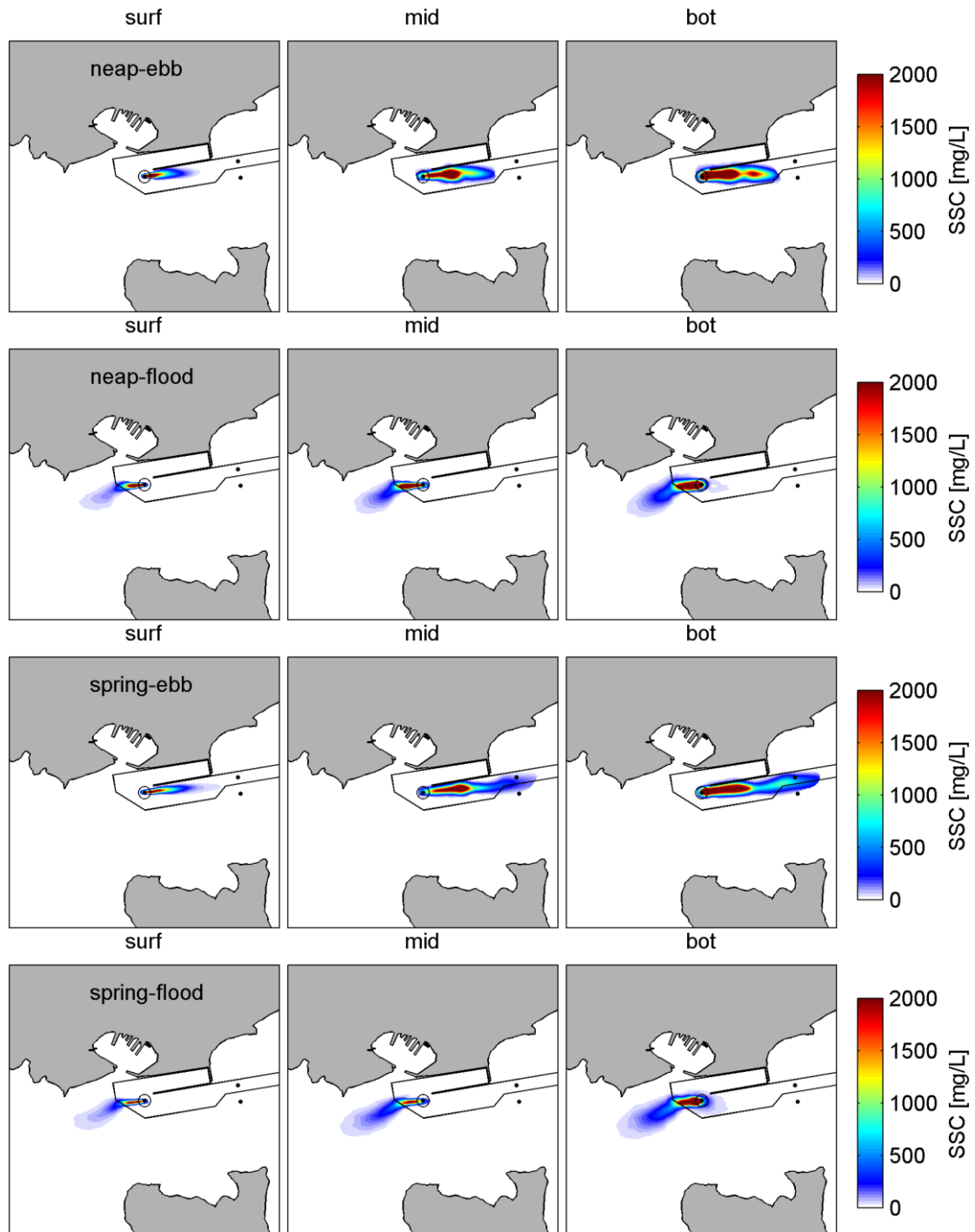


Figure A 1.16 Snapshots of suspended sediment concentrations plumes during overflow at site C1 during peak tidal flows (top to bottom) over the Scenario 2 bathymetry, at three levels in the water column (left to right).

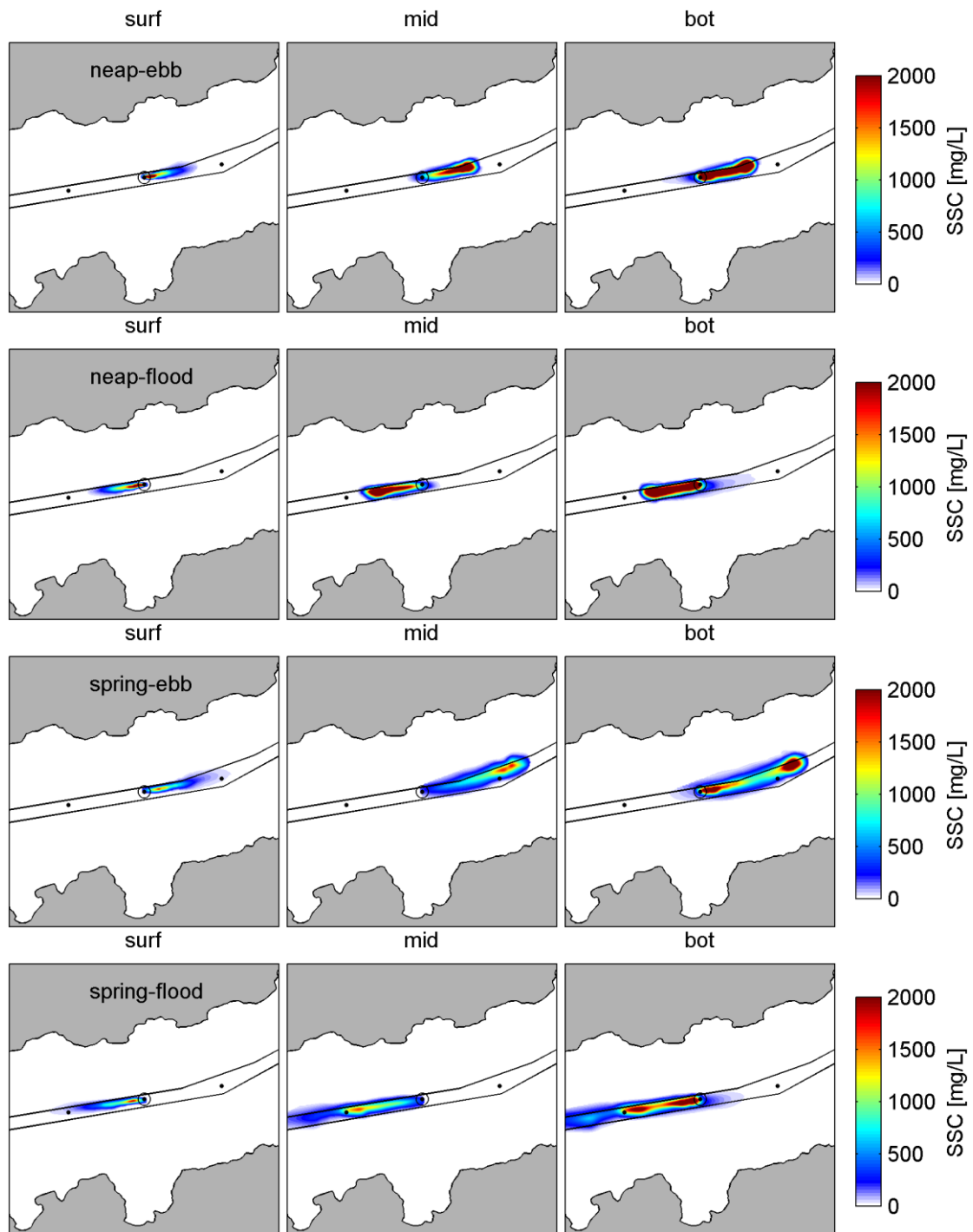


Figure A 1.17 Snapshots of suspended sediment concentrations plumes during overflow at site C5 during peak tidal flows (top to bottom) over the Scenario 2 bathymetry, at three levels in the water column (left to right).

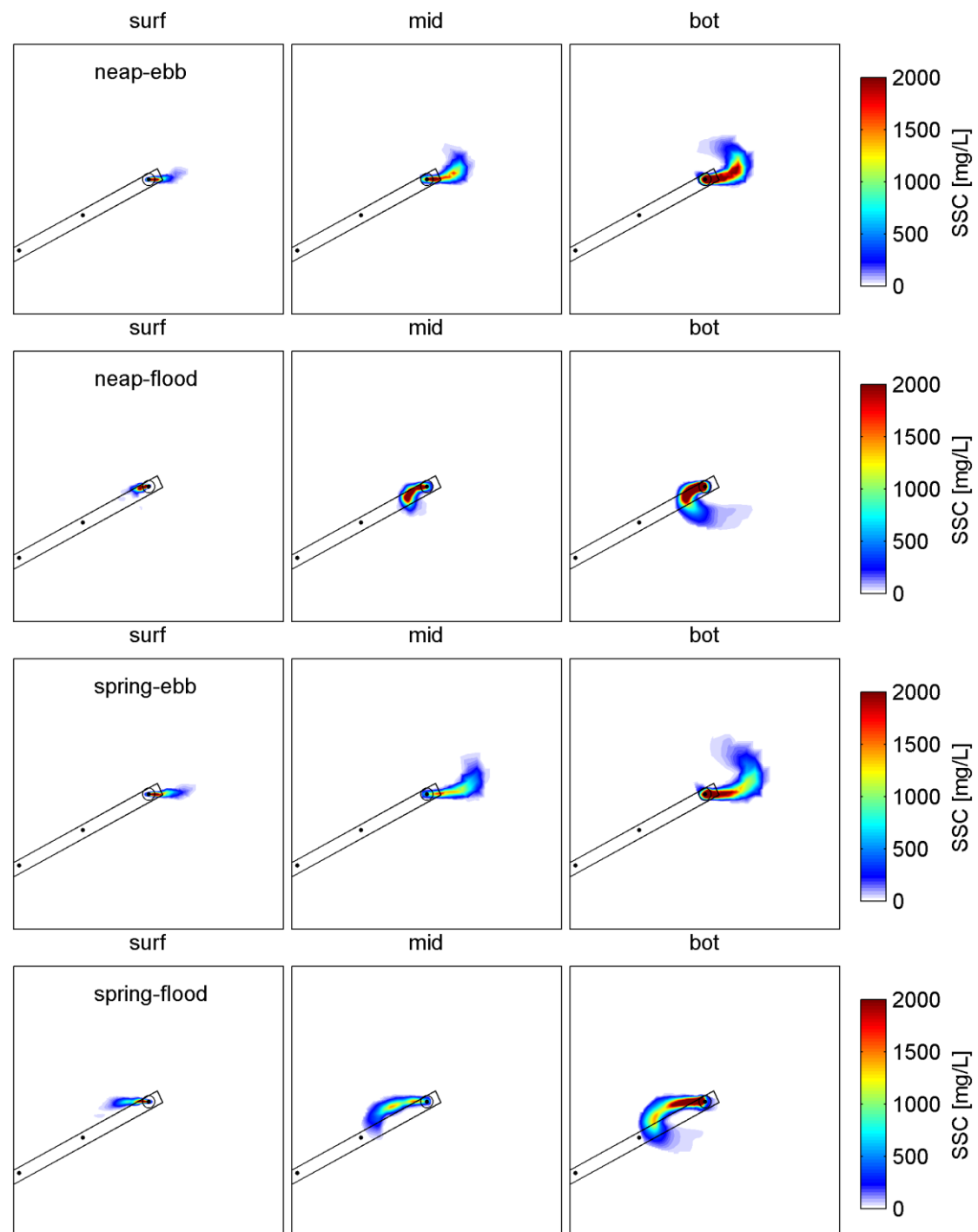


Figure A 1.18 Snapshots of suspended sediment concentrations plumes during overflow at site C11 during peak tidal flows (top to bottom) over the Scenario 2 bathymetry, at three levels in the water column (left to right).

A1.2.3 Existing bathymetry with surge signal

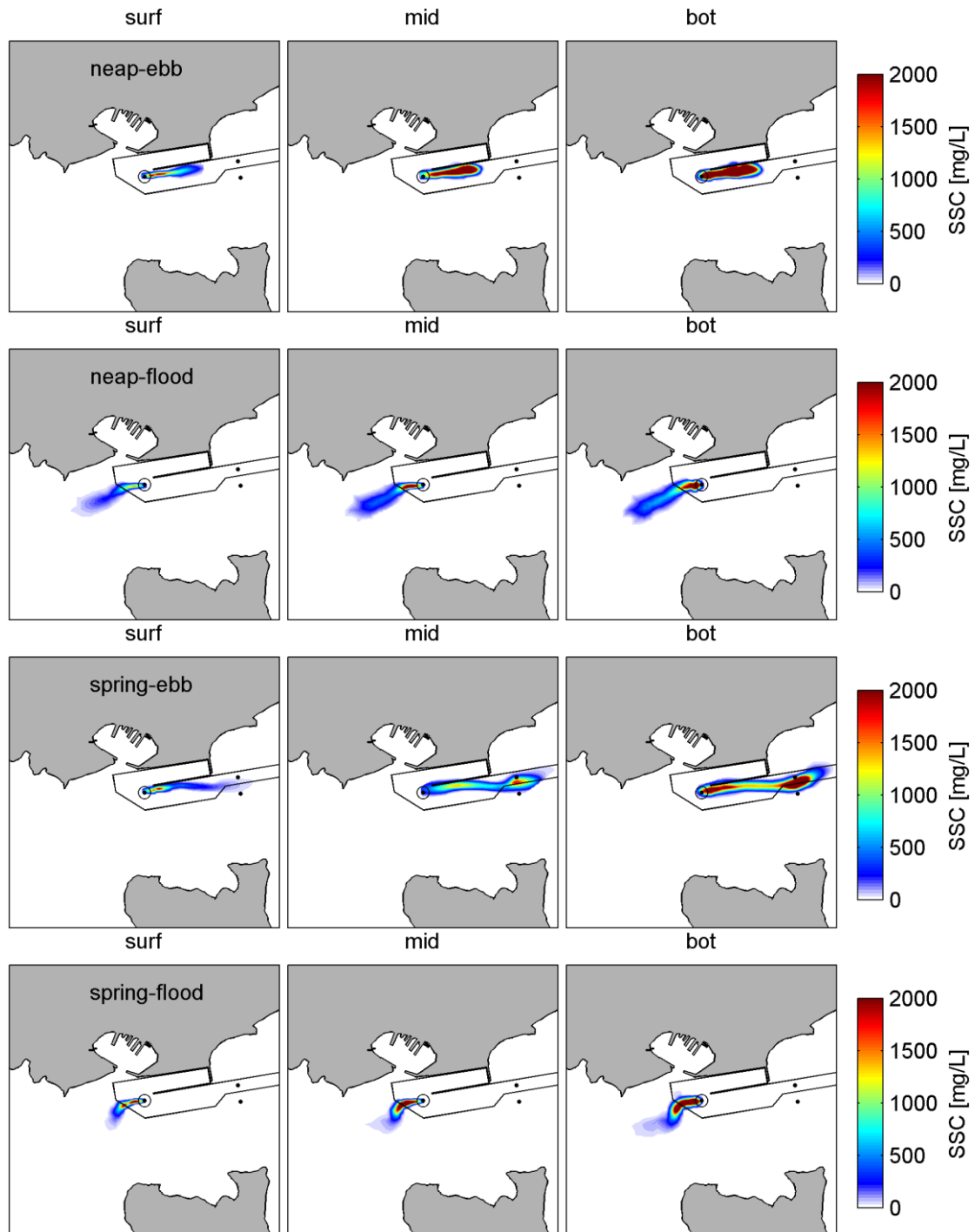


Figure A 1.19 Snapshots of suspended sediment concentrations plumes during overflow at site C1 during peak tidal flows (top to bottom) over the existing bathymetry, including a surge signal, at three levels in the water column (left to right).

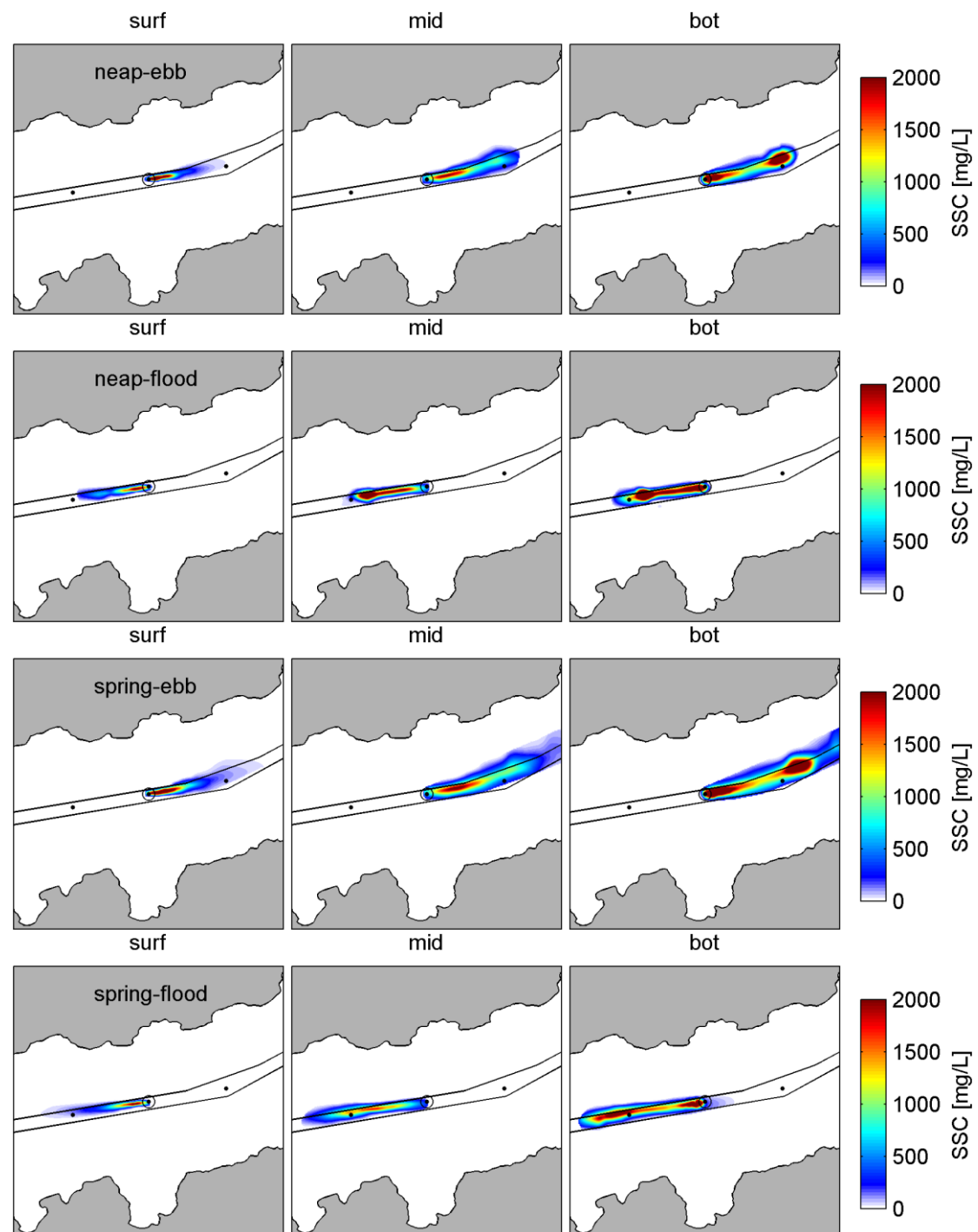


Figure A 1.20 Snapshots of suspended sediment concentrations plumes during overflow at site C5 during peak tidal flows (top to bottom) over the existing bathymetry, including a surge signal, at three levels in the water column (left to right).

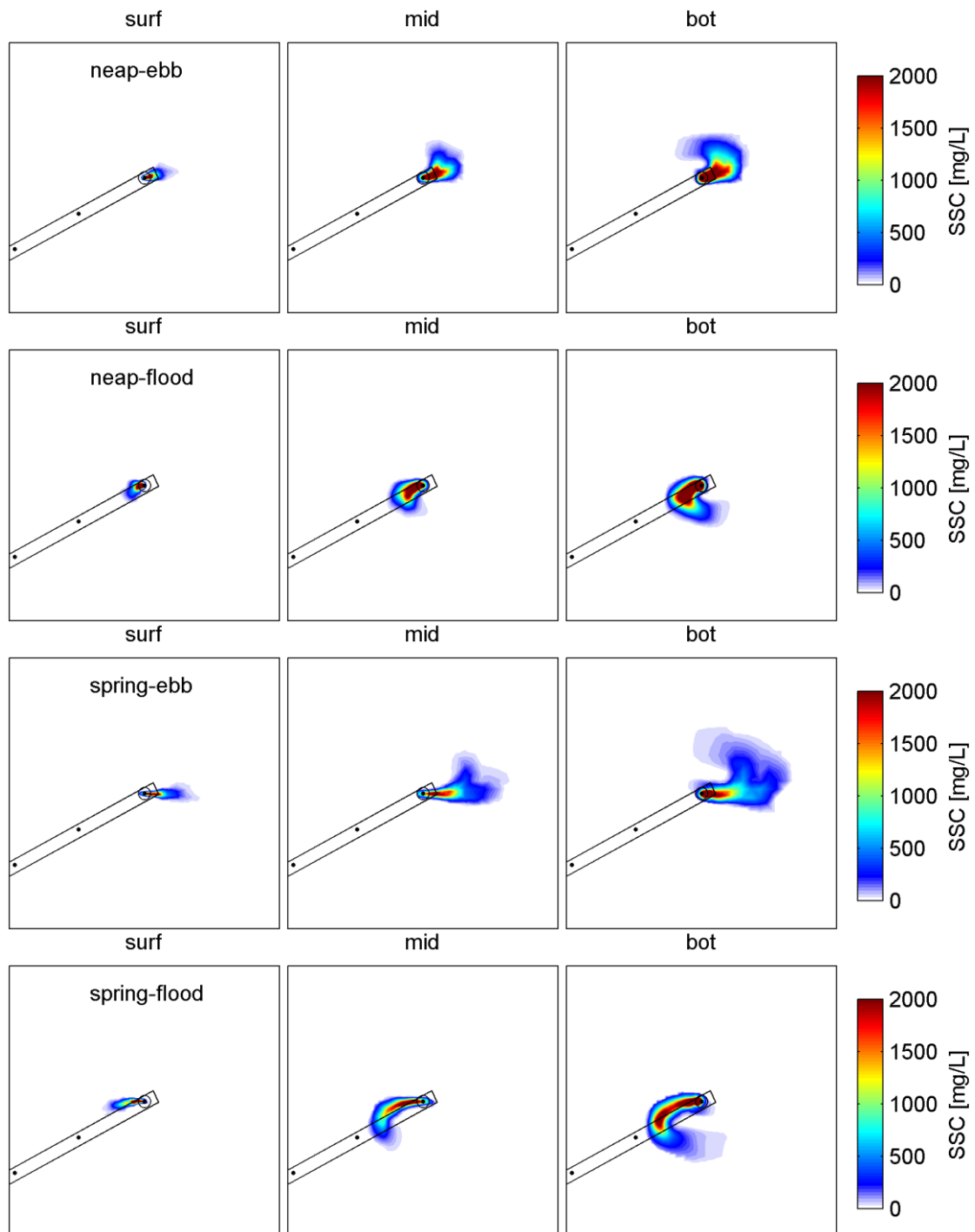


Figure A 1.21 Snapshots of suspended sediment concentrations plumes during overflow at site C11 during peak tidal flows (top to bottom) over the existing bathymetry, including a surge signal, at three levels in the water column (left to right).

A1.2.4 Scenario 2 bathymetry with surge signal

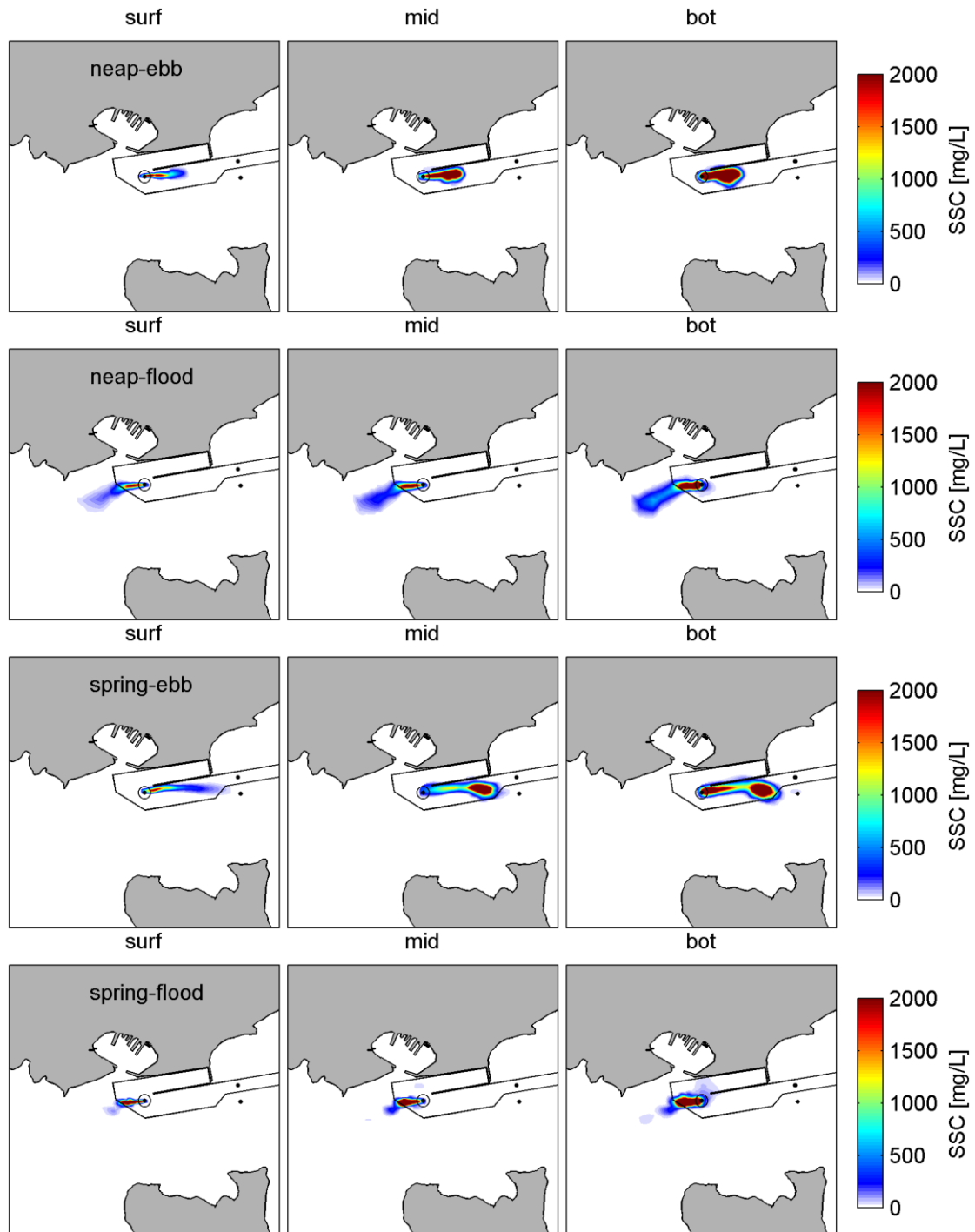


Figure A 1.22 Snapshots of suspended sediment concentrations plumes during overflow at site C1 during peak tidal flows (top to bottom) over the Scenario 2 bathymetry, including a surge signal, at three levels in the water column (left to right).

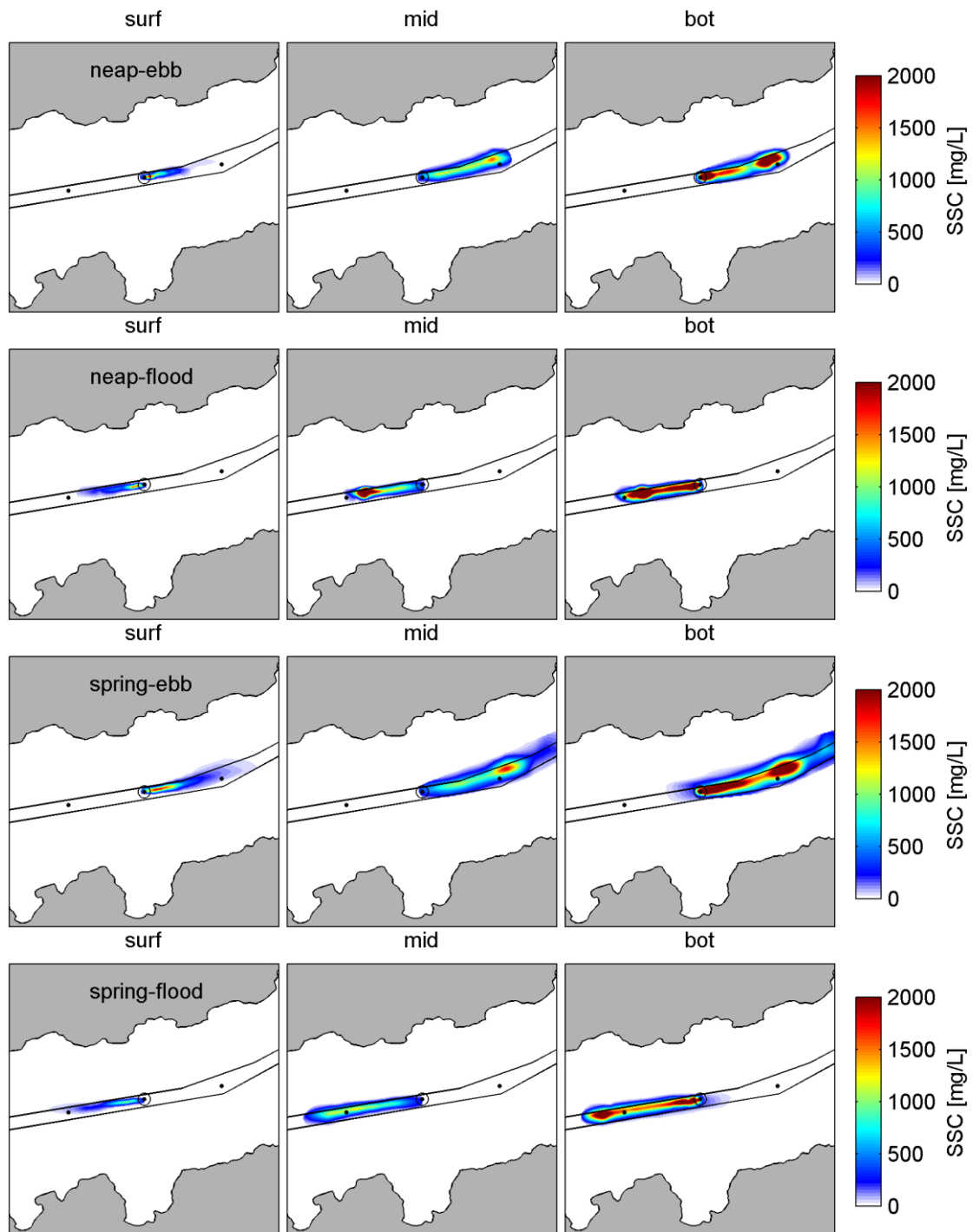


Figure A 1.23 Snapshots of suspended sediment concentrations plumes during overflow at site C5 during peak tidal flows (top to bottom) over the Scenario 2 bathymetry, including a surge signal, at three levels in the water column (left to right).

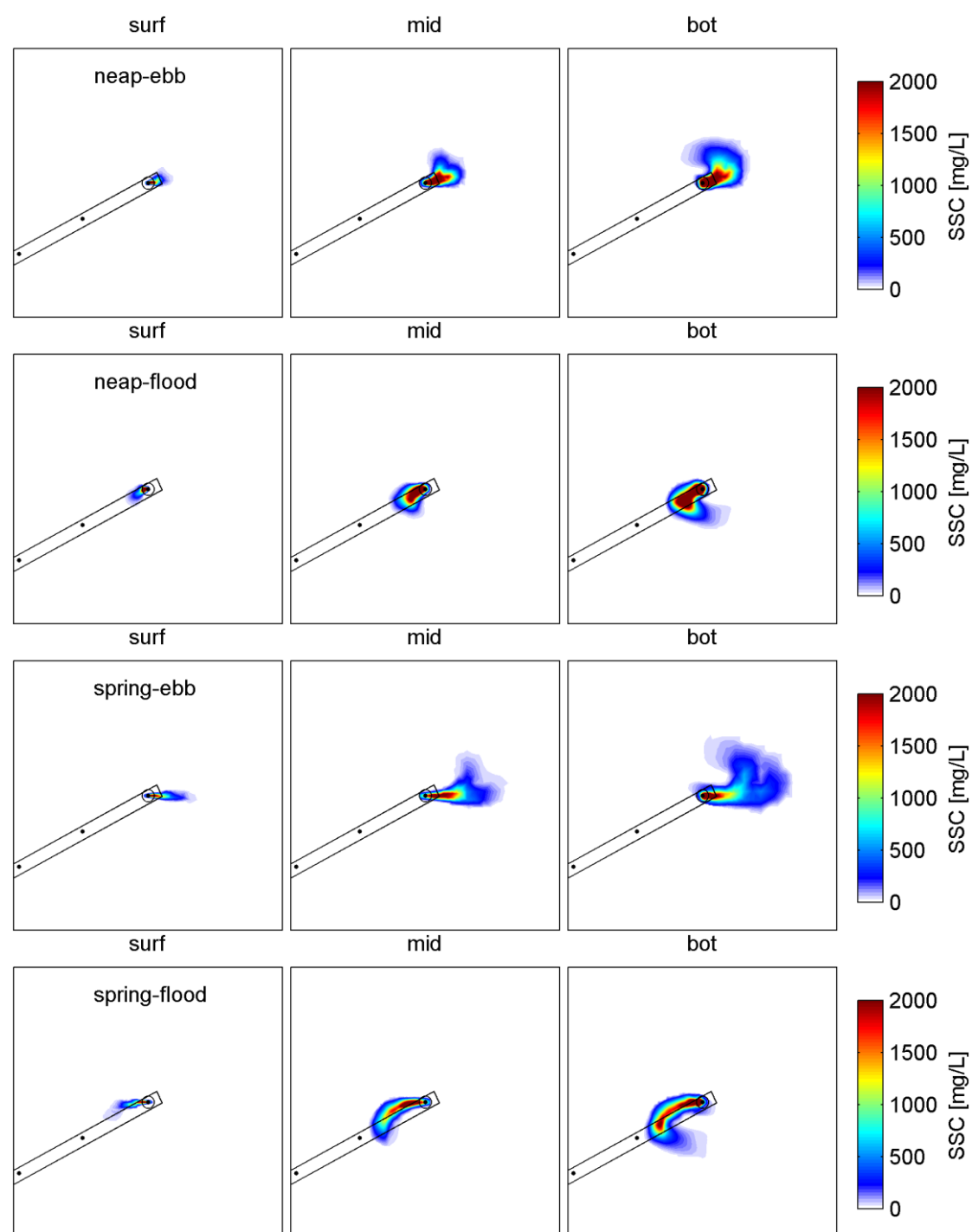


Figure A 1.24 Snapshots of suspended sediment concentrations plumes during overflow at site C11 during peak tidal flows (top to bottom) over the Scenario 2 bathymetry, including a surge signal, at three levels in the water column (left to right).

A2. PROBABILISTIC DREDGING PLUMES

A2.1 Dredging Mode

A2.1.1 Existing bathymetry

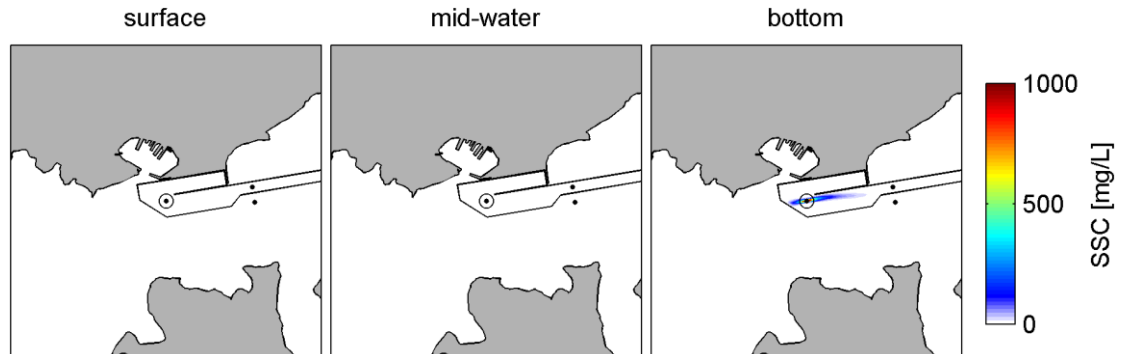


Figure A 2.1 Probabilistic SSC plumes during dredging at site C1, over the existing bathymetry, at three levels in the water column (left to right).

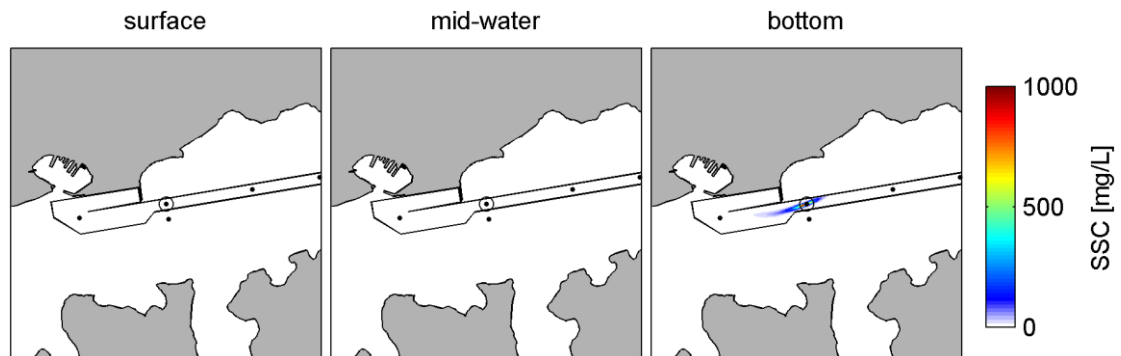


Figure A 2.2 Probabilistic SSC plumes during dredging at site C2, over the existing bathymetry, at three levels in the water column (left to right).

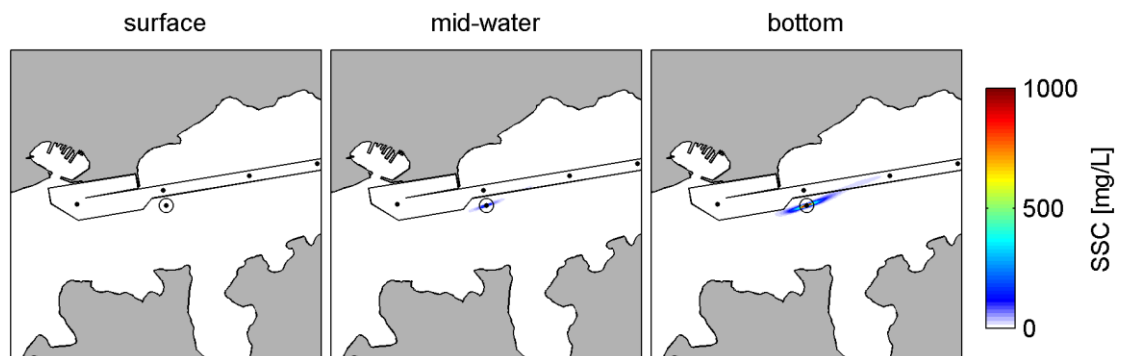


Figure A 2.3 Probabilistic SSC plumes during dredging at site C2_2, over the existing bathymetry, at three levels in the water column (left to right).

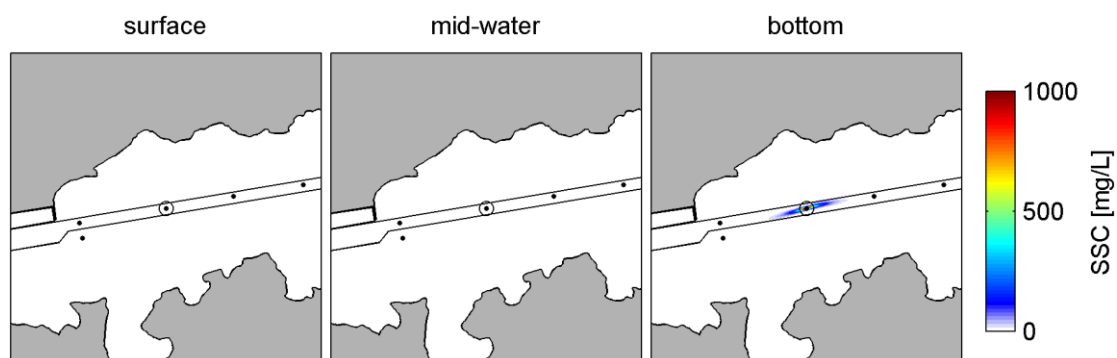


Figure A 2.4 Probabilistic SSC plumes during dredging at site C3, over the existing bathymetry, at three levels in the water column (left to right).

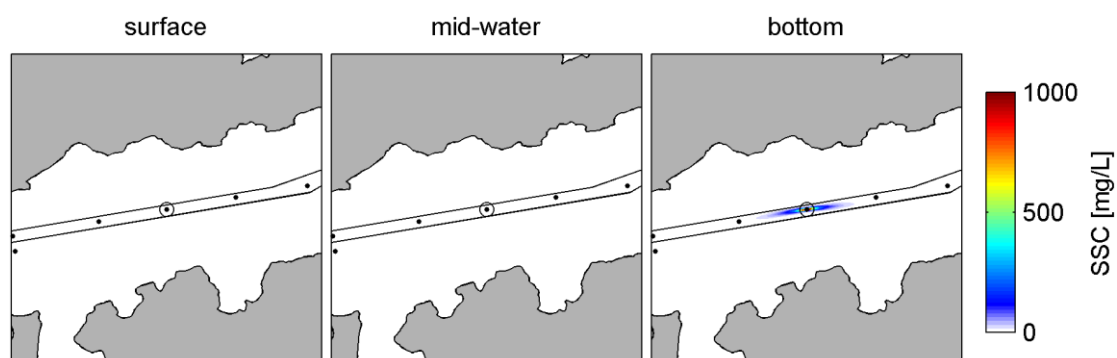


Figure A 2.5 Probabilistic SSC plumes during dredging at site C4, over the existing bathymetry, at three levels in the water column (left to right).

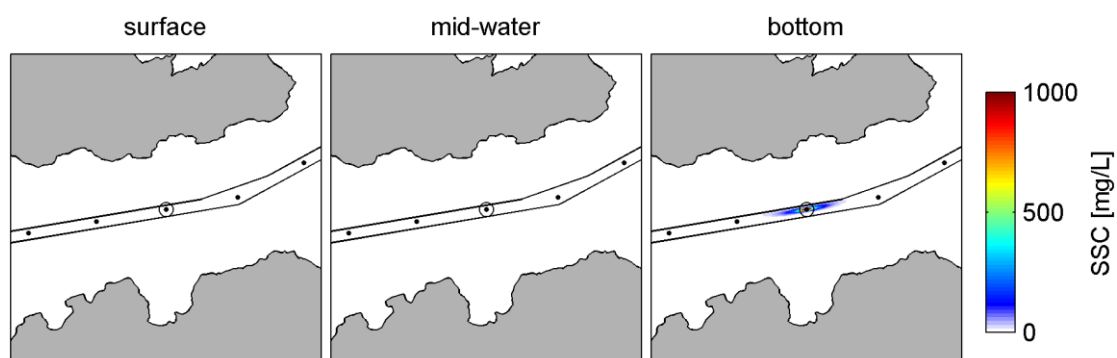


Figure A 2.6 Probabilistic SSC plumes during dredging at site C5, over the existing bathymetry, at three levels in the water column (left to right).

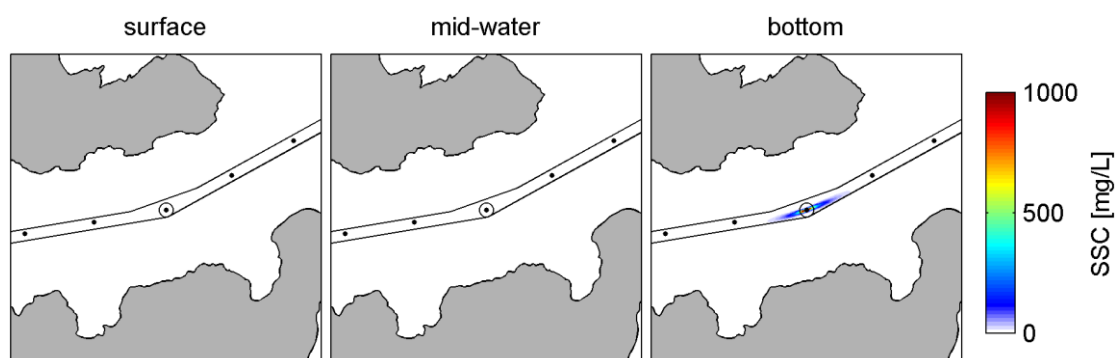


Figure A 2.7 Probabilistic SSC plumes during dredging at site C6, over the existing bathymetry, at three levels in the water column (left to right).

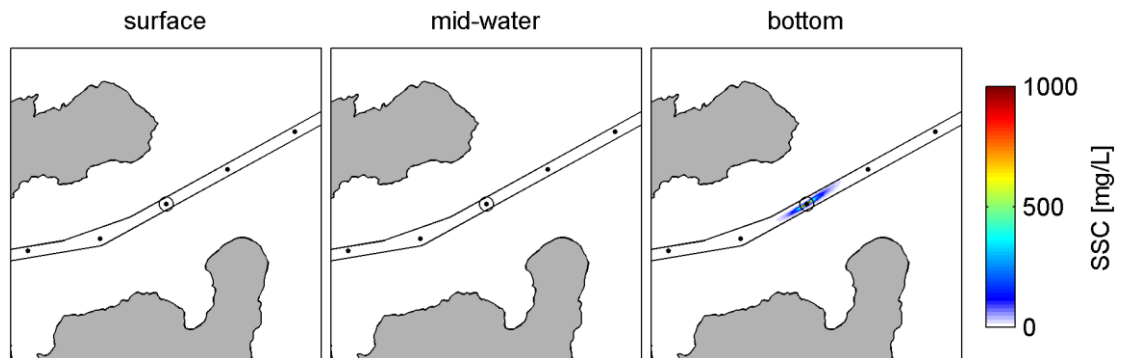


Figure A 2.8 Probabilistic SSC plumes during dredging at site C7, over the existing bathymetry, at three levels in the water column (left to right).

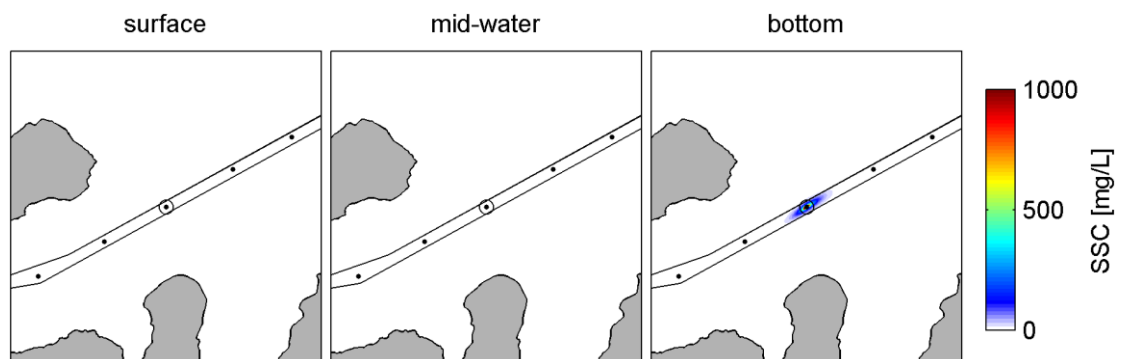


Figure A 2.9 Probabilistic SSC plumes during dredging at site C8, over the existing bathymetry, at three levels in the water column (left to right).

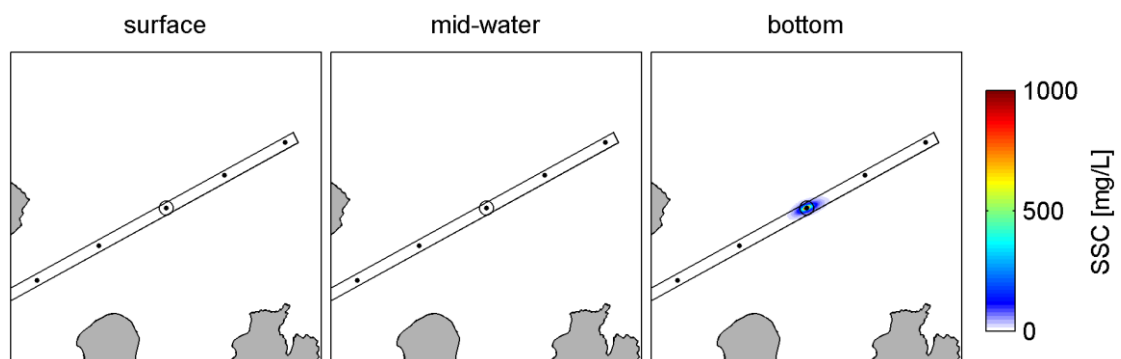


Figure A 2.10 Probabilistic SSC plumes during dredging at site C9, over the existing bathymetry, at three levels in the water column (left to right).

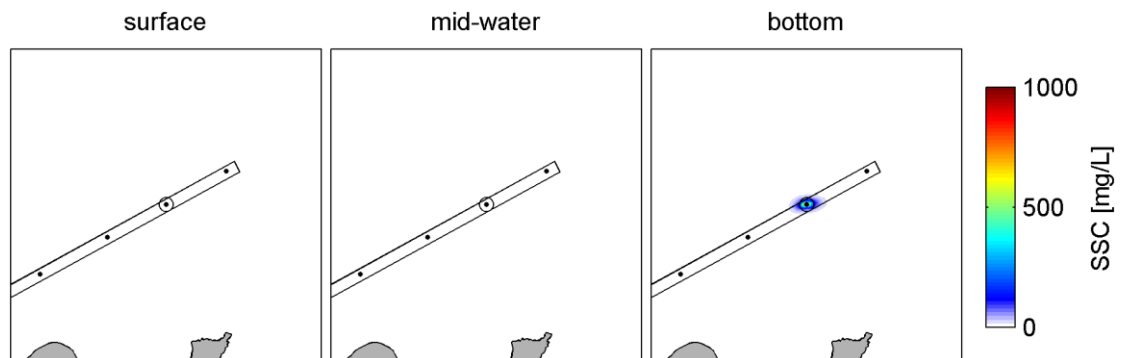


Figure A 2.11 Probabilistic SSC plumes during dredging at site C10, over the existing bathymetry, at three levels in the water column (left to right).

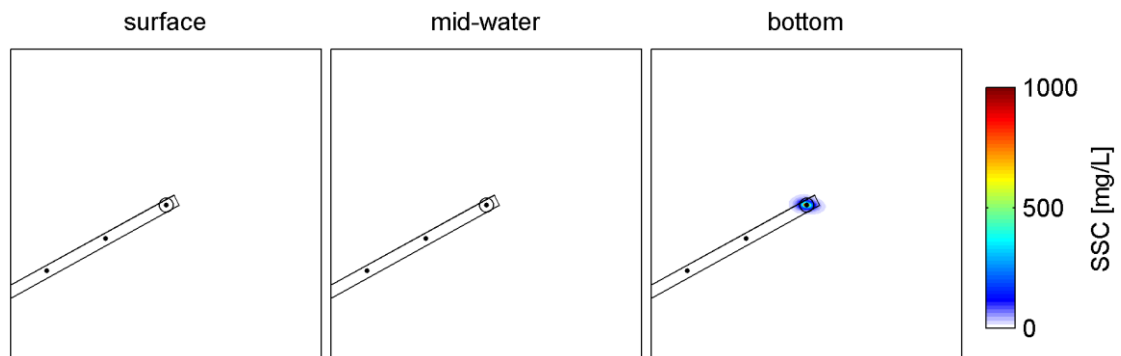


Figure A 2.12 Probabilistic SSC plumes during dredging at site C11, over the existing bathymetry, at three levels in the water column (left to right).

A2.1.2 Scenario 2 bathymetry

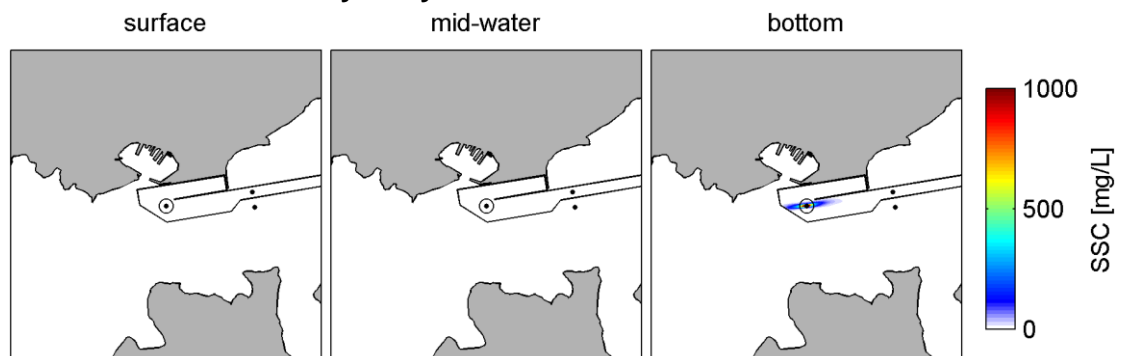


Figure A 2.13 Probabilistic SSC plumes during dredging at site C1, over the Scenario 2 bathymetry, at three levels in the water column (left to right).

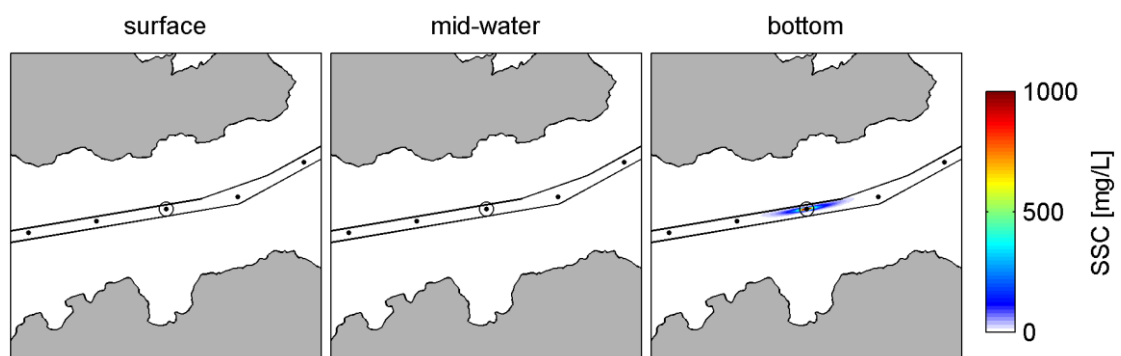


Figure A 2.14 Probabilistic SSC plumes during dredging at site C5, over the Scenario 2 bathymetry, at three levels in the water column (left to right).

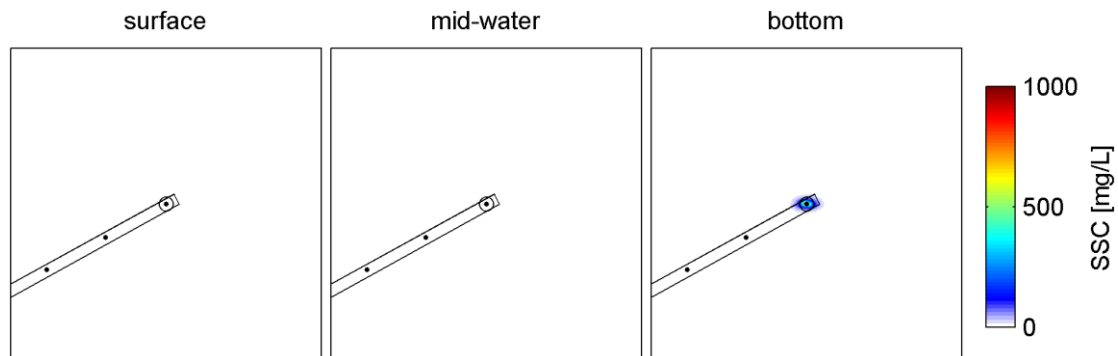


Figure A 2.15 Probabilistic SSC plumes during dredging at site C11, over the Scenario 2 bathymetry, at three levels in the water column (left to right).

A2.1.3 Existing bathymetry with surge signal

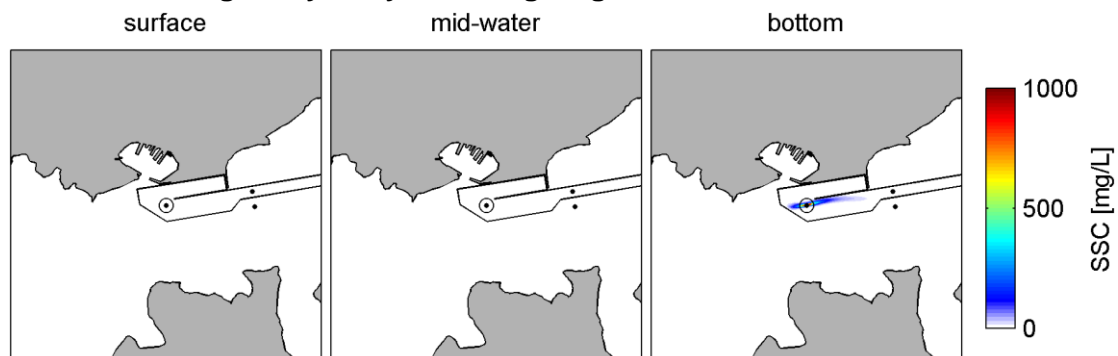


Figure A 2.16 Probabilistic SSC plumes during dredging at site C1, over the existing bathymetry, including a surge signal, at three levels in the water column (left to right)

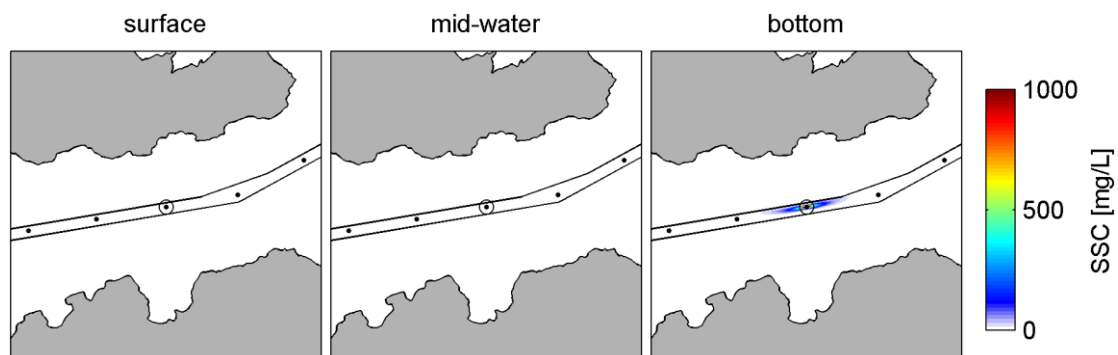


Figure A 2.17 Probabilistic SSC plumes during dredging at site C5, over the existing bathymetry, including a surge signal, at three levels in the water column (left to right).

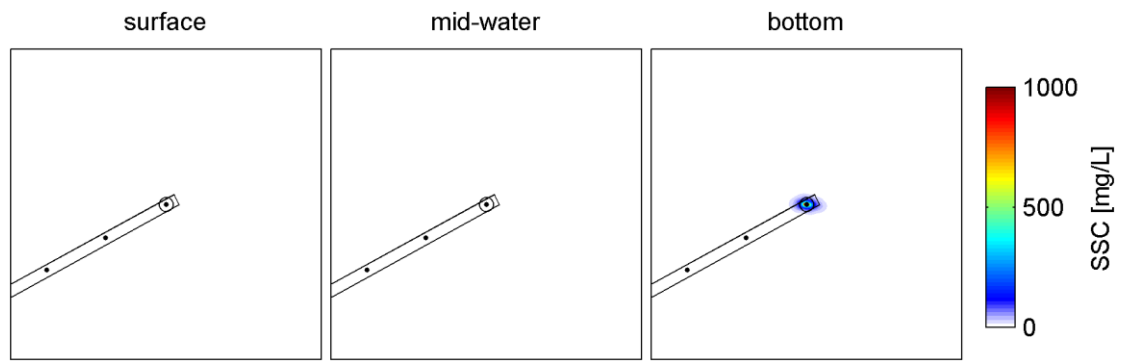


Figure A 2.18 Probabilistic SSC plumes during dredging at site C11, over the existing bathymetry, including a surge signal, at three levels in the water column (left to right).

Scenario 2 bathymetry with surge signal

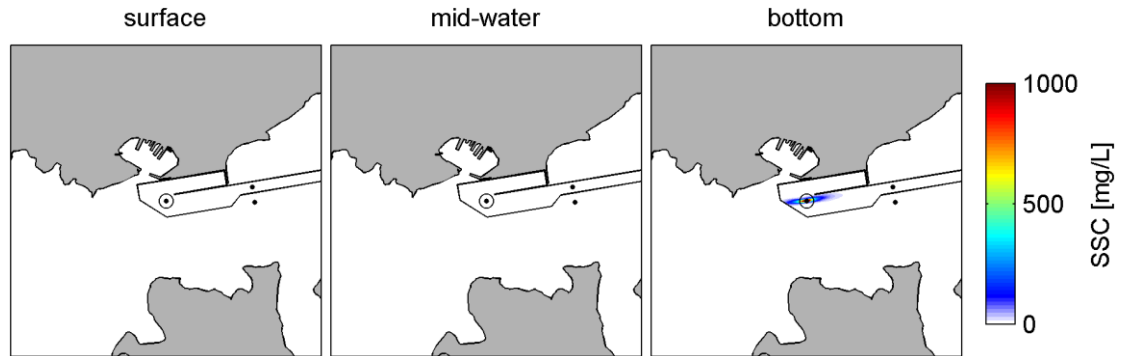


Figure A 2.19 Probabilistic SSC plumes during dredging at site C1, over the Scenario 2 bathymetry, including a surge signal, at three levels in the water column (left to right).

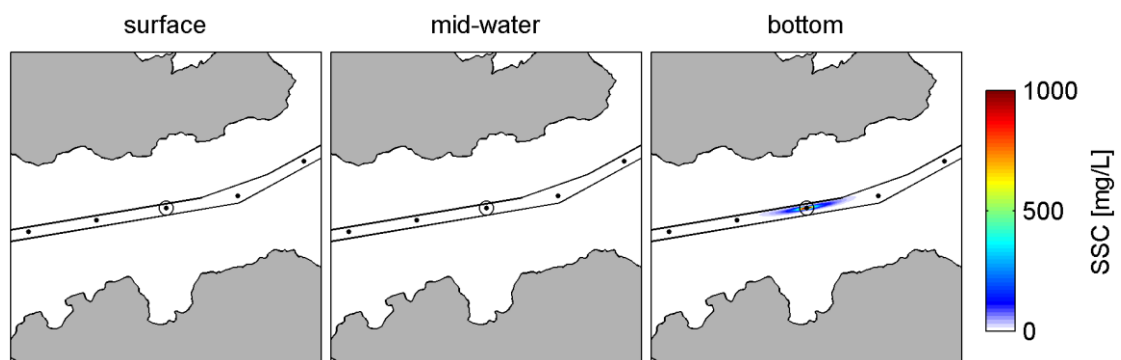


Figure A 2.20 Probabilistic SSC plumes during dredging at site C5, over the Scenario 2 bathymetry, including a surge signal, at three levels in the water column (left to right).

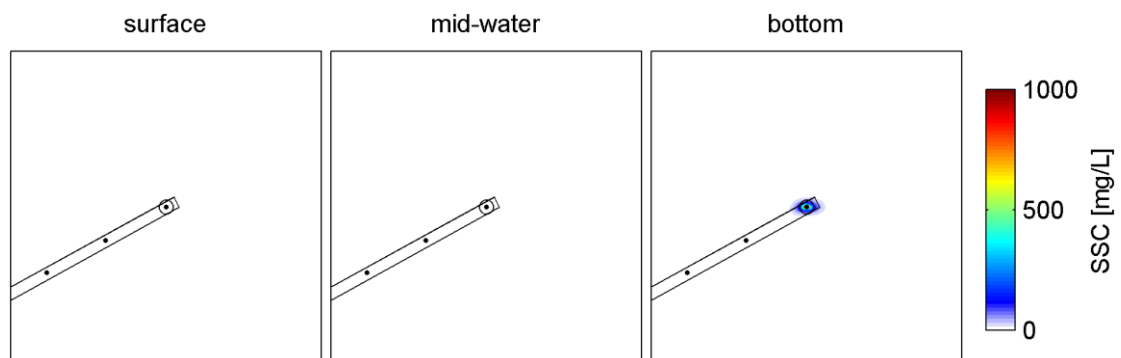


Figure A 2.21 Probabilistic SSC plumes during dredging at site C11, over the Scenario 2 bathymetry, including a surge signal, at three levels in the water column (left to right).

A2.2 Overflow Mode

A2.2.1 Existing bathymetry

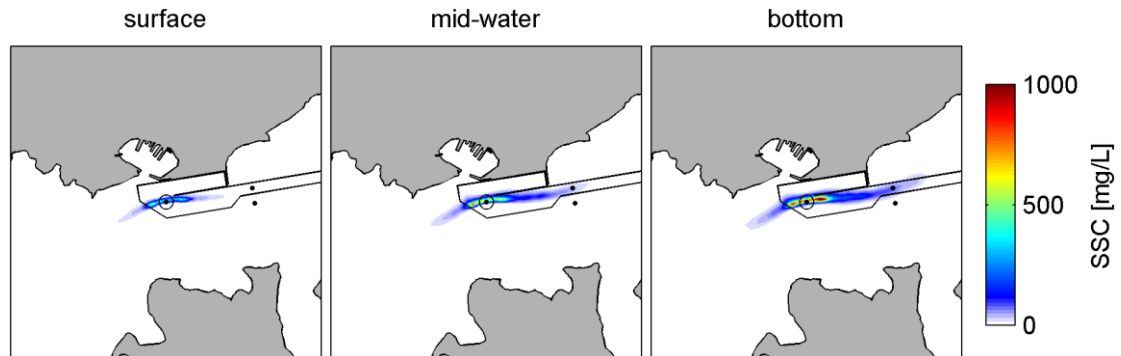


Figure A 2.22 Probabilistic SSC plumes during a 10-minute overflow phase at site C1, over the existing bathymetry, at three levels in the water column (left to right).

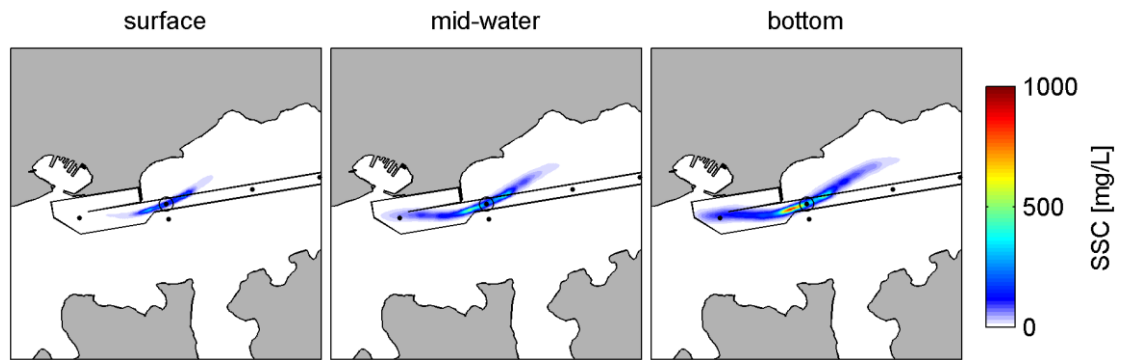


Figure A 2.23 Probabilistic SSC plumes during a 10-minute overflow phase at site C2, over the existing bathymetry, at three levels in the water column (left to right).

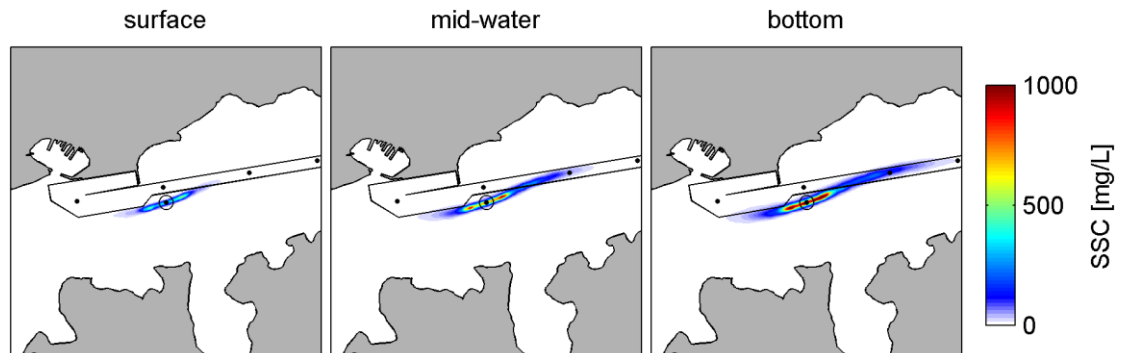


Figure A 2.24 Probabilistic SSC plumes during a 10-minute overflow phase at site C2_2, over the existing bathymetry, at three levels in the water column (left to right).

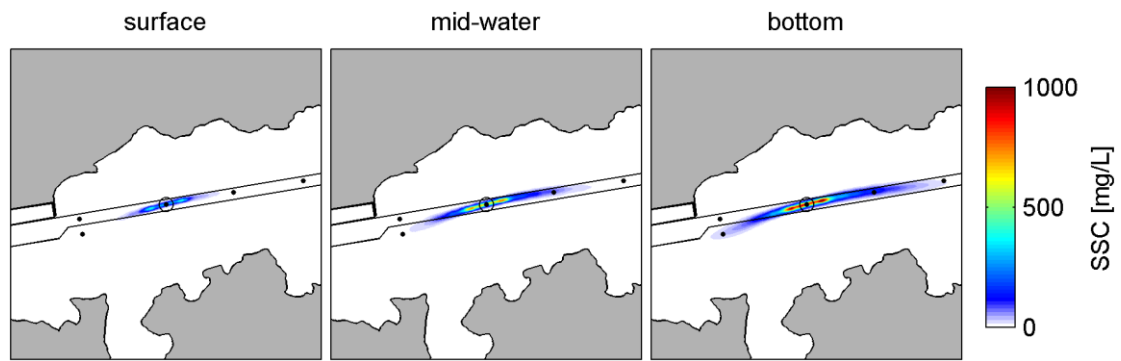


Figure A 2.25 Probabilistic SSC plumes during a 10-minute overflow phase at site C3, over the existing bathymetry, at three levels in the water column (left to right).

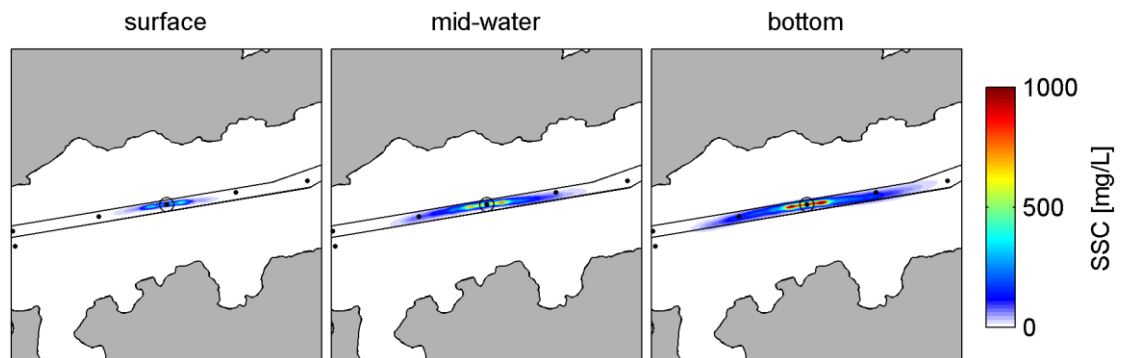


Figure A 2.26 Probabilistic SSC plumes during a 10-minute overflow phase at site C4, over the existing bathymetry, at three levels in the water column (left to right).

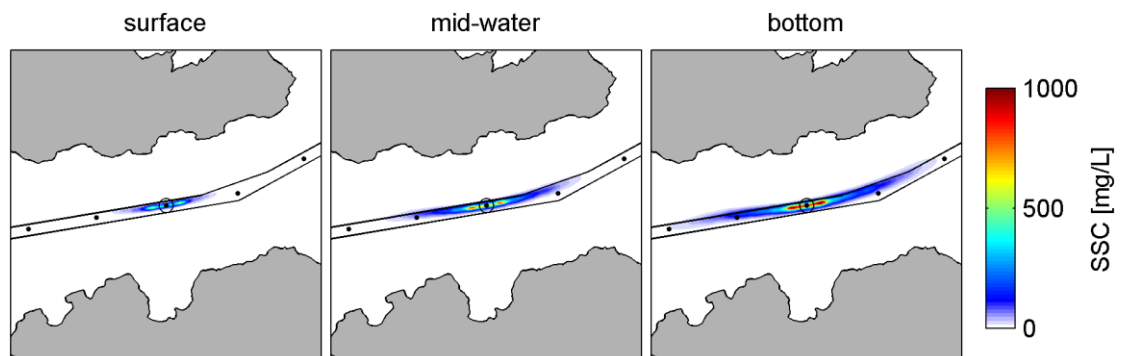


Figure A 2.27 Probabilistic SSC plumes during a 10-minute overflow phase at site C5, over the existing bathymetry, at three levels in the water column (left to right).

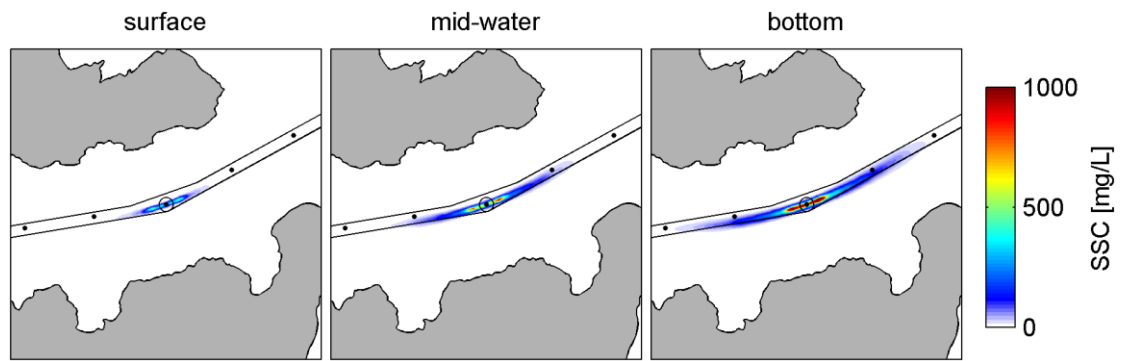


Figure A 2.28 Probabilistic SSC plumes during a 10-minute overflow phase at site C6, over the existing bathymetry, at three levels in the water column (left to right).

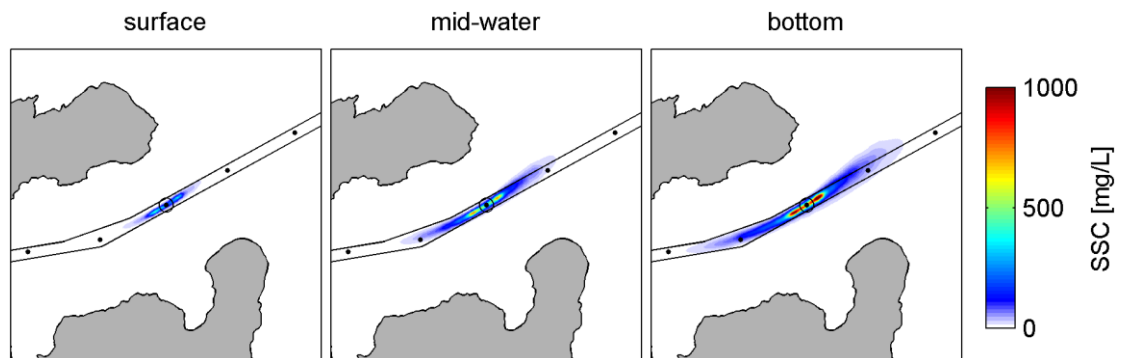


Figure A 2.29 Probabilistic SSC plumes during a 10-minute overflow phase at site C7, over the existing bathymetry, at three levels in the water column (left to right).

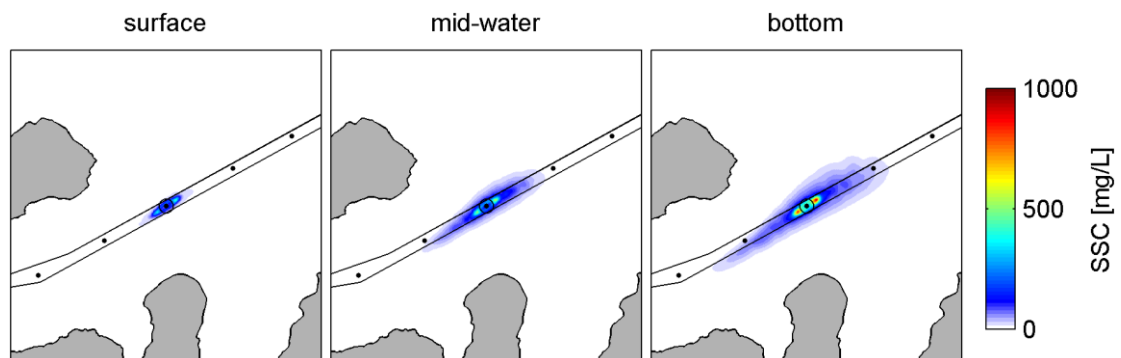


Figure A 2.30 Probabilistic SSC plumes during a 10-minute overflow phase at site C8, over the existing bathymetry, at three levels in the water column (left to right).

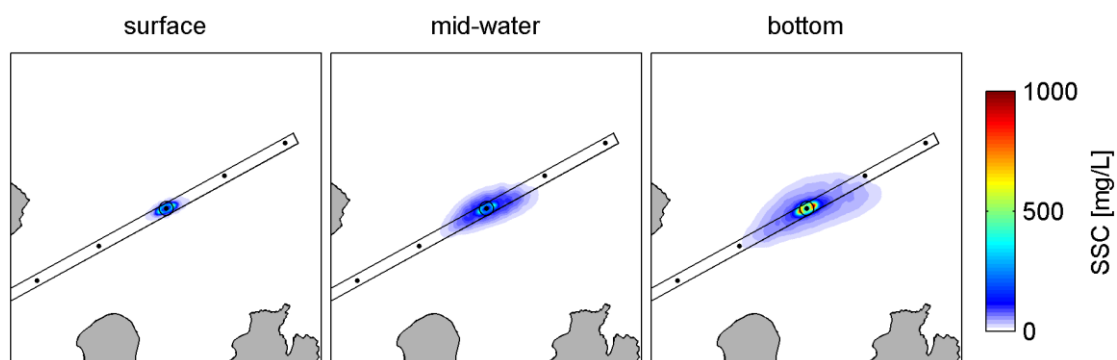


Figure A 2.31 Probabilistic SSC plumes during a 10-minute overflow phase at site C9, over the existing bathymetry, at three levels in the water column (left to right).

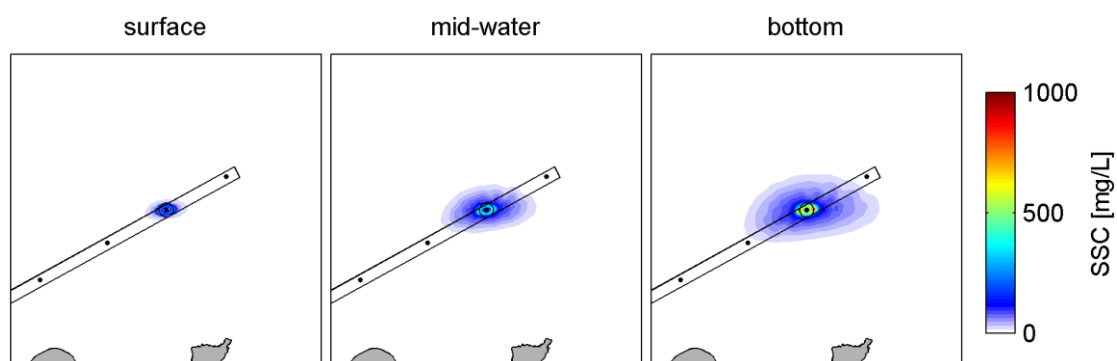


Figure A 2.32 Probabilistic SSC plumes during a 10-minute overflow phase at site C10, over the existing bathymetry, at three levels in the water column (left to right).

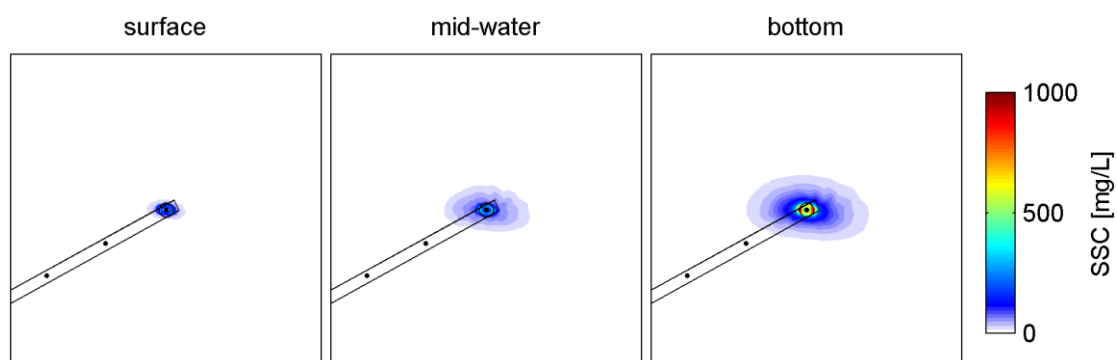


Figure A 2.33 Probabilistic SSC plumes during a 10-minute overflow phase at site C11, over the existing bathymetry, at three levels in the water column (left to right).

A2.2.2 Scenario 2

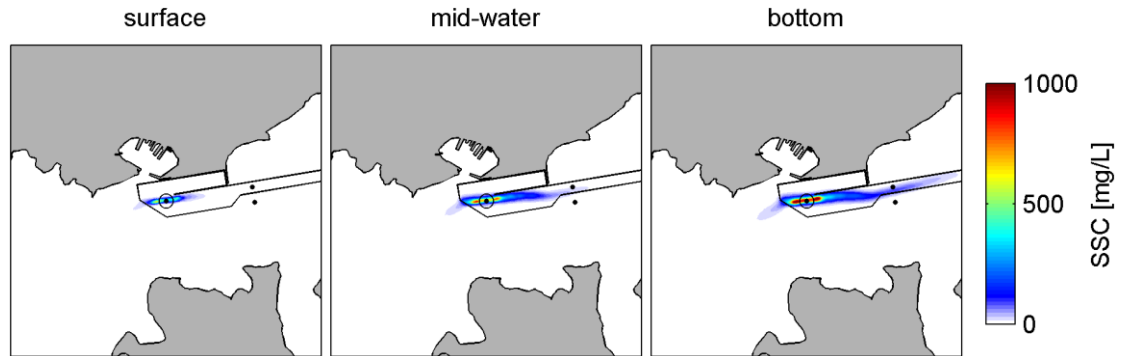


Figure A 2.34 Probabilistic SSC plumes for a 10-minute overflow phase at site C1, over the Scenario 2 bathymetry, at three levels in the water column (left to right).

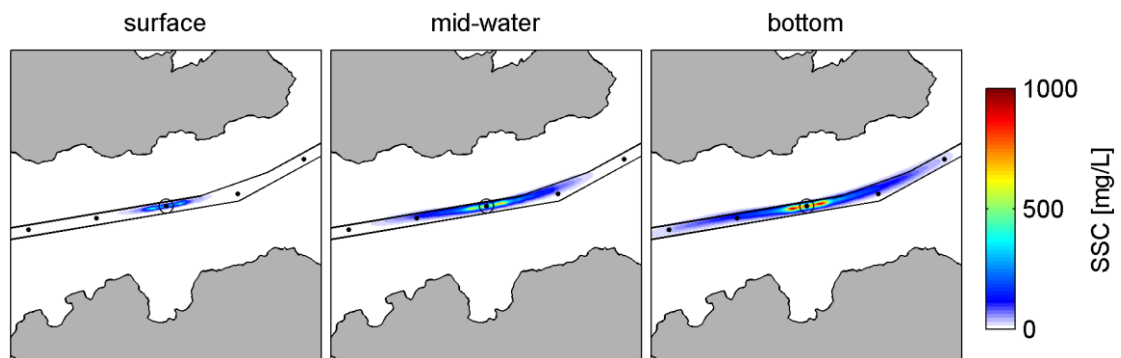


Figure A 2.35 Probabilistic SSC plumes for a 10-minute overflow phase at site C5, over the Scenario 2 bathymetry, at three levels in the water column (left to right).

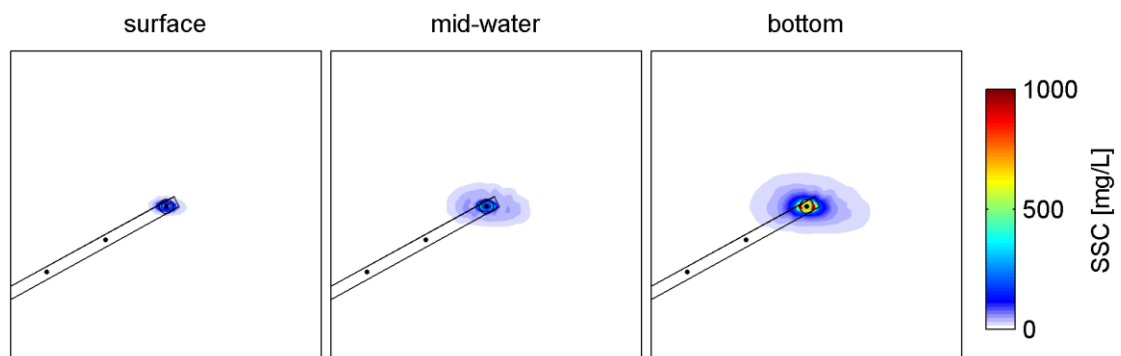


Figure A 2.36 Probabilistic SSC plumes for a 10-minute overflow phase at site C11, over the Scenario 2 bathymetry, at three levels in the water column (left to right).

A2.2.3 Existing with surge signal

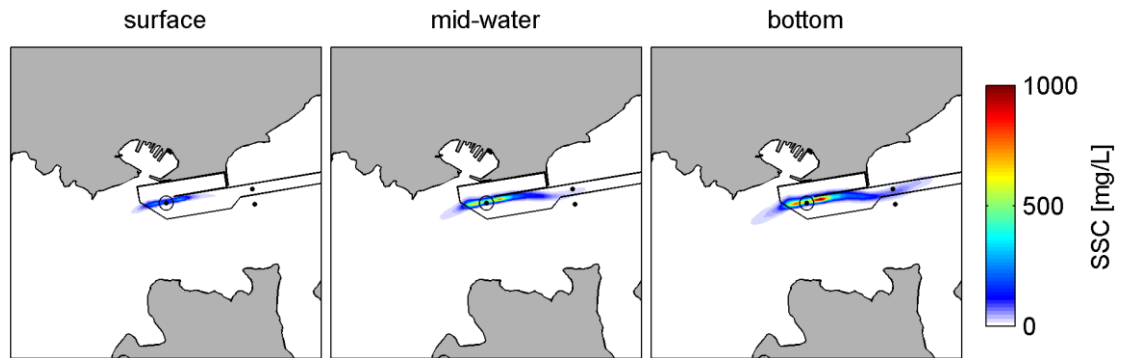


Figure A 2.37 Probabilistic SSC plumes for a 10-minute overflow phase at site C1, over the existing bathymetry, including a surge signal, at three levels in the water column (left to right).

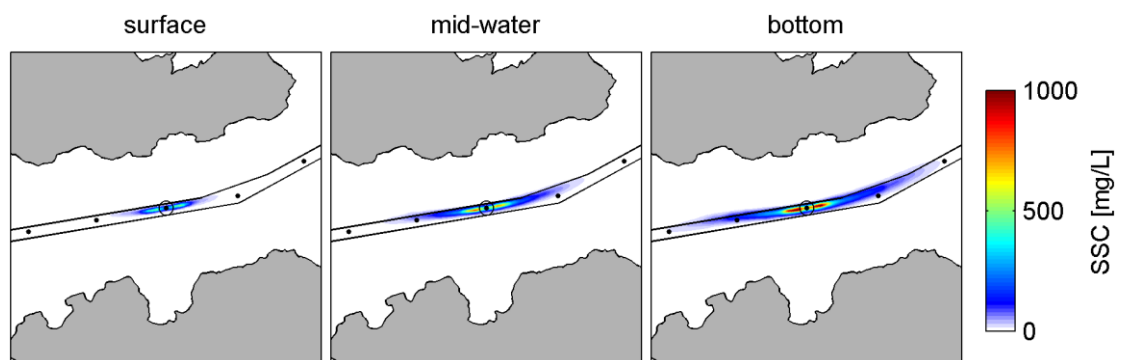


Figure A 2.38 Probabilistic SSC plumes for a 10-minute overflow phase at site C5, over the existing bathymetry, including a surge signal, at three levels in the water column (left to right).

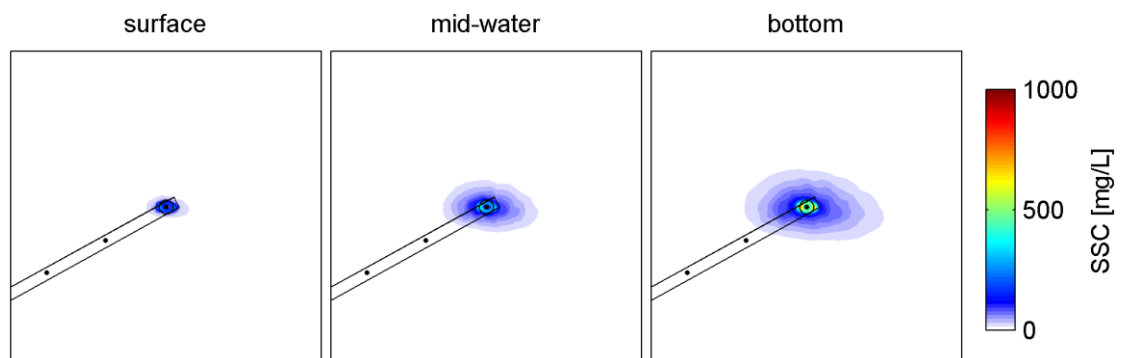


Figure A 2.39 Probabilistic SSC plumes for a 10-minute overflow phase at site C11, over the existing bathymetry, including a surge signal, at three levels in the water column (left to right).

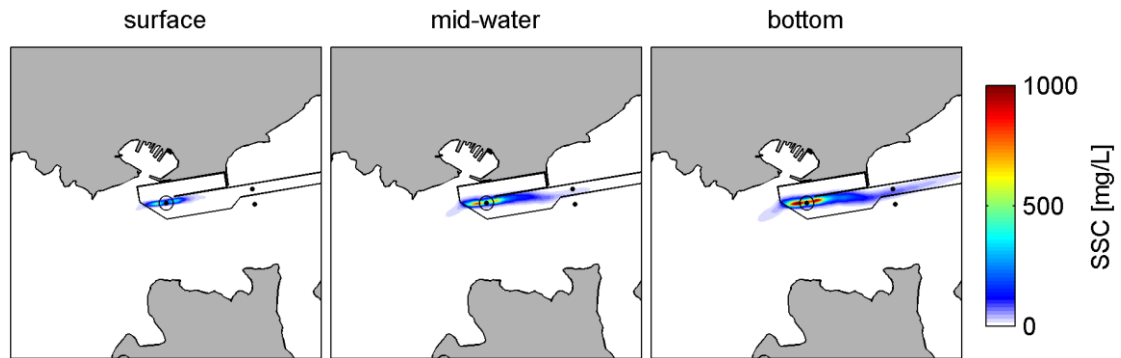
A2.2.4 Stage3 with surge signal

Figure A 2.40 Probabilistic SSC plumes for a 10-minute overflow phase at site C1, over the Scenario 2 bathymetry, including a surge signal, at three levels in the water column (left to right).

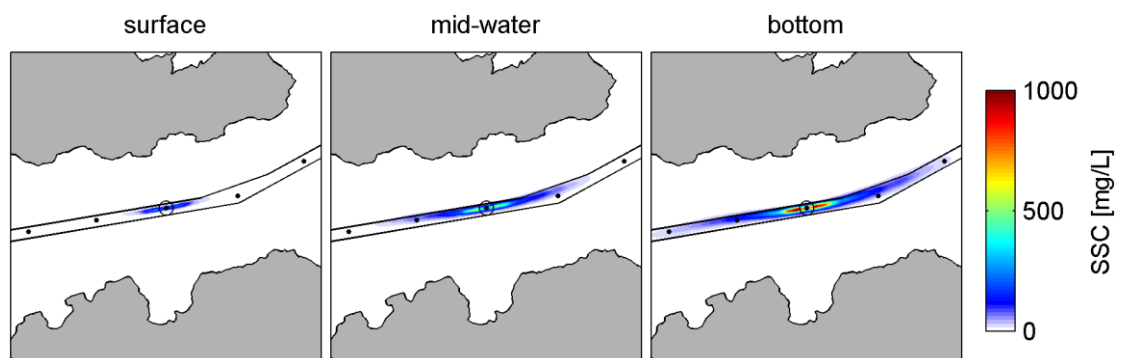


Figure A 2.41 Probabilistic SSC plumes for a 10-minute overflow phase at site C5, over the Scenario 2 bathymetry, including a surge signal, at three levels in the water column (left to right).

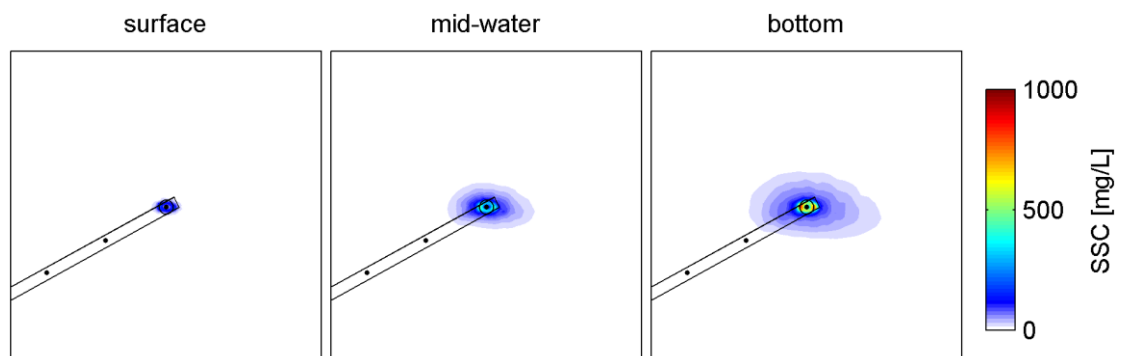


Figure A 2.42 Probabilistic SSC plumes for a 10-minute overflow phase at site C11, over the Scenario 2 bathymetry, including a surge signal, at three levels in the water column (left to right).

A2.3 Comparison of 10, 20, 30 min overflow scenario

A2.3.1 Existing bathymetry

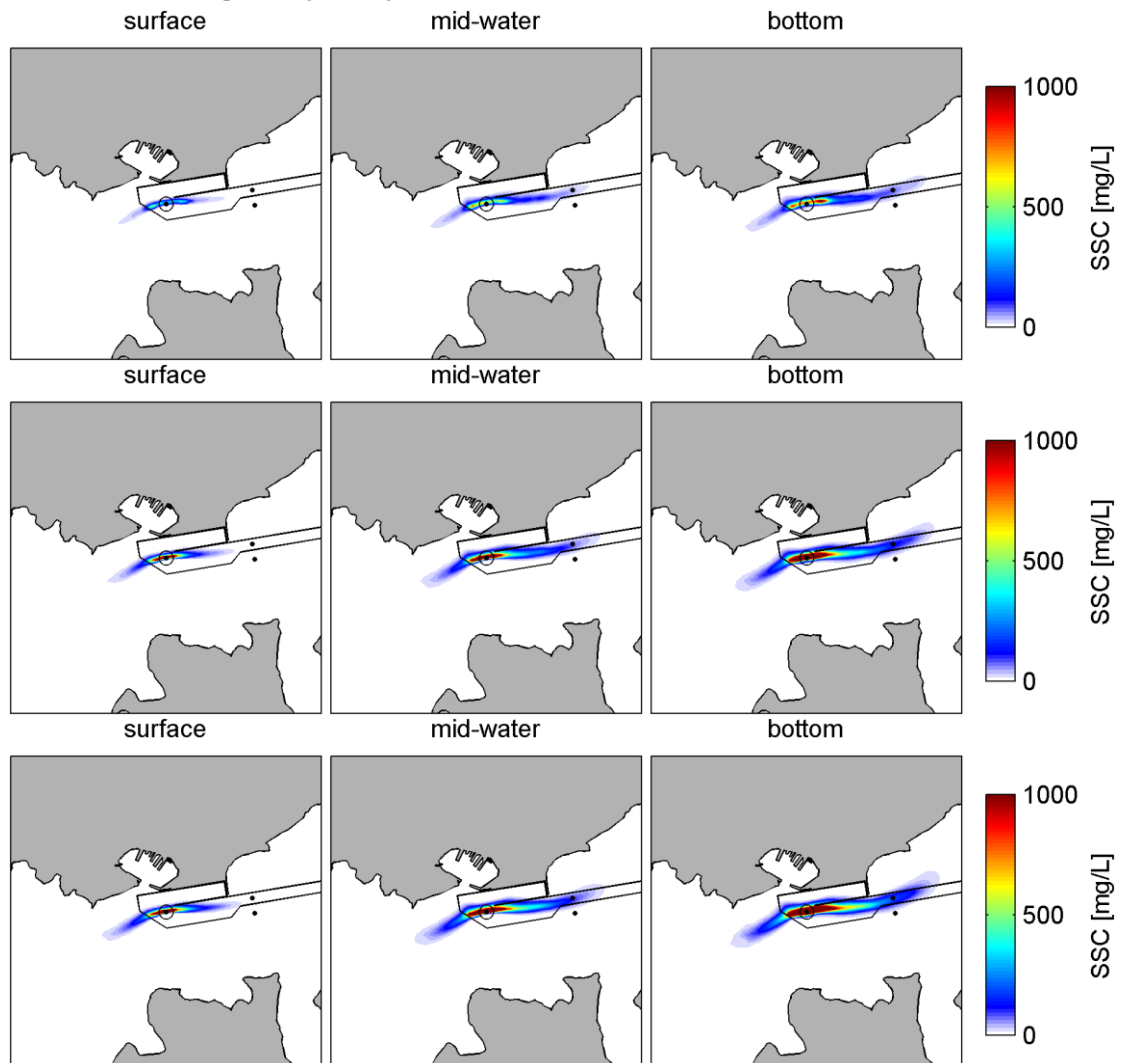


Figure A 2.43 Probabilistic SSC plumes for 10, 20 and 30 minute overflow phases (top to bottom) at site C1, over the existing bathymetry, at three levels in the water column (left to right).

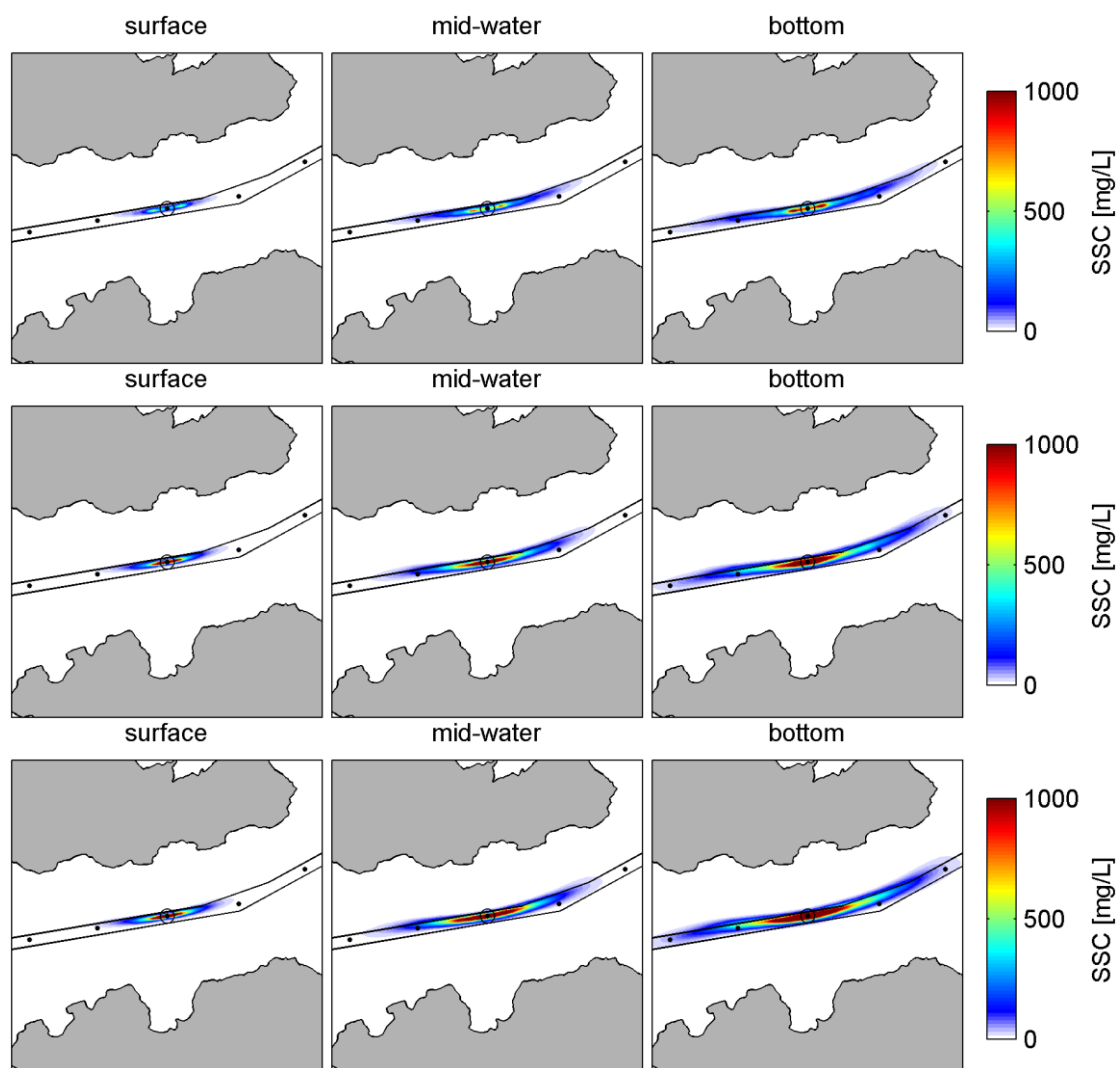


Figure A 2.44 Probabilistic SSC plumes for 10, 20 and 30 minute overflow phases (top to bottom) at site C5, over the existing bathymetry, at three levels in the water column (left to right).

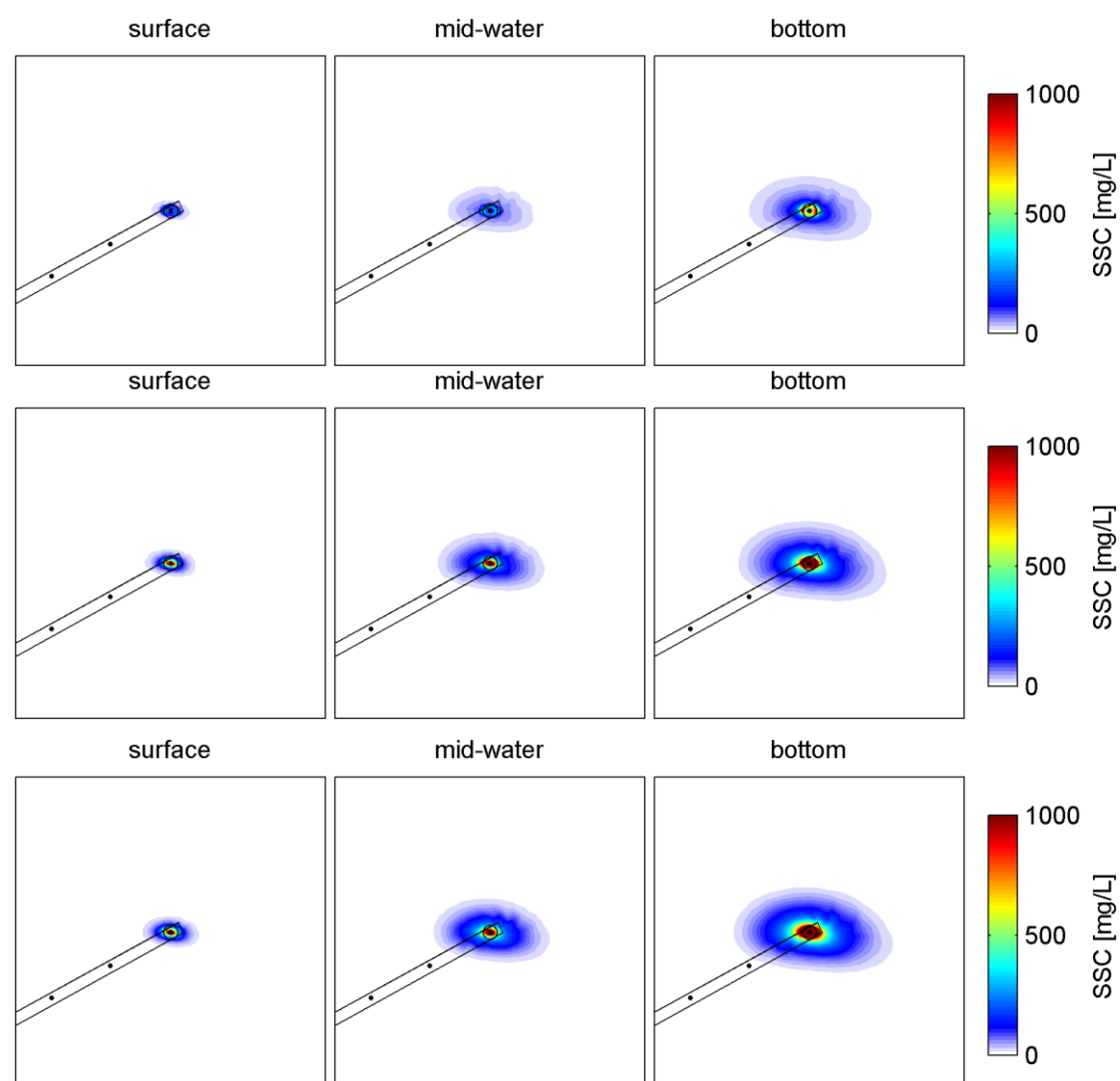


Figure A 2.45 Probabilistic SSC plumes for 10, 20 and 30 minute overflow phases (top to bottom) at site C11, over the existing bathymetry, at three levels in the water column (left to right).

A3. CONCENTRATION EXCEEDENCE

A3.1 Existing bathymetry

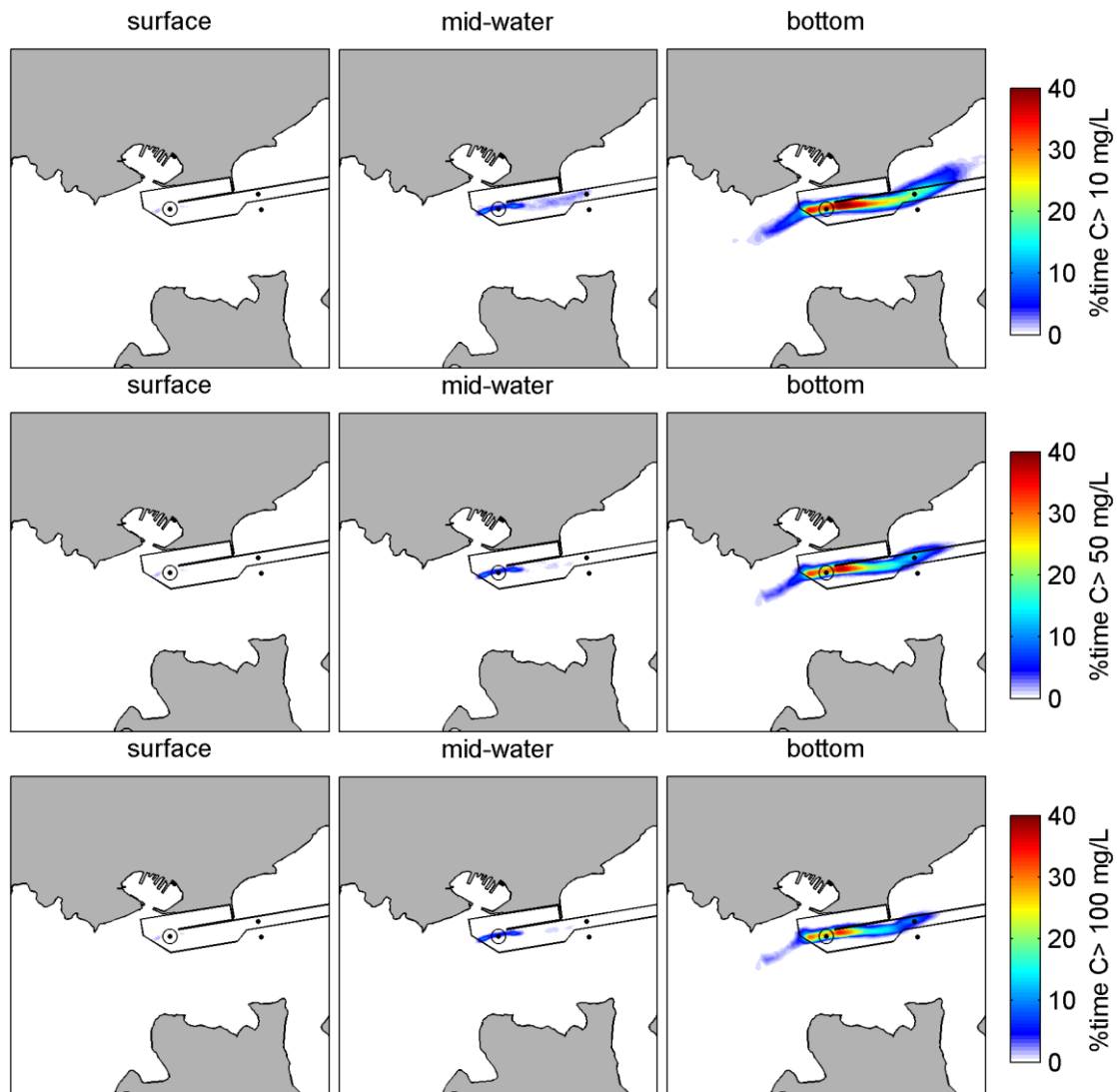


Figure A 3.1 Percentage of time SSC thresholds of 10, 50, 100 mg/L (top to bottom) are exceeded during dredging activities at site C1, including dredging (25 min), overflow (10 min) and travel to and from disposal site (85 minutes). The exceedence percentages are computed over a full spring neap tidal cycle (28 days).

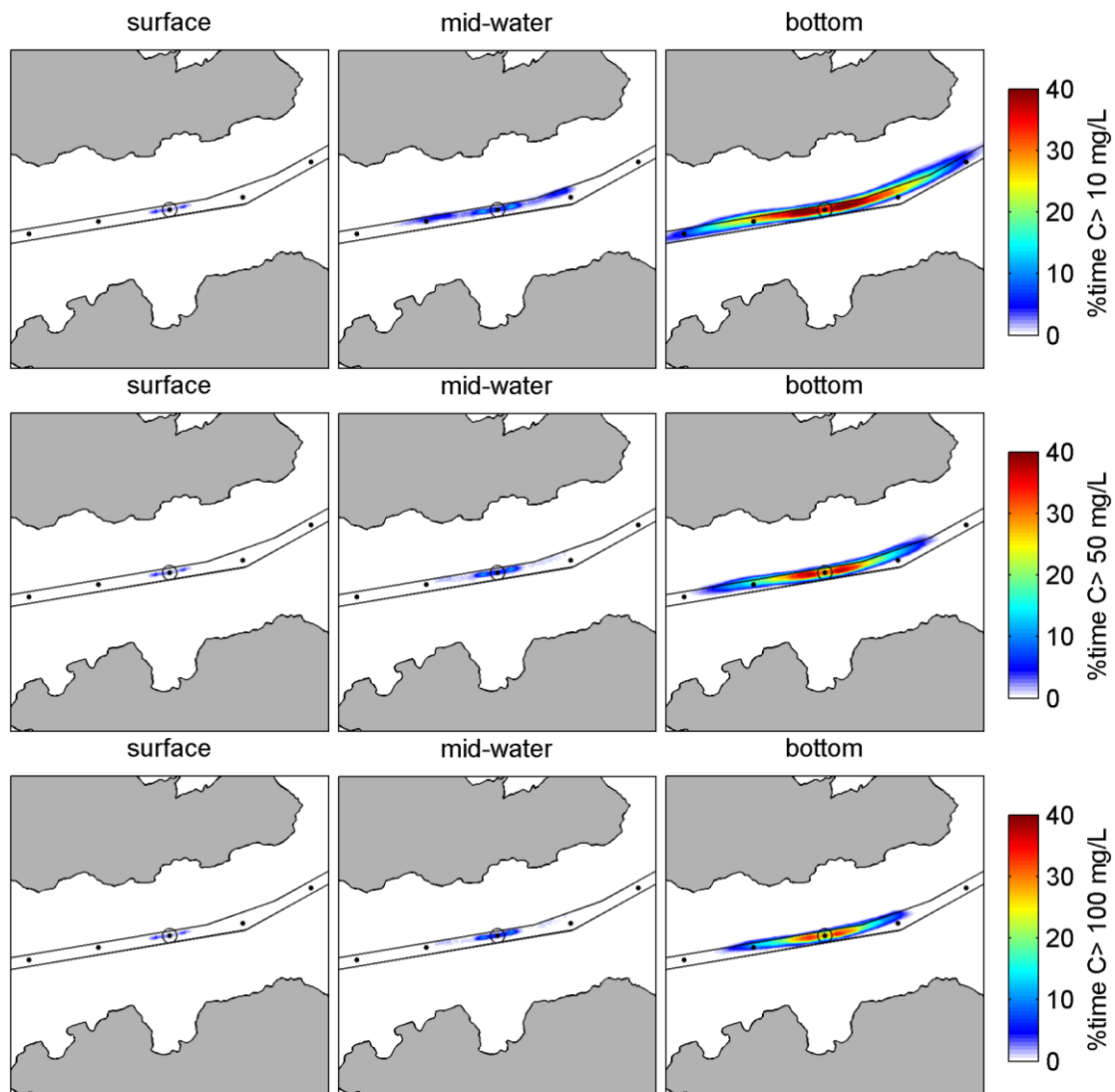


Figure A 3.2 Percentage of time SSC thresholds of 10, 50, 100 mg/L (top to bottom) are exceeded during dredging activities at site C5, including dredging (25 min), overflow (10 min) and travel to and from disposal site (85 minutes). The exceedence percentages are computed over a full spring neap tidal cycle (28 days).

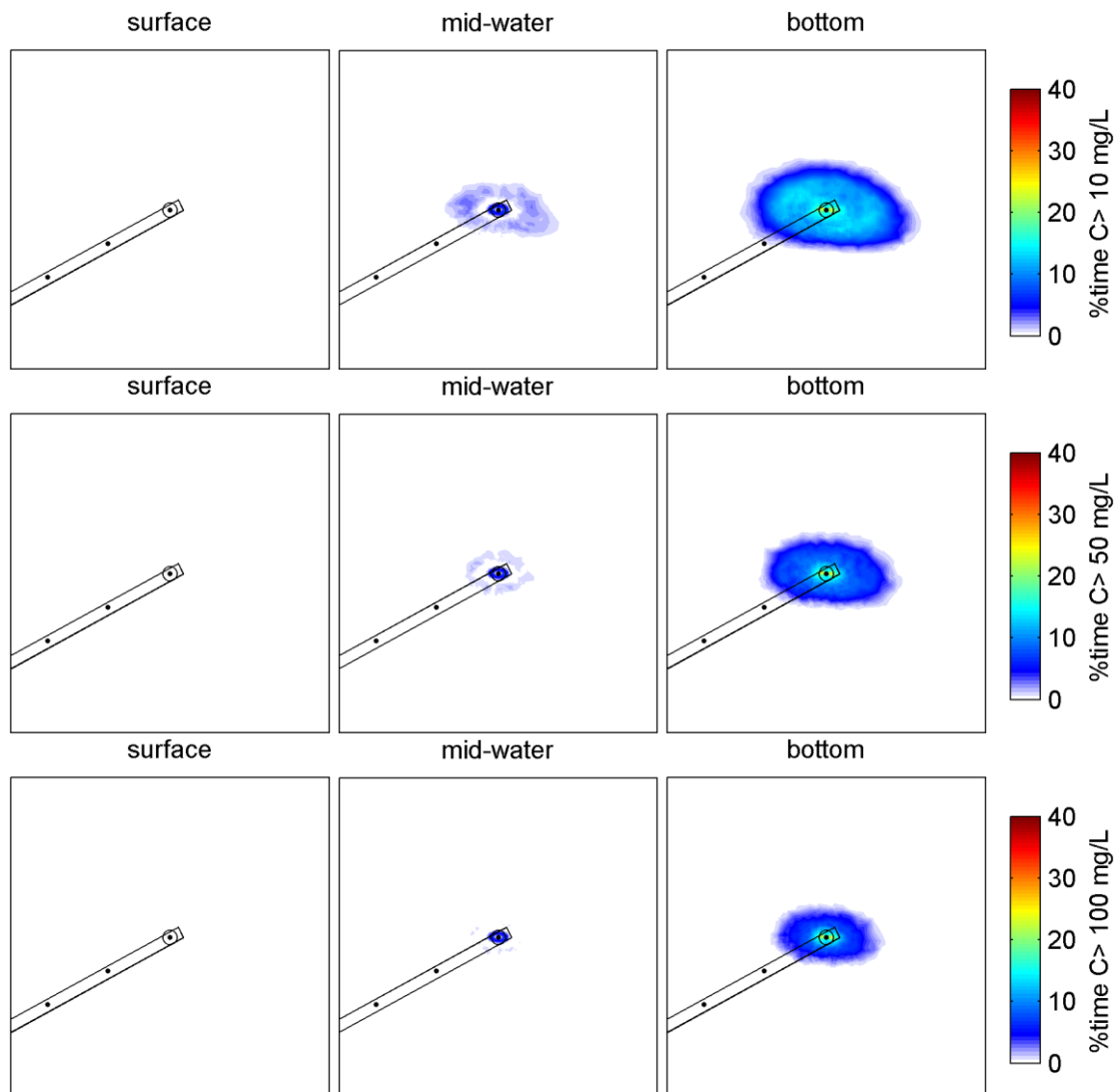


Figure A 3.3 Percentage of time SSC thresholds of 10, 50, 100 mg/L (top to bottom) are exceeded during dredging activities at site C11, including dredging (25 min), overflow (10 min) and travel to and from disposal site (85 minutes). The exceedence percentages are computed over a full spring neap tidal cycle (28 days).